TÉCNICO LISBOA

Buckling Optimization of Composite Panels with Curvilinear Fibers and Grid Stiffeners

Sofía Arranz Hernando

Thesis to obtain the Master of Science Degree in

Aerospace Engineering

Supervisors: Dr. Abdolrasoul Sohouli
Professor Afzal Suleman

Examination Committee

Chairperson: Professor Fernando Parracho Lau
Supervisors: Dr. Abdolrasoul Sohouli
Professor Afzal Suleman
Member of the Committee: Professor Aurelio L. Araujo

September 2021

Declaration

I declare that this document is an original work of my own authorship and that it fulfills all the requirements of the Code of Conduct and Good Practices of the Universidade de Lisboa.

Acknowledgements

I would like to start by expressing my gratitude to Professor Afzal Suleman. Thank you for taking me on as a student and helping me to speed up the completion of my thesis. I appreciate very much your critical advice on my analysis and writing.

I am extremely grateful to Professor Abdolrasoul Sohouli for the exceptional guidance and continuous support. Thank you for taking the time to answer any questions I had and for pointing out the right path to follow.

I also thank my colleagues of the research group on composite materials. Every Wednesday meeting made me feel more accompanied during this time.

My friends, although this summer I have not seen you as much as I would have liked, I have felt your love more than ever.

My last words of gratitude, as it could not be otherwise, are to my parents and my brother. Thank you for believing in me and being there every step of the way. Thank you for giving me the best education I could ever had. I dedicate this thesis and the bachelor degree to you. Os quiero.

Abstract

Automated Fiber Machines (AFP) can manufacture composite panels with curvilinear fibers. The stiffness of the panel depends on the spatial location. This can be tailored to improve the structural performance. In this work, the buckling performance of composite panels with curvilinear fibers and grid stiffeners is optimized using a genetic algorithm. To this end, the objective is to maximize the critical buckling load. The skin is composed of layers in which the fiber orientation varies along one spatial direction. Two design variables define each unique layer: the fiber angle at the center and side of the panel. The stiffener layout is parametrized by other two design variables, which are the stiffener location and its curvature. Manufacturing constraints in terms of maximum curvature allowable by the AFP machine are imposed for both skin and stiffener fibers. The effect of manufacturing-induced gaps in the laminates is also incorporated. The finite element method is used to perform the buckling analyses. The skin is modeled with shell elements and the stiffeners are idealized by beam elements. The panels are subjected to in-plane compressive loads and shear loads under several boundary conditions. Optimization results show the use of curvilinear fibers for both skin and stiffeners can increase the critical buckling load. The improvement over the straight fiber design depends on the load case and boundary conditions. The optimization framework developed can help the designer to evaluate in which scenarios grid-stiffened curvilinear fiber composite panels provide the greatest benefit for the critical buckling load

Keywords: Variable Stiffness composite structures, Curvilinearly grid-stiffened panel, Manufacturing constraints, Buckling, Finite element analysis, Optimization.

Resumo

As máquinas automáticas de fibra (AFP) podem fabricar painéis compósitos com fibras curvilíneas. A rigidez do painel depende da localização espacial. Isto pode ser utilizado para melhorar o desempenho estrutural. Neste trabalho, o comportamento de encurvadura dos painéis compósitos com fibras curvilíneas e reforços de grelha é optimizado utilizando um algoritmo genético. O objectivo é maximizar a carga crítica de instabilidade. Duas variáveis de projeto definem cada capa única do laminado da pele: o ângulo de fibra no centro e lado do painel. A disposição de reforços é parametrizada por duas variáveis de projeto, que são a localização e a curvatura do reforço. A curvatura das fibras da pele e dos reforços é limitada ao máximo permitido pela máquina AFP. O efeito de vazios induzidos pelo fabrico em laminados é incorporado. O método dos elementos finitos é utilizado para realizar análises de encurvadura. A pele é modelada com elementos de casca e os reforços com elementos de viga. Os painéis são submetidos a cargas compressivas e cargas de cisalhamento no plano e várias condições de fronteira. Os resultados da optimização mostram que o uso de fibras curvilíneas para a pele e reforços pode aumentar a carga crítica de instabilidade. A melhoria sobre o desenho de fibra recta depende do caso de carga e das condições de fronteira. A estrutura de optimização elaborada pode ajudar o projetista a determinar em que cenários os painéis compósitos de fibras curvilíneas com reforços curvilíneos proporcionam o maior benefício para a carga crítica de instabilidade.

Palavras-Chave: Estruturas compósitas de rigidez variável, Painel com grelha curvilínea, Restrições de fabricação, Encurvadura, Análise de elementos finitos, Optimização.

Contents

List of Figures

List of Tables

Acronyms

AFP	Automated Fiber Placement
BF	Buckling Factor
CTS	Continuous Tow Shearing
CS	Constant Stiffness
FEA	Finite Element Analysis
FEM	Finite Element Model
GA	Genetic Algorithm
GCMMA	Globally Convergent Method of Moving Asymptotes
LU	Lower–Upper
MIGA	Multi Island Genetic Algorithm
MMA	Method of Moving Asymptotes
NURBS	Non-Uniform Rational B-Splines
PSO	Particle Swarm Optimization
SA	Simulated Annealing
VAT	Variable Angle Tow
VS	Variable Stiffness

Chapter 1

Introduction

This chapter aims to provide an overview of the goal of this thesis: the design of composite panels with curvilinear fibers and grid stiffeners. Section 1.1 discusses the motivation of the thesis. Section 1.2 states the objectives to be achieved. And Section 1.3 briefly explains the contents of the chapters of this thesis

1.1 Motivation

In the aerospace industry, weight is crucial. Weight savings mean less fuel is required, which in turn results in a higher payload capacity or a longer range for the aircraft. The call for weight reduction drives the aerospace industry to continually search for lighter or stronger structures.

Composite materials have been increasingly employed in aerospace structures due to their high specific strength and stiffness. Traditional composite laminates are composed of plies with straight fibers. The material properties can be tailored by combining plies with different fiber orientations and changing the number of plies. In addition, structural performance can be enhanced through grid-stiffened composite skins. Typically, orthogrid or isogrid panels in which the stiffeners follow straight paths are used.

Recent advances in the manufacturing technologies of composites have made it possible to steer the fibers. The Automated Fiber Placement (AFP) machines can manufacture laminates in which the fiber orientation continuously varies. The stiffness of these laminates is not constant and depends on the spatial location. Therefore, they are called variable stiffness laminates. It is also possible to manufacture composite panels reinforced with curvilinear stiffeners. The use of curvilinear fibers for the laminate and for the stiffener path provides a larger design space to exploit the directionality of the material properties.

Composite laminates can be employed to manufacture wing or fuselage skins. Skins are thin-walled panels subjected to in-plane loads and are prone to buckling. Hence, the study of buckling is essential for the structural design of an aircraft.

The present thesis aims to determine whether the use of curvilinear fiber composite panels leads to a significant increase in buckling load over straight fiber designs. In other words, the motivation of the study is to answer the following question: *To what extent tailoring the stiffness variation can improve the buckling performance?*

1.2 Objectives

To the best of the author's knowledge, there is no study on the buckling optimization of curvilinear fiber composite panels reinforced with curvilinear stiffeners that simultaneously considers the manufacturing aspects in terms of the maximum curvature allowed by the AFP machine and induced gaps on the laminate. And that constitutes the main goal of this thesis. To this end, an integrated optimization framework will be developed following the steps indicated:

- Modeling of variable stiffness laminates and curvilinearly grid-stiffened layouts.
- Modeling the effect of gaps in variable stiffness laminates.
- Development of a Python-Abaqus script to conduct the buckling analysis of the panels
- Integration of the Python script and the Genetic Algorithm in MATLAB to perform the optimization
- Implementation of curvature constraints for both skin and stiffener fibers
- Optimization of panels for buckling performance under several loading cases and boundary conditions

1.3 Thesis Outline

This thesis has been structured in six chapters. The contents of the five subsequent chapters are explained below.

Chapter 2 presents a short background on the relevance of composite materials in the aeronautical industry and describes the manufacturing of composite materials by fiber placement technology. A literature review of the design of variable stiffness laminates and curvilinearly grid-stiffened panels is next given. The manufacturing-induced defects of VS laminates and their impact on the design phase are also addressed. A brief explanation of the linear buckling analysis is then provided. Lastly, the optimization strategies available to maximize the buckling performance of curvilinear fiber composite panels are discussed.

Chapter 3 first outlines the workflow of the Python script developed to build the FE model and process the FE analysis results. Next, the methodology for modeling variable stiffness laminates and for including the effect of gaps in the FE model is described. This chapter follows with the geometry parameterization and modeling of curvilinearly grid-stiffened panels. Finally, the mesh convergence study is presented.

Chapter 4 presents the optimization framework. In this chapter, the optimization problem is defined. The chapter describes the objective function, the design variables and constraints in terms of allowed curvature for both skin and stiffener fibers. The theoretical basis of Genetic Algorithms as well as the genetic parameters and functions selected are then explained. The last section discusses how to integrate the FE module into the optimization module.

Chapter 5 describes the case studies to be optimized. Several boundary conditions and load cases are considered in the optimization. The results for ideal panels are presented and discussed. Next, the optimized panels including the effect of gap are introduced and analysed. A comparison is finally made between the different scenarios of boundary conditions and loads and panels with or without considering the gap effect.

Chapter 6 discusses the conclusions drawn from the present work as well as several aspects that may be of interest for future research.

Chapter 2

State of the Art

This chapter first addresses the importance of composite materials in the aerospace industry. The manufacturing of composite materials by Fiber Placement is presented in Section 2.2. Variable stiffness laminates and available modeling methods are discussed in Section 2.3. The manufacturing-induced defects of VS laminates and how their impact has been included in the design phase are described in Section 2.4. Next, the design of curvilinearly grid-stiffened panels are introduced in Section 2.5. Section 2.6 explains the fundamentals of the linear buckling analysis. Finally, Section 2.7 provides a literature review of the buckling optimization of VS laminates and curvilinearly grid-stiffened panels.

2.1 Relevance of Composite Materials in the Aerospace Industry

The main driver in the development of materials for aerospace structures is weight reduction. The decrease in structural weight results in fuel savings that allow for higher payload capacity or a larger range of the aircraft. Besides structural efficiency, aerospace structure materials must demonstrate adequate damage tolerance, fatigue resistance, safety level, durability, affordable costs, and availability.

The call for weight reduction in the aerospace industry has led to the increasing use of composite materials due to their higher specific strength and stiffness compared to metals. In general, the usage of composite materials reduces the structural weight by 20–30%.

Composite materials can be defined as a combination of materials that differ in composition or form on a macroscopic scale. The constituents maintain their identity in the composite, i.e., they do not dissolve or melt into each other although they work together. The constituents can be physically identified and show a definite interphase between them. The composite material presents beneficial physical characteristics that are very distinct from those that the individual components can offer.

Fiber-reinforced composites are composed of two constituents: the fibers and the matrix. The main function of the fibers is to support and carry loads along their direction. They provide strength and stiffness to the composite. The mechanical properties of the composite material will be proportional to the volume and characteristics of the fibers. The matrix holds the fibers in their proper position and protects them from environment. It transfers and redistributes the load to and between the fibers and

provides interlaminar shear strength.

In the aerospace industry, the most common reinforcements are glass and carbon fibers. For the matrix, thermoset and thermoplastic polymeric resins are the most used ones. The type of composite material considered in this thesis is thermoset carbon fiber reinforced plastic (CFRP) in the form of laminate, which is currently the most widespread primary/secondary structures in the aeronautical industry.

Fiber-reinforced composites are orthotropic materials. The composite exhibits high strength and stiffness in the fiber direction, but much lower in the direction perpendicular to the fiber. Hence, the stiffness and strength properties of the laminate can be varied by combining layers with different orientations and changing the number of layers. This characteristic allows engineers to tailor the material properties according to the loads supported by the structure, resulting in weight savings.

Composites have also an outstanding fatigue resistance and by themselves do not corrode, which can decrease the maintenance cost of the aircraft. When using composite materials, fewer integration operations are required, so there is a reduction in the number of parts and the cost of assembly. Complex shapes are easier to obtain and the material waste is less than in metals.

Composites are a good alternative from an environmental perspective. Despite the higher environmental impact in the manufacturing phase and more complex disposal or recycling, the environmental benefits are due to the lower fuel consumption of the aircraft, which reduces atmospheric emissions over its lifetime.

The introduction of composite materials in aircrafts occurred progressively over time. Firstly, composite materials were employed in the tertiary components, such as interior parts, sidewalls and galleys. Then they were incorporated into secondary structures like control surfaces. Over the last two decades, composite materials have been implemented in primary structures such as the wing, fuselage and stabilizers.

The mid-1960s and early 1970s saw the first application of composite materials, developed in the military field. Examples of this were the empennages of the F-14 and F-15 fighter aircrafts. The use of composite materials steadily expanded from only 2% of the F-15 airframe to 20% of modern fighter aircraft, including significant parts like the wing (skins and substructure), forward fuselage and horizontal stabilizer [1].

Composite materials went through a similar path in commercial aviation. Figure 2.1 shows the increase in the percentage of structural weight attributed to composite materials in commercial aircraft. The Airbus A320 with its all-composite tail was the first commercial aircraft to employ composite materials on a large scale. Until recently, Airbus has relied more on composite materials than Boeing, reaching up to 15% of composite materials relative to overall airframe weight for the A320, A330 and A340 families of aircraft. Airbus has continued to incorporate composites into primary load-carrying airframe structures with the A380 development. The major Airbus commitment to composite materials has come with the A350 XWB aircraft model. Half of the A350 XWB's structure is made of composite materials, which accounts for more than 50% of composite in terms of weight.

However, in the last decade, Boeing has taken a step forward by introducing its 787 Dreamliner.

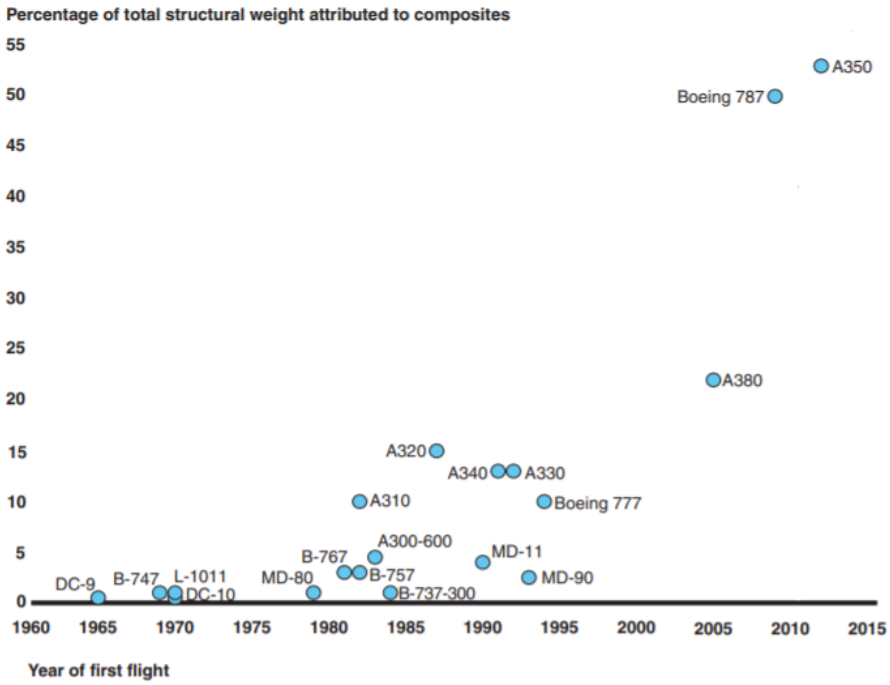

Figure 2.1: Evolution of the percentage of structural weight attributed to composite in commercial aviation, reproduced from [2]

The Boeing 787 makes extensive use of composite materials in its airframe and primary structure, such as the wing and fuselage. Figure 2.2 schematizes how materials are applied throughout the Boeing 787 Dreamliner. As can be seen, 50% of the structural weight corresponds to composite materials. Aluminum alloys represent only 20% and titanium 15%.

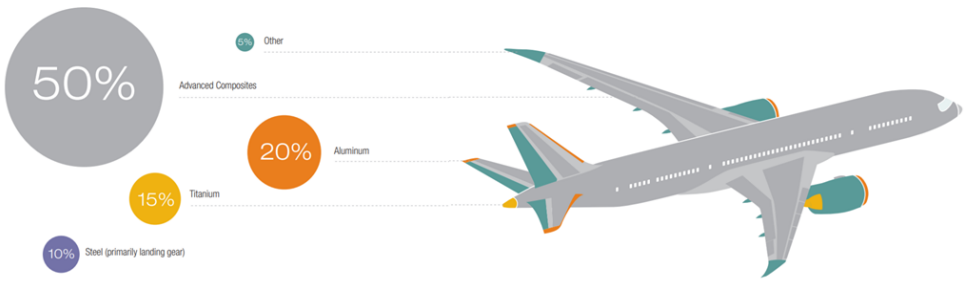

Figure 2.2: Materials used throughout the Boeing 787 expressed as a percentage of total structural weight, reproduced from [3]

In addition to military and commercial aircrafts, helicopters or General Aviation airplanes have incorporated composite materials into their structures. Another application for the use of composite materials is in the growing Urban Air Mobility (UAM) vehicles. In these segments, the aircrafts are smaller and the incorporation of composite materials is easier. The percentage of composites is very significant to the extent that some vehicles can be considered 'all-composite aircraft'.

The strong growth of the aeronautical composites market is largely due to a better understanding of the behavior and capabilities of composite materials, increasing demand for lighter and more fuel-efficient aircrafts, and improved manufacturing processes. However, some challenges must be overcome before composites can fully displace aluminum and other metal alloys, especially, in large aircrafts.

Composites are a relatively new material and, consequently, have a high cost. They require intensive labor and complex and expensive manufacturing machines. Development, testing, certification, maintenance, and end-of-life costs must also be considered. Composites are difficult to inspect for flaws and can absorb moisture or be affected by temperature. These materials are susceptible to damage by impact and delamination can occur, which are not simple to repair. There is still a shortage of "standard" design rules and knowledge on some aspects of their behavior. Recycling of parts is also another concern.

The aerospace industry needs to address these hurdles through innovative design and manufacturing technologies since the use of composite materials has shown significant benefits over metallic alloys. The developments in automated manufacturing methods, specifically in Automated Fiber Placement machines, have broadened the number of design possibilities. The fiber placement technology is discussed next.

2.2 Fiber Placement Technology

2.2.1 Automated Fiber Placement

Automated Fiber Placement (AFP) machines are a recent advance in composite manufacturing techniques. They can manufacture complex structures that may not be created with other manufacturing techniques. The AFP machine can continuously vary the orientation of the fibers. This fiber steering capability allows manufacturing variable stiffness laminates and curvilinearly grid-stiffened composite panels. Typical aircraft components manufactured by fiber placement include engine cowls, inlet ducts, fuselage sections, pressure tanks, nozzle cones, tapered casings, fan blades, among others.

The most commonly employed materials in AFP machines are thermoset prepegs, however, thermoplastic materials or dry fibers can also be used. Depending on the machine design, the prepeg tows are grouped from 8 to 32, named collectively as a course. Common values for tow width are 3.175×10^{-3} m, 6.35×10^{-3} m and 12.7×10^{-3} m [4].

Modern AFP machines employ an active and passive feeding system to deposit the tows onto the surface. The tows are moved from the material spools to the delivery head by means of guide rollers. These rollers press and transport the tows to the compaction roller. The compaction roller transfers the tows to the nip point and, by rotating and moving, places them on the tool surface. The compaction roller helps to decrease the trapped air and gaps between tows. These two previous steps are considered as active feeding. At that point, the rollers are released because the adhesive between the tow and the tool is increased, allowing the tow to move at its own speed (passive feeding). It should be mentioned that the tow tension must be kept constant, as it is a crucial parameter in the AFP process. Figure 2.3 shows the scheme of the delivery head of an AFP machine.

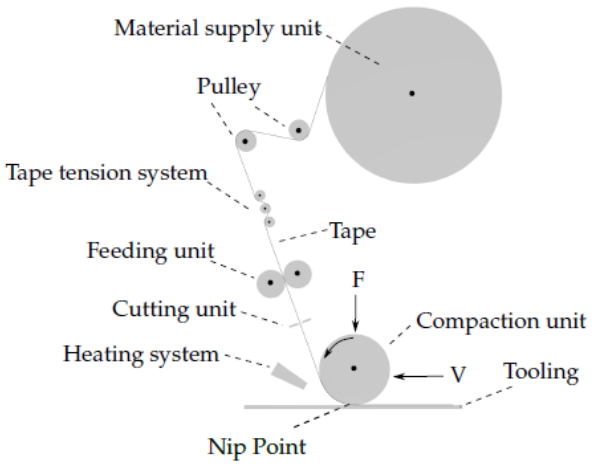

Figure 2.3: AFP delivery head, reproduced from [5]

A major feature of the AFP delivery head is the capability to individually control the speed each tow is deposited on the surface. Termed as differential tow payout, this is the key when dealing with curved trajectories. If one considers Figure 2.4, it can be observed that path A is longer than path B. This is possible because the head places tows at different rates.

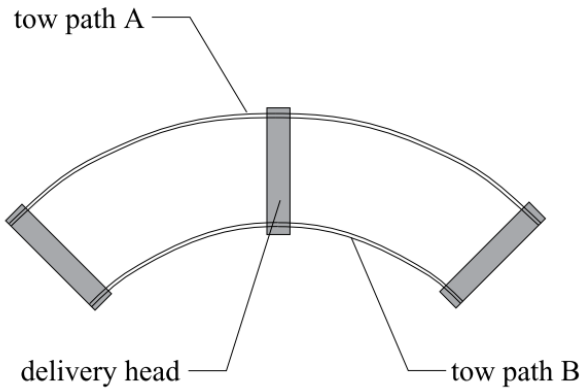

Figure 2.4: Manufacture of curved fiber paths using different speeds on AFP machines, reproduced from [6]

Curved tows require in-plane deformation. Therefore, compressive forces will occur along the inner edge and tensile forces along the outer edge, as it can be seen in Figure 2.5. If a tow is overly curved, the compression force will be high enough to produce local tow buckling or wrinkling. This fiber deformation out-of-plane is undesirable due to the decrease in the laminate quality. It results into imperfections and reduces the structural load carrying capability. Hence, a maximum curvature, k_{max}, or the equivalent minimum turning radius, R_{min}, has to be established. The value depends on the tow width, material stiffness and tackiness, layup rate and compaction pressure used by the machine [7].

AFP machines can also cut and restart individual tows while continuing to lay the remaining tows. This capability allows parts to be manufactured closer to their final shape and, therefore, the scrap rate is lower. In addition, as tows can be added or dropped at any point, the course width can vary along the

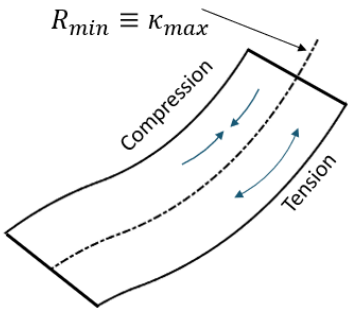

Figure 2.5: Compressive and tensile forces generated on a curved course

path of the AFP head. This can be employed to avoid large gaps or overlaps formed between tow steered courses.

In the case of thermoset materials, to increase the tackiness and thus the adhesion to the mould, a heat unit is employed. This unit is placed in the delivery head and prior to the material deposition. On the other hand, cooling can be used to reduce tackiness when performing cutting, clamping and restating processes.

The great flexibility of the AFP machine to position the delivery head onto the surface is due to its seven axes of motion. Three components make it possible to achieve this seven degrees of freedom. The fiber delivery head is attached to a robotic wrist that can rotate about three axes (yaw, pitch and roll). The sled for positioning the delivery head can move in two directions (cross-feed and carriage traverse) and rotate on one axis (arm tilt). The mandrel rotates the mould.

The AFP machine is also computer controlled. The software converts the CAD part and tooling data into commands for the seven axes of motion, determining the tow path and boundaries. Then a manufacturing simulation is run to confirm that the predefined paths are valid.

2.2.2 Continuous Tow Shearing

Continuous Tow Shearing (CTS) is presented as an alternative technique to the conventional AFP process. It has recently been developed by B.Kim, P.Weaver and K.Potter at the Advanced Composites Collaboration for Innovation & Science (University of Bristol) [8–10]. The key feature is that the CTS head provides a continuous in-plane shear deformation to the tow as opposed to the AFP head that places the tow using in-plane bending. The difference is that while the AFP head keeps the axis perpendicular to the tow path, the CTS head moves along the shifting direction. Figure 2.6 shows the tow arrangement and the head rotation for AFP method and CTS method.

The aim of this novel technique is to minimize the defects generated by the AFP process such as fibre wrinkles, resin-rich areas and fibre discontinuities. Shearing the tow constantly can decrease the minimum radius of curvature, and avoid the gaps/overlaps induced by the shifted method as the fibers can exactly follow the designed path. The design process is simplified as it is no longer necessary to model the geometry of the gaps/overlaps. However, the tow subjected under shear and with fixed boundaries

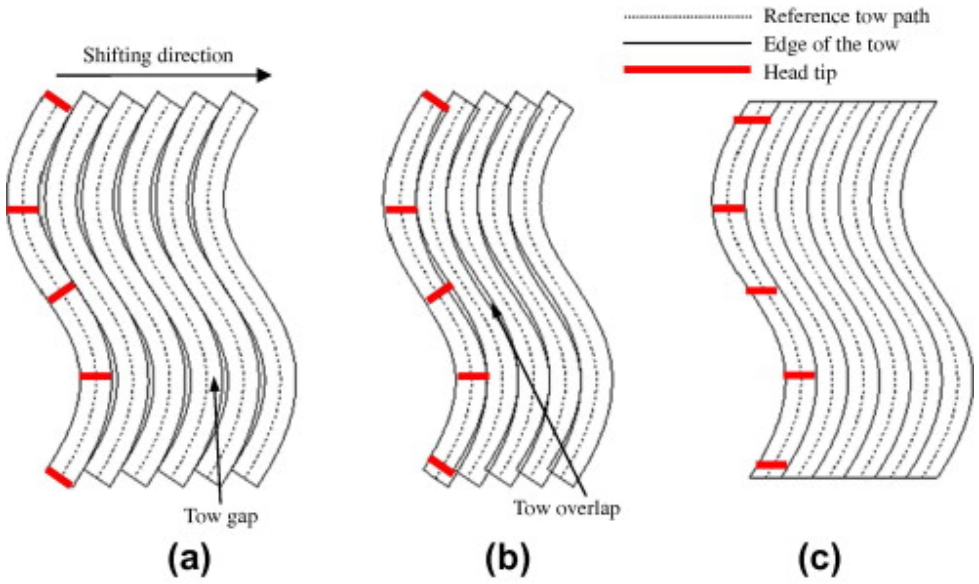

Figure 2.6: Tow arrangement and head rotation for AFP (a,b) and CTS (c) techniques, reproduced from [8]

experiences an increase in thickness that has to be taken into account in the design [9].

The conventional pre-impregnated tow material is not utilized in the CTS method. The relatively high viscosity of its resin matrix prevents the fibers from shearing easily and, instead, fiber wrinkles will appear. Thus, a hybrid between the prepeg and a dry tow is used. The CTS machine impregnates a dry tow in situ to form a semi-impregnated tow [8].

Although Continuous Tow Shearing is a promising technology, it is not as mature as the AFP technology in terms of design, manufacturing, testing and certification [10]. Therefore, in this work, the AFP method has been chosen to manufacture the variable stiffness laminates.

2.3 Variable Stiffness Laminates

The stiffness of a laminate depends on the number of plies and the fiber orientation within the plies. Traditionally, the fiber angle orientation is uniform (straight fibers), resulting in Constant Stiffness (CS) laminates. As discussed in Section 2.2, advances in manufacturing technology have made it possible to curve the fibers. Therefore, laminates in which the fiber orientation of the plies is not constant can be manufactured. This results in laminates with variable stiffness that can be tailored to produce more efficient load paths than CS laminates. The design space is enlarged and substantial improvements in structural performance or weight savings can be obtained. Another approach to spatially vary the stiffness is to add patches of plies over the laminate, thus changing the stacking sequence and the number of plies in a discrete manner.

In this thesis, Variable Stiffness (VS) laminates refer to laminates composed of plies in which the fiber orientation changes continuously with the spacial location. This type of laminate may also be termed tow-steered laminate or Variable Angle Tow (VAT) laminate.

In the literature, different approaches are available to model VS flat panels. Several authors have used mathematical modeling common in computer graphics to represent curves as a direct method to parameterize curvilinear fibres. Nagendra et al. [11] modeled the fiber paths by using Non-Uniform Rational B-Splines (NURBS) with a fixed number of control points. Honda et al. [12] employed a linear combination of B-Splines to represent arbitrarily shaped fibers. Other works, including [8, 13], selected Bézier curves to model the fiber paths. The above fiber paths can be easily read by the fiber placement machine. However, the definition of appropriate basis paths and control points is not straightforward, limiting the feasibility of these methods [7].

Gürdal and Olmedo [14, 15] were the first to introduce a parameterization scheme to describe fibers which orientation varied linearly along the x or y direction. Later, Tatting and Gürdal [16] generalize the reference path formulation so that the fiber angle, $\theta(x')$, can vary linearly along an arbitrary axis, x', as expressed in Equation 2.1.

$$\theta(x') = \phi + (T_1 - T_0)\frac{|x'|}{d} + T_0 \tag{2.1}$$

where T_0 and T_1 are the fiber angles at the beginning and the end of the characteristic length d. The angle ϕ defines the orientation of the $x' - y'$ coordinate system with respect to the $x - y$ global coordinate system. These three magnitudes are sufficient to define a linearly varying ply. The compact notation that has been adopted by convention is of the form $\phi\langle T_0, T_1\rangle$. Figure 2.7 schematized the terms of Equation 2.1. Note that the angles are considered positive in a counter-clock wise direction.

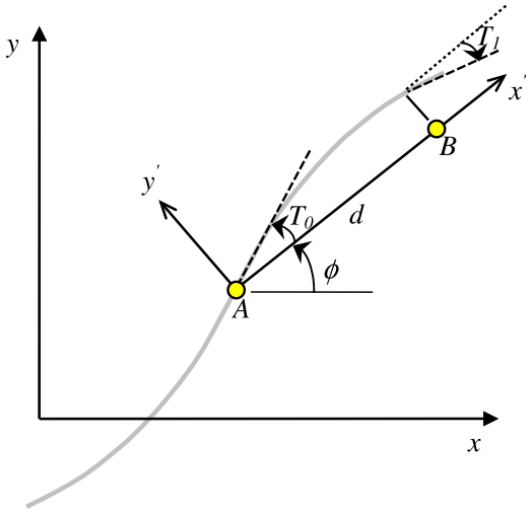

Figure 2.7: Reference path of linear angle variation fibers, reproduced from [17]

By using the relation $dy'/dx' = tan(\theta - \phi)$ and performing the integration with respect to x', the reference fiber path y' is expressed in Equation 2.2.

$$y'(x') = \begin{cases} \frac{d}{T_1 - T_0}\left\{-ln\left[cosT_0\right] + ln\left[cos\left(T_0 + (T_0 - T_1)\frac{x'}{d}\right)\right]\right\}, & \text{for } -d \leq x' \leq 0 \\ \frac{d}{T_0 - T_1}\left\{-ln\left[cosT_0\right] + ln\left[cos\left(T_0 + (T_1 - T_0)\frac{x'}{d}\right)\right]\right\}, & \text{for } 0 \leq x' \leq d \end{cases} \tag{2.2}$$

where

$$x' = xcos\phi + ysin\phi \tag{2.3}$$

More recently, Gürdal et al. [18] developed another parametrization to describe curvilinear fibers. The definition of the fiber path was based on circular arcs, using the same parameters as the formulation of the linear angle variation: the fiber angles at the start and end, T_0 and T_1, of the characteristic length d. With this formulation, the manufacturing constraint of AFP machines in terms of the curvature can be directly imposed by restricting the curvature value of each arc of the fiber path. Figure 2.8 schematizes a fiber path defined by circular arc variation in which each segment has the same radius, i.e., the same curvature.

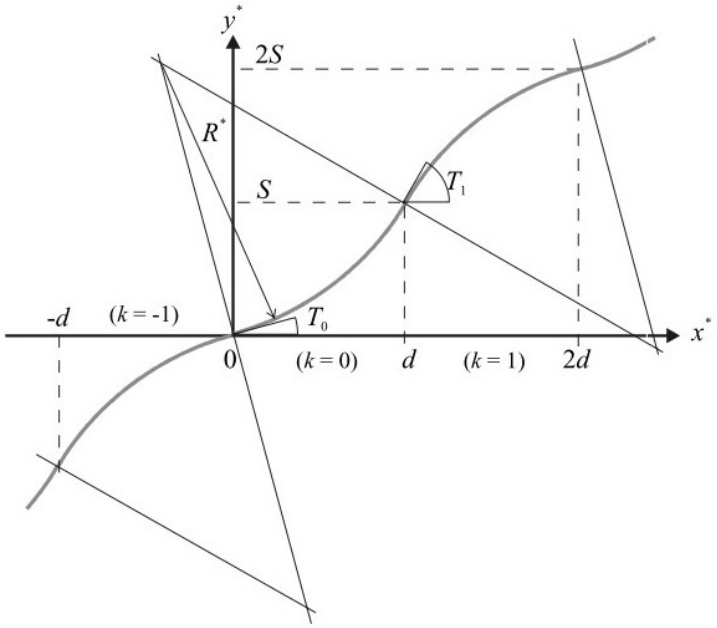

Figure 2.8: Fiber reference path defined by using circular arc variation, reproduced from [18]

Since the curvature is a signed quantity, previous to calculating its value, it was necessary to determine on which side of the arc it was located. The curvature, $\kappa(x)$, was then obtained by Equation 2.4.

$$\kappa(x) = \frac{(-1)^k (\sin T_1 - \sin T_0)}{d}, \quad k = \text{floor}\left[\frac{x}{d}\right] \tag{2.4}$$

The fiber angle was calculated with Equation 2.5. Note that it is a linear variation of the sine but not of the angle itself.

$$\sin\theta(x) = \left\{ \begin{matrix} \sin T_0 + (\sin T_1 - \sin T_0)\left(\frac{x}{d} - k\right), & k \quad \text{even} \\ \sin T_1 + (\sin T_0 - \sin T_1)\left(\frac{x}{d} - k\right), & k \quad \text{odd} \end{matrix} \right\}, \quad k = \text{floor}\left[\frac{x}{d}\right] \tag{2.5}$$

Other researches proposed alternative definitions for fiber angle variation along a single axis, including parabolically shaped fiber [19] or cubic polynomial fibers [13]. Honda et al. [20] introduced a cubic polynomial surface, $f(x, y)$, to represent curved fibers using Equation 2.6.

$$f(x, y) = c_{00} + c_{10}x + c_{01}y + c_{20}x^2 + c_{11}xy + c_{02}y^2 + c_{30}x^3 + c_{21}x^2y + c_{12}xy^2 + c_{03}y^3 \tag{2.6}$$

The fiber paths were the projections of the surface contour lines on the horizontal plane, as illustrated in Figure 2.9. Different surface shapes were described by varying the values of the c_{ij} polynomial coefficients.

The fiber angle θ was defined as the tangential direction of the contour lines and calculated with Equation 2.7.

$$\theta = \tan^{-1}\left(-\frac{\partial f/\partial x}{\partial f/\partial y}\right), \quad \text{when} \quad \partial f/\partial y = 0, \theta = 90^\circ \tag{2.7}$$

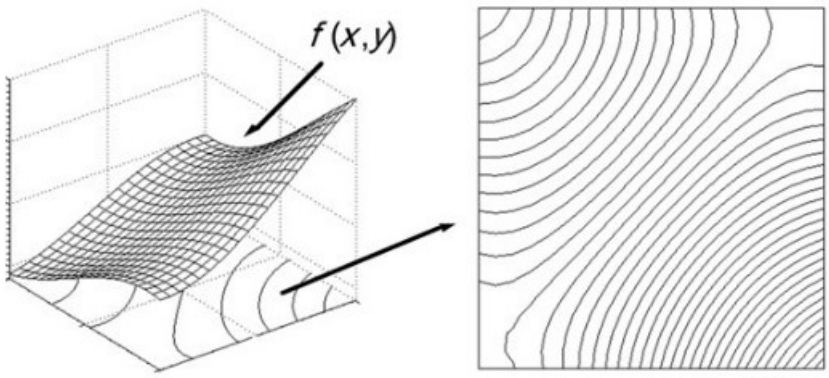

Figure 2.9: Cubic polynomial surface and its projection on the horizontal plane representing the fiber paths, reproduced from [20]

Authors [21, 22] presented a formulation for the nonlinear variation of the fiber angle along x and y directions. The definition of the fiber angle was based on Lobatto-Legendre polynomials in which the coefficients were the design variables. Wu et al. [23] proposed an alternative definition of the nonlinear distribution of fiber angles on an x-y plane using Lagrangian polynomials. A set of $M \times N$ reference points was selected in the plate domain. A double series function of $(M-1)$ by $(N-1)$ order polynomials was used to interpolate the nonlinear fiber angle distribution. The benefit of employing Lagrangian polynomials was that the coefficients of the polynomial were the fiber angle at the reference points. The nonlinear distribution of the fiber orientation , $\theta(x, y)$, was expressed as in Equation 2.8. Note that Equation 2.8 is simplified to the definition of linear variation if the fiber angle varies only in the x-direction and two reference points are used.

$$\theta(x, y) = \sum_{m=0}^{M-1} \sum_{n=0}^{N-1} T_{mn} \cdot \prod_{m \neq i} \left(\frac{x - x_i}{x_m - x_i}\right) \cdot \prod_{n \neq j} \left(\frac{y - y_i}{y_n - y_i}\right) \tag{2.8}$$

The reference points (x_m, y_n) could be randomly chosen. The selection would influence the optimization process. Generally, a uniform distribution of reference points was preferred, as illustrated in Figure 2.10.

Blom et al. [24] employed a streamline analogy for the construction of fiber paths. Each streamline represented the center line of the fiber course. The solution of the stream function and consequently, the location of the streamlines depended on the boundary conditions. Additional considerations on the physics of the problem were necessary. Later, Niu et al. [25] presented a method for path planning of variable stiffness laminates based on the potential flow field theory. The flow field function to characterize the fiber path contained a uniform linear flow field and several vortex fields. Two plies were considered: one ply was based on the stream function and the other on the potential function of the flow field. Since potential flow theory states that the cocurrent and equipotential lines passing through any point in the

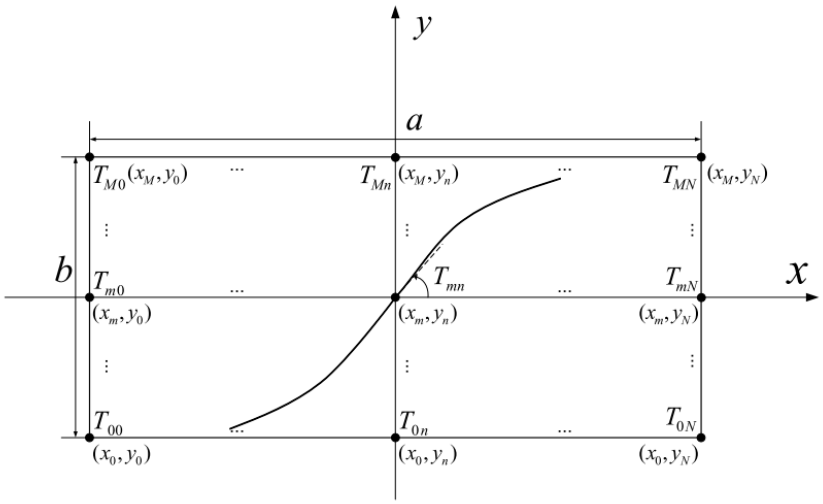

Figure 2.10: Nonlinear distribution of fiber angle using Lagrangian polynomials with $M \times N$ reference points, reproduced from [23]

flow field are orthogonal, the fiber paths of the laminate were orthogonal at each intersection, improving its properties.

Lamination parameters have also been employed to analyze variable stiffness composites (see, for instance, [7, 26–28]). Tsai et al. [29, 30] demonstrated that the ABD stiffness matrix can be fully defined by twelve lamination parameters (in the most general case) and the total laminate thickness. A symmetrical laminate requires only eight parameters and a symmetric balanced laminate four. Lamination parameters are trigonometric functions of the ply orientation. The functions are interrelated, so it is necessary to set a feasible region for the lamination parameters. The advantage of using the lamination parameters as design variables to define the local stiffness properties is that no explicit knowledge of the final stacking sequence is required. This allows to model any laminate with a minimum number of design variables, regardless of the number of layers. However, a postprocessing step is necessary to convert the optimal distribution of lamination parameters into a fiber angle distribution and then into a continuous fiber paths for manufacturing.

Considering that the objective of this thesis is to optimize the buckling behavior of composite panels with curvilinear fibers, a literature review has been carried out to identify the most commonly adopted approach. Linear variation of the fiber orientation offers a compact form to describe curvilinear fibers. Only two fiber angles are required, thus reducing the number of design variables. This parameterization is characterized by its simplicity, an extensive background in the analysis, design and manufacture of tow-steered composite materials and accurate results. It is therefore not surprising that the linear variation of fiber orientation has been widely used to analyze the buckling response of variable stiffness laminates [6, 14, 16, 31–34]. Consequently, the linear variation of the fiber angle is the approach utilized in this work.

2.4 Manufacturing-induced defects in VS laminates

Shifted method is used to manufacture variable-stiffness laminates. First, the AFP machine deposits the reference course. The distance between the course top and bottom boundaries changes along the horizontal since the fiber path is curvilinear. Figure 2.11 shows a reference curvilinear course in which the vertical distance, D, has the maximum value at the plate edges and the minimum at the center. W_{course} indicates the width of the course, which is constant here.

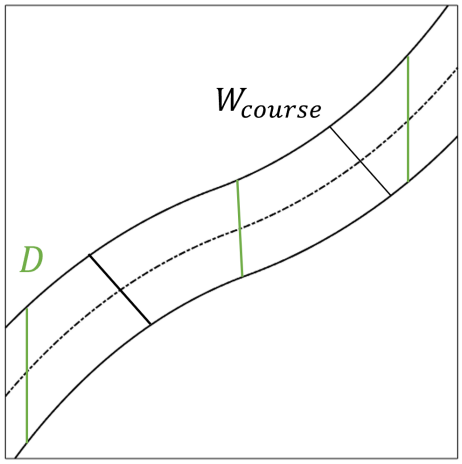

Figure 2.11: A curvilinear reference course

The AFP head then moves in the vertical direction with a constant value to lay down the next course. If the course width remains constant, large areas of overlap will occur between the two courses, as it can be seen in Figure 2.12a.

Therefore, the course width should vary continuously. This variation is actually discrete, as the AFP can only cut finite tow widths. Small areas of defects are then generated, as depicted in Figure 2.12b. Note that this can be achieved thanks to the AFP capability of cutting each tow independently.

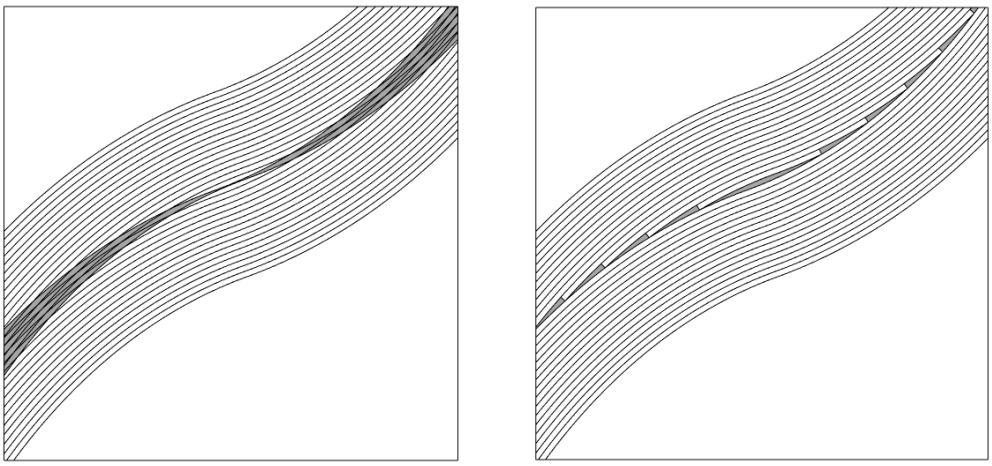

(a) Overlap area

(b) Gaps generated

Figure 2.12: Intersection of two curvilinear courses

Two techniques can be employed to cut the tows: one-sided tow drop or both-sided tow drop. The former implies that one course boundary, either the top or the bottom one, is cut and the other remains smooth. The latter modifies both course boundaries. One-sided tow drop strategy has been adopted as it results in fewer defects within the laminate [35].

Depending when a tow is cut, gaps or overlaps will be generated. A gap is a small wedge-shaped without fibers which, after curing, will be filled with resin. An overlap occurs when a small jagged patch of the composite tow lies on top of the adjacent composite course. If the AFP machine drops a tow as soon as one of its edges reaches the boundary of the adjoining course, a gap is formed. Conversely, if the tow is cut when the second edge touches the boundary course, an overlap is created. 0% coverage strategy means that all defects generated are gaps while 100% coverage involves that all defects are overlaps. It is also possible to have intermediate scenarios. The 100% coverage strategy has been shown to provide increased structural performance, however, the thickness of the laminate is not constant. Many aeronautical applications require a smooth surface to maintain aerodynamics, which will not be possible to manufacture with this technique [36]. Therefore, in this work, 0% coverage or complete gap strategy has been chosen.

The study of the influence of defects in variable-stiffness laminates has attracted the interest of many authors. A.Blom et al. [37] presented a method to localize gap areas within tow-steered layers. To implement these defect areas in a finite element model was first determined whether or not the element lied in the tow-drop area. Elements in the gap areas were modeled with resin material properties. Otherwise, regular composite material properties were assigned. Thus, the element size was small enough to capture the tow-drop area. Studies were carried out on the influence of gaps on the strength and stiffness of the laminate. It was concluded that a larger gap area led to lower strength and stiffness.

Fayazbakhsh et al. [36] introduced a novel method, called *defect layer method*, to characterize the influence of defects created in a variable stiffness laminate. The location of gaps or overlaps was first obtained using MATLAB subroutines. Another MATLAB subroutine received that information as an input as well as that of the mesh to calculate the area percentage of a defect in each element. This area percentage was used to modify the characteristics of the nondefect composite layer. If the defect produced was a gap, the area percentage scaled the elastic properties. If the defect was an overlap, the area percentage scaled the thickness. The modified properties were computed for each element of each layer of the laminate. Next, a finite element analysis was performed to calculate the in-plane stiffness and buckling load of composite panels with embedded defects. Results showed that gaps degraded the structural behaviour while overlaps improved it.

V.Mishra et al. [38] proposed a methodology to study the effect of gaps on the stiffness and buckling load of the laminates. The method was called *smearing method*. The novelty of their approach was the estimation of the gap volume fraction in a ply without explicitly modeling the defects, reducing computational cost. The gap volume fraction was calculated using the gradient of the fiber angle distribution. Results showed that the stiffness of the laminate was within 5% error comparing to the *defect layer method* and on the conservative side. However, the buckling load was over-predicted because the stress concentration was not captured as well as in the *defect layer method* .

T.Brooks and J.Martins [39] developed a mathematical formulation to provide a relationship between the gap/overlap propagation rate in a tow-steered composite ply with the divergence of a 2D vector field. The streamlines of the vector field represented the tow paths of the ply. The relationship between divergence and defect growth can be described locally taking a small control volume. If the divergence had a positive value, the density of tow paths entering the control volume was greater than the density of tow paths exiting. This implied a gap formation. Likewise, if the divergence had a negative value, the entering tow paths' density was less than the existing tow paths' density, indicating an overlap formation. In the case of zero divergence, tow paths were parallel and no defects were formed. The amount of gaps and overlaps created in the ply was implemented in the optimization framework by constraining the magnitude of the divergence. Although the gap/overlap rate of growth was restricted in the optimization process, its effect on the local stiffness of the panel was not considered.

Since the aim of this thesis is to optimize the buckling performance of variable-stiffness panels, the method for modeling laminates with embedded defects should provide reliable results as well as computational time efficiency. The approach performed by Fayazbakhsh et al. [36] is the one considered to meet all the above criteria. The element size is smaller than that of A.Blom et al. [37], but sufficient to obtain more accurate results than V.Mishra et al. [38] in the buckling load. The influence of defects in the laminate is taken into account in the finite element analysis and is not limited to the optimization process as T.Brooks and J.Martins [39] do.

2.5 Curvilinearly Grid-Stiffened panels

Curvilinearly grid-stiffened panels provide a larger design space than the traditional orthogrids or isogrids panels with straight stiffeners. Tailoring the stiffener location and shape can lead to substantial improvements in the buckling performance.

Different approaches have been reported for modeling curvilinearly grid-stiffened panels. Several authors, including [31, 33, 40, 41], used the linear variation of the angle to define the stiffener path. The definition was the same as that formulated by Gürdal [14] to describe the curvilinear fibers in variable stiffness panels. The stiffener path was determined by the orientation values at the center and sides of the panel. The orientation angle was chosen to vary along the x-direction. The stiffener reference path was shifted vertically and mirrored about the y-axis to construct a grid-stiffened panel. The stiffness distribution was, therefore, influenced by the variation of the angle on the x-axis and the distance between the stiffeners on the y-axis. Generally, equidistant stiffeners were employed, although non-uniformly distributed stiffeners were also proposed to widen the design space. Figure 2.13 illustrates an example of a grid-stiffened panel defined by the linear variation of the angle.

Kapania and his co-authors' researches have employed NURBS or third-order B-Splines to describe the reference path of curvilinear stiffeners (see for instance [34, 42, 43]). In most of the works, three points were chosen to shape the curve to not further increase the number of design variables. The start and end points were assumed to be on the panel boundary. These points influenced the stiffener placement. A perimeter parameter, which varied from 0 to 1, was used instead of the physical coordinates to reduce

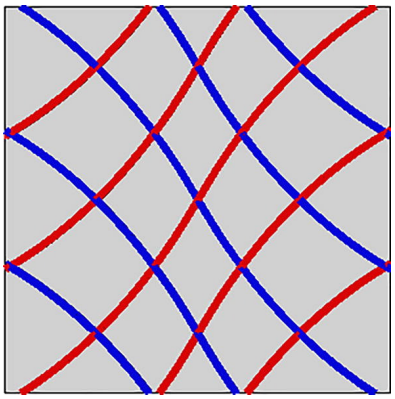

Figure 2.13: A curvilinearly grid-stiffened panel with the stiffener path defined by the linear variation of the angle, reproduced from [31]

the number of design variables. The third point was located in the perpendicular direction of the straight line joining the start and end point. A curvature parameter was defined to determine the position of the control point and, thus, the stiffener shape. Three design variables were needed to define one curvilinear stiffener. A scheme of this geometry parametrization for the stiffener path is shown in Figure 2.14.

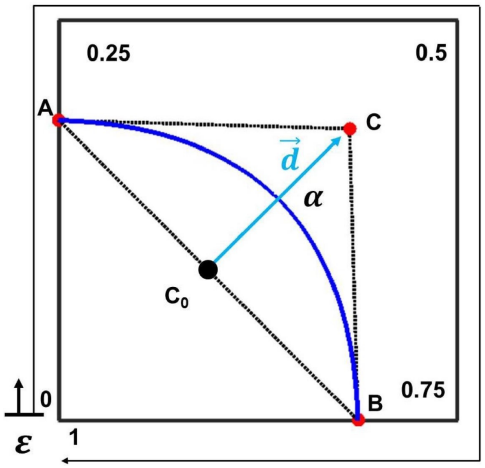

Figure 2.14: Geometry parameterization for the stiffener path using NURBS, reproduced from [42]

NURBS curves have the convex hull property which ensures that the curve lies within the region of the control points. However, since NURBS only pass through the start and end points and not through the control points, an additional step is necessary to check if the stiffener is inside the panel. This also means that it is difficult to set the upper and lower bounds of the curvature parameter for the optimization problem.

Other authors such as [44, 45] parametrized the stiffener geometry using Bézier curves. Three control points were employed to define the curvilinear path. The start and end points were fixed at the panel edges, which required two design variables to define their location. The control point was defined by its x-y coordinates, setting the two remaining design variables to define the stiffener shape. Bézier curves, like NURBS, do not pass through all control points. Hence, additional calculations as well as extra attention to choose the appropriate bounds for the design variables were necessary to ensure that the

stiffener lied within the panel boundary.

In the present thesis, the stiffeners are modeled using the spline tool in Abaqus. Therefore, the approach adopted by [34, 42–45] which employs NURBS or Bézier curves to model the stiffener, is easier to implement than the approach taken by [31, 33, 40, 41] which describes the stiffener path using the analytical formula of linear angle variation. In addition, the stiffener paths in the latter approach are slightly biased toward the horizontal direction over the vertical direction because the angle variation is defined along the x-direction. In contrast, stiffeners modeled by the spline parameterization can flexibly stretch from the left to right edges or from the top to bottom edges of the panel [34]. The geometry parameterization with NURBS curves is modified as Abaqus interpolates the points using a natural cubic spline. This spline passes through all control points, which facilitates the stiffener being inside the panel and the choice of appropriate bounds for the design variables. Section 3.4.1 explains in detail the geometric parametrization utilised in this thesis to model the stiffener layout.

2.6 Linear Buckling Analysis

Buckling is a stability behaviour to which slender structural components (e.g., long columns or thin plates) under loads are susceptible. When a structure subjected to a gradually increasing load reaches a critical level, it suddenly changes shape and is said to have buckled. The buckling critical load marks the limits between possible configurations for the structure. The transition from a reference configuration (pre-buckling) to another different configuration (post-buckling) is at the bifurcation point. The latter configuration usually has a much lower stiffness leading to collapse, but some structures can continue to support loads even after buckling in a stable manner. Pre-buckling behaviour is commonly linearized, whereas post-buckling presents non-linearlities. Figure 2.15 schematizes the force-displacement curve that represents the buckling behaviour of the structures.

The buckling analysis of VS laminates reinforced with curvilinear stiffeners presents a high level of complexity due to the inherent geometry of the panel. The Finite Element approach can provide meaningful and accurate results regardless of the complexities in geometry, material properties, boundary conditions and loading [46]. Hence, finite-element procedures have been widely adopted to study the buckling response of curvilinear fiber composite panels (see for instance [16, 31, 34, 42]).

In the present thesis, the linear buckling analysis is performed by the FEA commercial software Abaqus. Abaqus can estimate the critical buckling load by linearized eigenvalue extraction. This method is particularly useful for stiff structures. Stiff structures are characterized by carrying their design loads primarily by axial or membrane action, rather than by bending action. Their response usually involves very little deformation prior to buckling (almost linear pre-buckling response). When the critical load is reached, the structure bends suddenly and exhibits a much lower stiffness (post-buckling state) [47].

In the eigenvalue buckling problem, the loads for which the stiffness matrix of the model becomes singular are sought, so that the problem has nontrivial solutions. The buckling loads are calculated relative to the base state of the structure. The base state can include preloads ("dead" loads), P_N. The preloads are often zero in classical eigenvalue buckling problems. In the present study, the eigenvalue

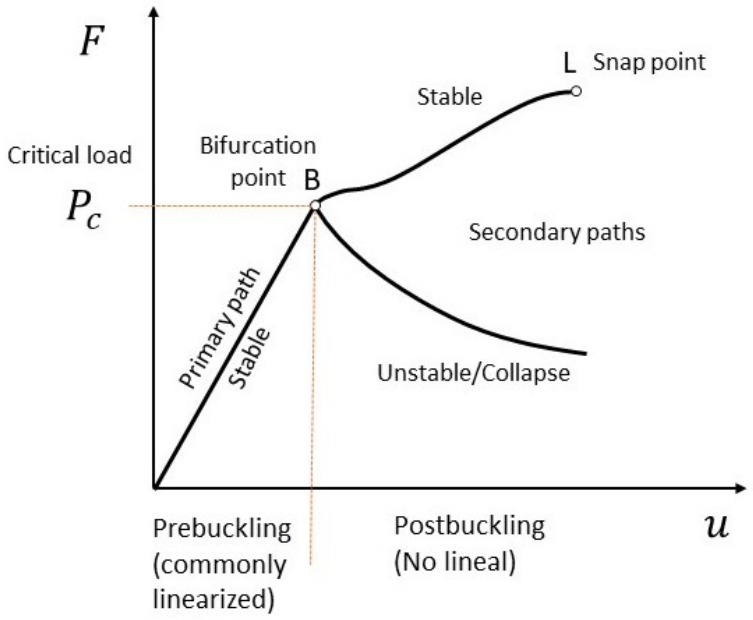

Figure 2.15: Load-displacement curve of buckling behaviour

buckling procedure is the first step in the analysis, thus preloads are not included.

The eigenvalue buckling problem requires first to define an incremental loading pattern, Q_N. The Q_N loading will be scaled by the load multipliers (eigenvalues), so its magnitude is not relevant. A static perturbation analysis is then performed to determine the incremental stresses, $\Delta\sigma$, due to Q_N. The incremental stresses are utilized to build the stiffness matrix K_Δ^{MN} due to Q_N. Next, Abaqus forms the stiffness matrix K_0^{MN} corresponding to the base state geometry. The eigenvalue problem expressed in Equation 2.9 can now be solved.

$$\left(K_0^{MN} + \lambda_i K_\Delta^{MN}\right) v_i^M = 0 \tag{2.9}$$

where λ_i are the eigenvalues and v_i^M the associated eigenvectors. M and N indicate the degrees of freedom of the whole model; and i indicates the ith buckling mode.

In the present analysis, only the lowest (first) eigenvalue, $\lambda_1 = \lambda$, is requested, which is normally the one of the most interest. The solver selected to extract the eigenvalue is the Subspace iteration method as it is particularly suited for the calculation of few eigenmodes (less than 20) of large finite element systems.

The critical buckling load is finally obtained by multiplying λ to the applied loads Q_N. The buckling mode shape, v^M, although it is a normalized vector and does not represent the actual magnitude of deformation, can be useful to represent it.

2.7 Buckling Optimization of Composite Panels with Curvilinear Fibers

The optimization of the buckling response of tow steered panels and/or curvilinearly grid-stiffened panels has been the subject of attention by several authors. Designing the optimum stacking sequence or the optimum stiffener layout and size to maximize the buckling performance often results in many local optima [43, 48]. In addition, the sensitivity information of the problem is not always easy to compute. Hence, global optimization techniques are required.

Genetic Algorithm (GA) is the most widely adopted for the optimization of this type of panels due to their robustness in finding a global optimum. Some works that are worthy of note are the following. Wu et al. [23] performed an optimization for the maximum buckling load of Variable Angle Tow plates. The VAT plates were described by a nonlinear variation of the fiber orientation in which the fiber angles at the reference points constituted the design variables. The design problem was non-convex and a Genetic Algorithm was selected as the solver for the optimization. Tatting et al. [16] developed an in-house software based on Genetic Algorithm to maximize the buckling load of tow-steered laminates. The laminates were characterized using the linear variation of fiber angle, so the parameters of the curvilinear fiber path within each ply were chosen as design variables.

Liu et al. [40] maximized the buckling load of an aluminium curvilinearly grid-stiffened panel. The stiffener layout was defined by a piecewise linear variation of the angle, taken from the parametrization of the curvilinear composite fibers. In their work, Multi Island Genetic Algorithm (MIGA) was employed to optimize the grid panel. MIGA differs from standard Genetic Algorithms in that the entire population is divided into several subpopulations, called islands. In each island, the GA standard conducts the optimization. Every few generations, individuals from each island will be randomly chosen to migrate to other islands to enhance the diversity of individuals.

Hao et al. [49] proposed a bi-level optimization framework for improving the buckling load of variable stiffness panels with cut-outs. In their study, the optimization was split into two small-set problems. In the first level, the optimization was performed for a constant stiffness panel, i.e., with straight fibers. The result was a quasi-optimum design that was used as the basis for the second level. In the second level, the fiber paths were curvilinear and defined with a flow field function. Curvature constraint was imposed here. MIGA was utilized to find the fiber angles for maximizing the buckling load at both optimization levels.

Other stochastic algorithm that has been used as an optimizer is Simulated Annealing (SA). The name and inspiration for SA comes from the process of annealing metals. The technique consists of heating the material and then slowly lowering the temperature to reduce the defects, minimizing the energy of the system. In general, SA algorithm adopts an iterative movement according to the variable temperature parameter, which imitates the annealing transaction of metals [50]. For instance, A.Ahmad [51] used global Simulated-Annealing optimizer to determine the optimal fiber paths within each ply of the laminate for maximum buckling load.

Particle Swarm Optimization (PSO) has been another alternative algorithm for the optimization of the design of variable stiffness panels. PSO is a population-based optimization technique that is inspired by the social behaviour of large groups in nature, such as such as bee swarms or fish schools. The system is initialized with a population of particles (potential solutions) moving through the search space. The new location of each particle is determined by a velocity term, which reflects the attraction of both its best local position found and the best global positions encountered by other particles. Singh et al. [34] presented a PSO parallel processing-based optimization framework for designing tow-steered composite laminates with metallic curvilinear stiffeners. The objective was to find the optimum laminate stacking sequence and the optimum stiffener placement and shape for maximizing the buckling load. A structural mass constraint was also implemented. In their work, Penalty Method was used to convert the constrained optimization problem into an unconstrained optimization problem.

Most design problems of variable stiffness panels to optimize buckling are parameterized by fiber orientation angles, which often results in nonconvex problems and difficult to obtain sensitivity information, and so stochastic methods are required. Another approach, mentioned in Section 2.3, to characterize VS panels is using the lamination parameters. Lamination parameters allow the local stiffness properties to be defined using a finite set of convex and continuous design variables, well suited to gradient-based algorithms as reported by IJsselmuiden et al. [7], who performed a buckling load optimization for VS panels described with these parameters. Wu et al. [52] also used lamination parameters to conduct a buckling optimization of VAT plates. In their work, a two-level optimization framework was proposed. In the first step, a gradient-based algorithm called the Globally Convergent Method of Moving Asymptotes (GCMMA) was adopted to find the optimal lamination parameters for the maximum buckling load. At the second step, the fiber orientation angle distributions were retrieved from the lamination parameters via a genetic algorithm. The use of lamination parameters guided the design process to determine the best possible laminate configuration in the second step.

Another work within gradient-based optimization that is worth highlighting is that carried out by Wang et al. [33]. In their study, a curvilinearly grid-stiffened panel was optimized to improve the structural buckling resistance. The skin fibers were straight and the curvilinear stiffeners were represented by the linear variation of the angle. The stiffeners were not explicitly modeled in the finite element calculations with the aim of reducing the computational cost. Instead, an equivalent unstiffened model with a fixed mesh was employed to calculate the buckling load. The equivalent material properties were obtained by homogenization techniques and changed with the curvilinear path of the stiffener in the optimization. Taking advantage of the fixed mesh, it was possible to use a gradient-based optimization algorithm, specifically the Method of Moving Asymptotes (MMA). The sensitivities of the structural responses were calculated by the finite difference method.

In the present thesis, the Genetic Algorithm (GA) is selected to perform the optimization. As mentioned above, composite panels with curvilinear fibers and grid stiffeners may have local minima. In addition, the sensitivity information is not accessible in the present optimization framework. The above stated impedes the application of gradient-based algorithms and global search methods are required even though they are not as computationally efficient. The parameterization chosen for curvilinear skin fibers

and stiffeners involves a low number of design variables. Therefore, direct search methods are affordable in terms of computational time. Among stochastic methods, genetic algorithm is the most popular due to its robustness and ease of implementation. Section 4.3 explains in more detail the GA and its operators.

Chapter 3

Numerical Modeling

This chapter describes how composite panels with curvilinear fibers and grid stiffeners have been modeled. Section 3.1 outlines the workflow of the tasks performed in the Finite Element Module. The modeling of the variable stiffness laminates and the manufacturing-induced gaps are described in Sections 3.2 and 3.3, respectively. The modeling of curvilinear stiffeners is given in Section 3.4. Finally, the mesh convergence study is presented in Section 3.5.

3.1 FE Module

In the present thesis, variable angle tow laminates are modeled, i.e., laminates with curved fibers. This is done by assigning a local stacking sequence to each element of the mesh. Thousands of elements may be employed which makes the process infeasible to set up "manually". In addition, during the optimization process, the design variables are changed and so the geometry of the panel. A simulation of the panel model is performed as many times as the parameters vary. Hence, an automated process to create the FE model, run the FE analysis, and extract the results is essential for optimization.

The Abaqus Scripting Interface can effectively automate the workflow. Abaqus scripting interface scripts are Python scripts that enable to create and modify a model, submit an analysis and read the results in a compact form [47]. The model geometry, material properties, loads, boundary conditions and more can be easily modified by scripting.

A Python script has been developed that Abaqus runs to generate the FE model, conduct the analysis and process the results, and that MATLAB can interact with. Figure 3.1 shows the workflow of the tasks performed by the FE module. Hereafter, a brief explanation of the sequential stages to build the FE model and extract the FE analysis output is presented.

First, the input data are provided. The inputs are the plate dimensions, the stiffener thickness and height, the material properties of the composite, the laminate definition (number of layers and their thickness), and the value of the design variables that come from the optimization module.

The sketches of the plate and stiffeners are generated with the input geometry. The materials and if necessary, other properties are next created. After the plate and stiffeners are assembled. The interaction

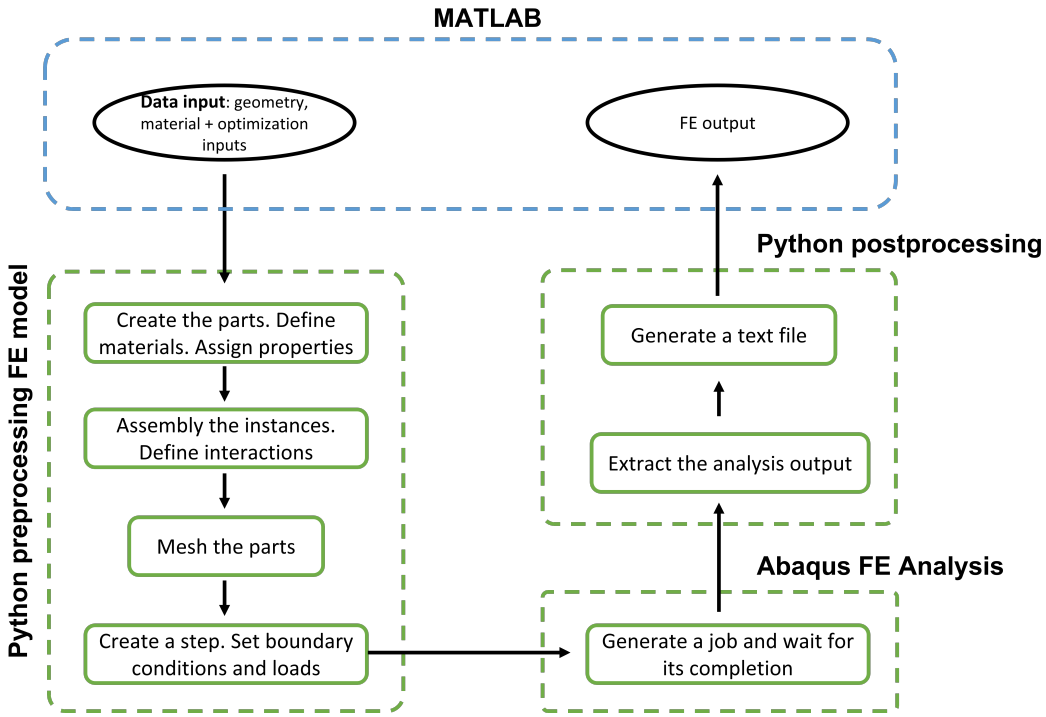

Figure 3.1: Workflow of the FE module

between the two instances is defined with a tie constraint. Plate and stiffeners are then meshed separately.

The step stage specifies the type of analysis. In this case, a linear buckling analysis is selected. The boundary conditions and loads are then applied to the plate. The stages indicated so far correspond to the creation of the FE model.

Next, a job is created with the model and Abaqus performs the FE analysis. The results from the linear buckling analysis are contained in the output database (.odb) file. The requested output is the first eigenvalue (the buckling factor). The Python file is scripted to read the odb file, extract the buckling factor and write it to a text file. Here, the Abaqus module ends and the text file is read by MATLAB. This is necessary since the buckling factor will be used in the evaluation of the objective function of the optimization process, explained in Chapter 4.

3.2 Modeling of Variable Stiffness Laminate

The VS laminates considered in the present thesis are formed by plies in which the fiber orientation varies along the x-direction. As discussed in Section 2.3, the linear variation of the fiber angle is the adopted approach. Henceforward, the origin of the coordinate system is fixed at the center of the panel. The characteristic length is considered to be half the width of the panel and designated by a. The two fiber orientation angles T_0 and T_1 are the major design variables, while ϕ is usually stipulated as 0 or 90 degrees for a rectangular panel [16]. The ϕ angle is set to 0 so the superscript $'$ is removed from the formulation. After these statements, the linear variation of the fiber angle is described by Equation 3.1.

Figure 3.2 schematized the terms of Equation 3.1. The reference fiber path is given in Equation 3.2.

$$\theta(x) = (T_1 - T_0)\,\frac{|x|}{a} + T_0 \tag{3.1}$$

$$y = \begin{cases} \frac{a}{T_1 - T_0}\left\{-ln\left[cosT_0\right] + ln\left[cos\left(T_0 + (T_0 - T_1)\,\frac{x}{a}\right)\right]\right\}, & \text{for } -a \leq x \leq 0 \\ \frac{a}{T_0 - T_1}\left\{-ln\left[cosT_0\right] + ln\left[cos\left(T_0 + (T_1 - T_0)\,\frac{x}{a}\right)\right]\right\}, & \text{for } 0 \leq x \leq a \end{cases} \tag{3.2}$$

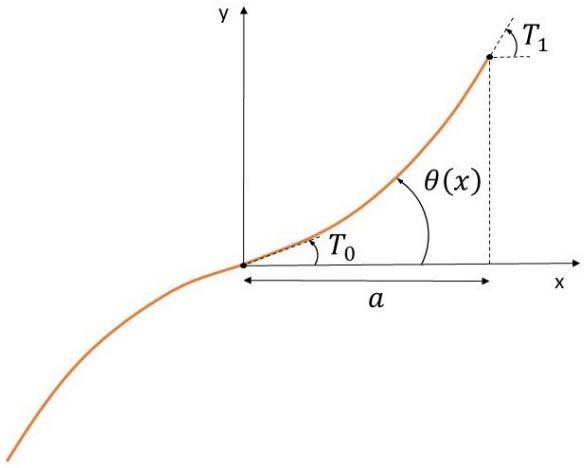

Figure 3.2: Reference path defined by the the linear variation of the fiber angle

The reference path is shifted vertically to create the remaining paths. Thus, the change in the fiber angle occurs only along the x-axis. To account for the variation of the fiber angle, the ply can be discretized into small parts. In this case, the plate is the part to be featured with the tow steered laminate. Therefore, the plate is meshed with a suitable number of elements. Abaqus S4R shell element is used.

S4R element is defined as a 4-node, quadrilateral, stress-displacement shell element with reduced integration and a large-strain formulation. These elements allow transverse shear deformation. It is included in the group of general-purpose shell elements and can model both thin and thick shells. It provides robust and accurate solutions to most applications [47].

Once the plate is meshed, the aim is to calculate the fiber angle within each element. For this purpose, a sequence of operations is carried out as outlined in Figure 3.3. The element connectivity is first requested and the node coordinates of the element are obtained. Using the nodal coordinates, the centroid of each element is calculated. At the centroid, the fiber angle is computed by using Equation 3.1. Since Equation 3.1 depends on T_0 and T_1, the variables that characterize a ply, a fiber angle is obtained for each different ply in the laminate. Note that each fiber orientation angle obtained is constant within an element.

The local stacking sequence is then built and assigned to the element. As a result, there are as many composite sections as there are elements. In this way, a variable stiffness composite panel with an arbitrary ply configuration can be modeled.

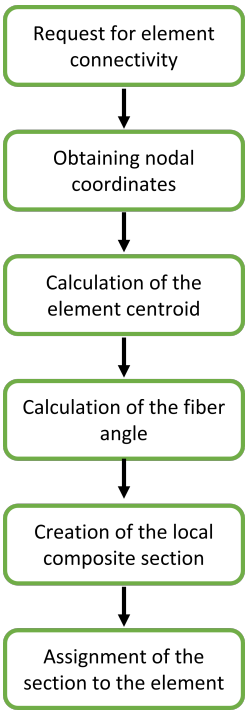

Figure 3.3: Steps for assigning the local fiber angle to the mesh element

Figure 3.4a illustrates the fiber paths for a $\langle 20, 50 \rangle$ ply. Figure 3.4b shows how the fiber paths of the ply are discretized in the Finite Element Model (FEM). The straight lines represent the fiber angle computed at the centroid of each element.

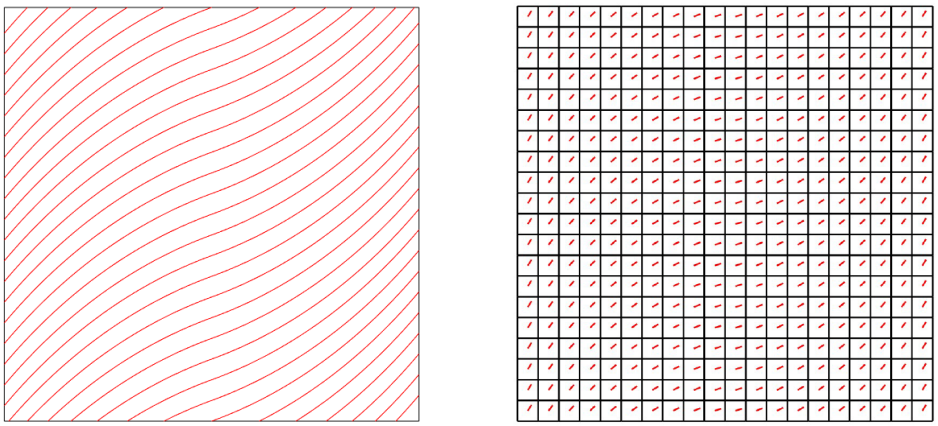

(a) Continuous fiber paths (b) Fiber angle within element

Figure 3.4: Modeling of tow steered $\langle 20, 50 \rangle$ ply

3.2.1 Verification study of VS laminates

The case study presented by Waldhart [6] is employed here to validate the present Python script for modeling VS composite laminates. In Waldhart's work, the buckling response of constant and variable stiffness laminates was investigated. The Ritz method was used to calculate the critical buckling load.

A square panel of dimensions 20 in × 20 in subjected to uniaxial compression in x-direction was studied. The transverse edges were free to expand. All edges were simply supported, i.e, the out-of-plane displacement was restrained. The in-plane displacement in the y-direction of the lower left corner was set to zero, $v(-10,-10)=0$, to avoid the vertical translation of the model. Figure 3.5 shows the loading and boundary conditions applied to the panel.

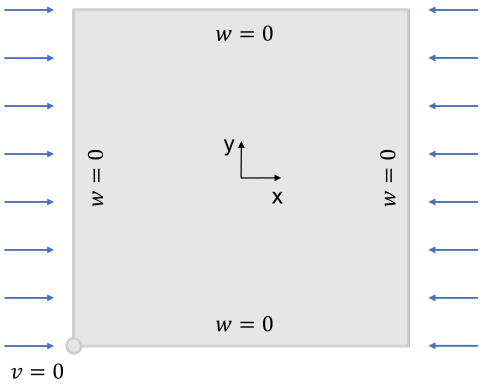

Figure 3.5: Load and boundary conditions applied to test case for VS modeling

The laminates consisted of 36 plies with a thickness of $t = 0.0055$ in. The material properties were as follows: $E_1 = 21.0$ Msi, $E_2 = 1.40$ Msi, $G_{12} = 0.80$ Msi and $\nu_{12} = 0.34$.

Constant and variable stiffness laminates were analyzed. For the modeling of CS laminates, the fiber angles were made equal, $T_0 = T_1$. In the VS laminate, the fiber orientation changed along the x-direction and, thus, Equation 3.1 and the methodology described above were employed.

The critical buckling loads reported by Waldhart using the Ritz method and those obtained by the present FE model for CS and VS laminates are given in Table 3.1. The percent error in all cases is less than 1%. Therefore, the present code to model variable stiffness composite laminates is verified.

Table 3.1: Comparison between the buckling loads of CS and VS laminates reported by Waldhart and those obtained by the present model

Buckling Load $[lbs/in]$			
	$[0]_{18s}$	$[90]_{18s}$	$[0 \pm \langle 15, 60 \rangle]_{9s}$
Waldhart [6]	-426.7	-240.9	-692.2
Present Model	-425.0	-239.6	-690.4
Percent error [%]	0.4	0.5	0.3

3.3 Modeling of Manufacturing-induced Gaps

When manufacturing a VS laminate by the AFP machine, defects are generated in the laminate. These manufacturing-induced defects should be accounted for at the design phase. As stated in Section 2.4, Fayazbakhsh et al. [36] used a constant curvature path to define the reference fiber path. This path

differs from the definition employed in this thesis: the linear variation of the fiber angle. The approach introduced by Fayazbakhsh et al. has been modified to model the induced gaps when the definition of linear variation of the fiber angle is considered. References [36] and [53] are used as a basis for developing one's own code. The process followed to model laminates with embedded gaps is detailed below.

The code has two modules. The first module consists of MATLAB functions to obtain the location of the gaps in the laminate. This is necessary to compute the gap area within each element of the mesh. The material properties are then modified according to the gap area for each layer and each element. This information is passed to the second module. The second module is a Python script to build the FEM of the composite laminate.

As mentioned above, linear variation of the fiber orientation is used to generate the geometry of a tow-steered layer. Equation 3.1 gives the variation of the fiber angle along x-direction and Equation 3.2, the corresponding reference path. The tow width, t_w, and the number of tows, n_t, are then selected to construct the reference course. When the AFP machine deposits the course, its head is perpendicular to the local fiber angle. This means that each point along the AFP head has the same fiber orientation as the one corresponding to the reference path. Thus, the points that form each tow of the course can be calculated by Equation 3.3.

$$\begin{aligned} x &= x^* - i \cdot t_w sin\theta^* \\ y &= y^* + i \cdot t_w cos\theta^* \end{aligned} \tag{3.3}$$

where the superscript $*$ is used to denote the points in the reference path and i is an index which range decreases by 1 from $n_t/2$ to $-n_t/2$. Figure 3.6 shows the reference course. The reference path ($i = 0$) and a point belonging to it (x^*, y^*) are colored in red. The blue lines represent the edges of the remaining tows and the blue dots the corresponding points. The point on the top course boundary ($i = n_t/2$) that is on the same perpendicular as the point of the reference path is indicated. Both points have the same fiber local orientation, θ^*.

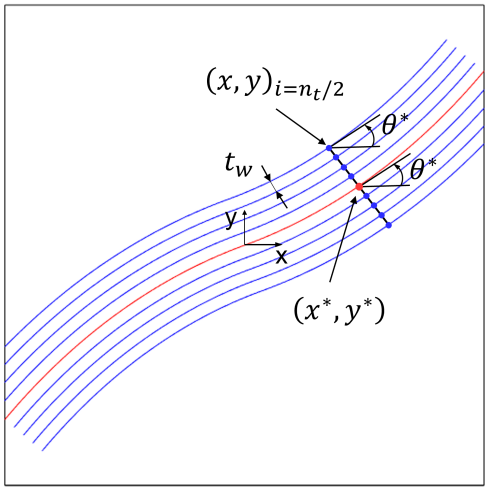

Figure 3.6: Reference course of a tow steered ply

It should be noted that the reference path must be extrapolated further from the plate edges, so that the reference course completely covers the plate. Figure 3.7 shows the reference course in which the part

coloured in green corresponds to the points extrapolated from the reference path.

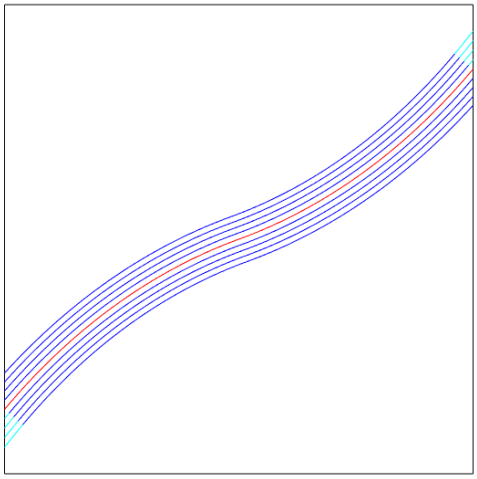

Figure 3.7: Extrapolated reference course

The next step is to compute the shift distance, i.e., the minimum vertical distance between the reference course top and bottom boundaries. The reference trajectory is antisymmetric, so it is sufficient to calculate the vertical distance for positive values. The shift distance is calculated with Equation 3.4. The extrapolated values of the reference path are not considered.

$$d_s = min\left(\frac{n_t t_w}{cos\theta^*}\right) \tag{3.4}$$

The AFP machine will move vertically with the shift distance to lay down the next course (the shifted course). The points of the shifted course are calculated by Equation 3.5.

$$\begin{aligned} x_s &= x^* - i \cdot t_w sin\theta^* \\ y_s &= y^* + i \cdot t_w cos\theta^* + d_s \end{aligned} \tag{3.5}$$

The intersections between the outer top edge of the reference course and the tows of the shifted course are next located. Figure 3.8 shows the intersection points between the shifted course and the reference course. A perpendicular line is then drawn from each intersection point up to the next corresponding tow edge. This reproduces the cut of a tow made by the AFP machine.

A polygon defined by 2D vertices is employed to generate the geometry of the gaps. The vertices to be linked are the intersection point , its corresponding perpendicular point and the points belonging to the tow edge of the shifted course and the reference outer edge. Hence, the gaps produced by the intersection of the reference course and the shifted course can be stored in an array. Figure 3.9a shows the gaps generated due to that intersection.

The reference course will intersect the top outer edge of the course shifted in the negative y-direction. Thus, the distance between two sets of gaps is the shift distance. The gap set is translated vertically to generate the defects across the entire ply. The gaps across the entire ply are shown in Figure 3.9b

It is important to highlight that depending on the values of the fiber angle at the center, T_0, and at the edge, T_1, of the plate, the way gaps are generated is slightly different. This is due to the position at

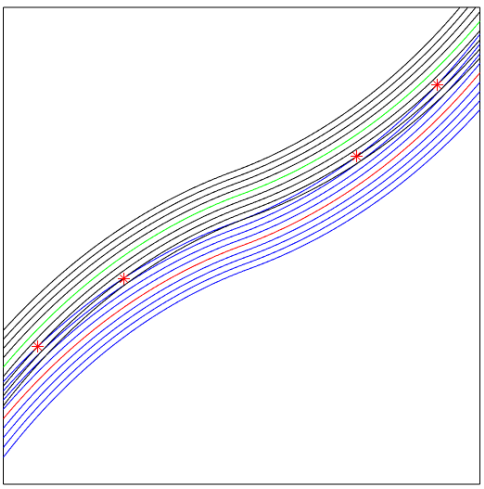

Figure 3.8: Intersection points between the shifted course and the reference course

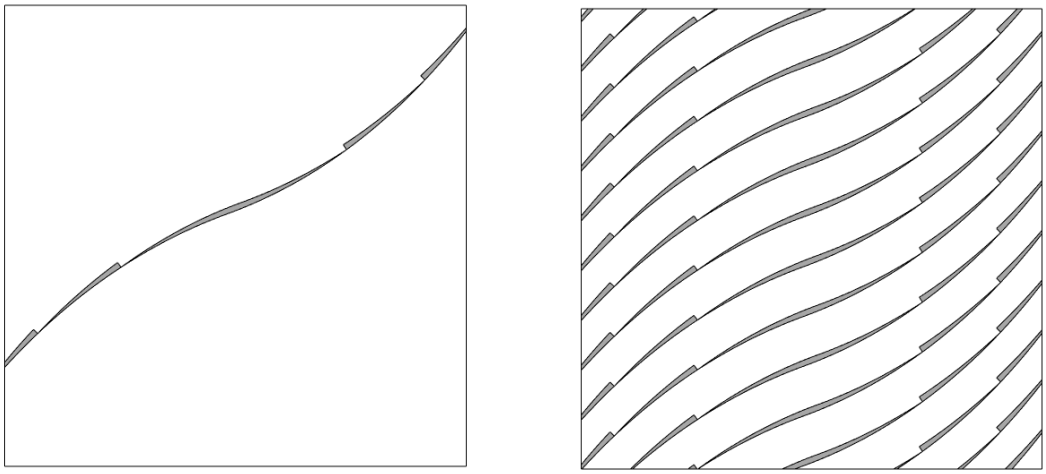

(a) Gaps due to one intersection

(b) Gaps generated across the entire layer

Figure 3.9: Gaps distribution

which the shift distance is obtained. In that position, the bottom tow of the shifted course is tangent to the reference course. In the others positions, intersections could occur.

Although the shift distance is calculated indistinctly from the values of T_0 and T_1, three different cases have been observed. When $T_0 > T_1$ and they have the same sign, the shift distance is obtained at the edge of the plate. If $T_0 < T_1$ and both are either positive or negative values, the shift distance is at the center. In the last case, when T_0 and T_1 have opposite signs, regardless of whether one is larger or smaller, the shift distance is somewhere between the center and the edge of the plate. Consequently, the way gaps are modeled varies depending on T_0 and T_1. Figure 3.10 indicates how the shifted course overlaps the reference course for the three cases mentioned above. The red asterisk marks the position where the shift distance has been computed. It also shows the gaps generated after the intersection of both courses. The variation in the shape of the gaps can be seen for the different cases.

The gap formation depends, in addition to the fiber angles T_0 and T_1, on the manufacturing parameters: number of tows, n_t, and the tow width, t_w. For example, to manufacture the $\langle 60, 30 \rangle$ ply a course of

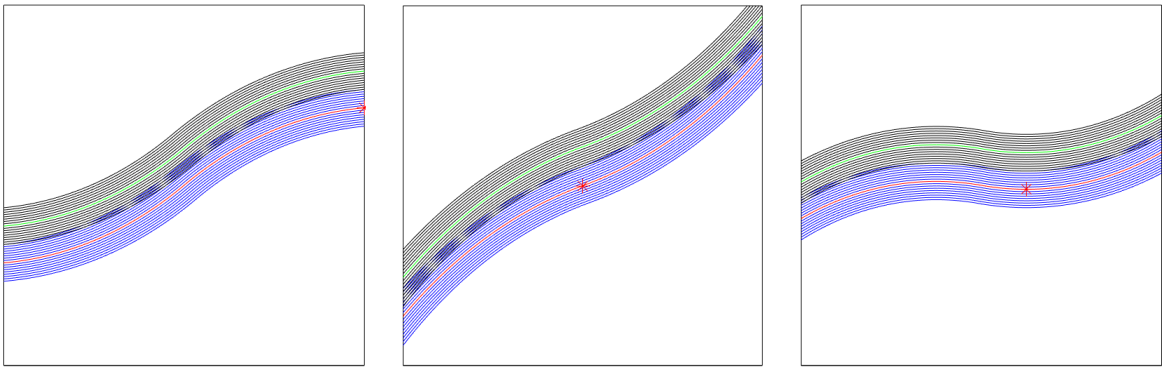

(a) Courses of $\langle 40, 5 \rangle$ ply (b) Courses $\langle 20, 50 \rangle$ ply (c) Courses of $\langle -10, 30 \rangle$ ply

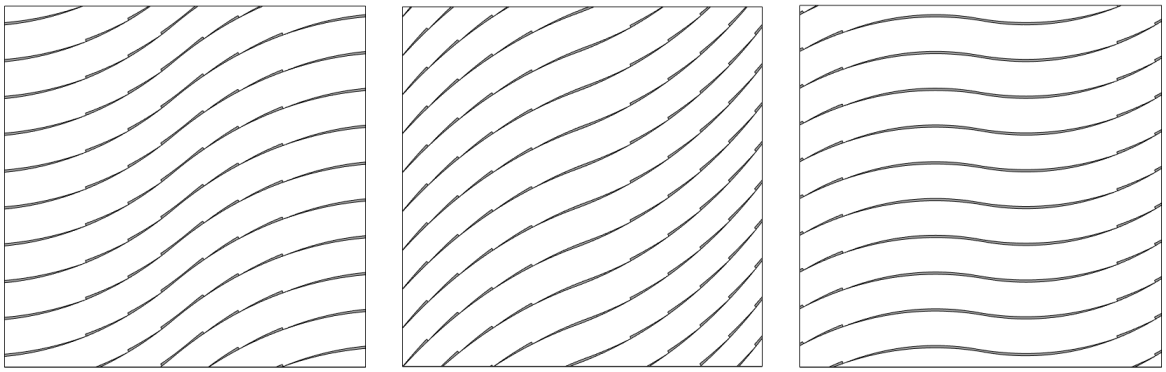

(d) Gaps of $\langle 40, 5 \rangle$ ply (e) Gaps of $\langle 20, 50 \rangle$ ply (f) Gaps of $\langle -10, 30 \rangle$ ply

Figure 3.10: Intersection of two coursed and gap distribution based on the conditions of T_0 and T_1. $T_0 > T_1$ & same sign (a,d); $T_0 < T_1$ & same sign (b,e); T_0 T_1 opposite sign (e,f).

1.016×10^{-1} m width is employed. This course can be formed by 8 tows with a width of 12.7×10^{-3} m, 16 tows of 6.35×10^{-3} m and 32 tows with a width of 3.175×10^{-3} m. One can observe in Figure 3.11 that the amount of gaps generated in the ply of the first configuration is larger than the third one. In fact, the area of gaps with respect to the total ply area is 8.5% for the 8 tows - 12.7×10^{-3} m width configuration, 4.1% for the 16 tows - 6.35×10^{-3} m width configuration and 2% for 32 tows - 3.175×10^{-3} m width configuration. Therefore, a larger number of tows with a smaller width results in a lower gap area and the laminate properties will be less affected.

The situation when $T_0 = T_1$ corresponds to straight fiber laminates. It is considered as an ideal layer without gaps. Hence, the calculation of the gap area is avoided and the value is set to zero.

Once the gap distribution of the ply has been generated, the next step is to intersect that gap distribution with the skin mesh, as shown in Figure 3.12. This step is necessary to compute the value of gap area for each element of the mesh. The gap area fraction, defined as the value of the gap area in each element divided by the area of the mesh element, is used to modify the material properties. The gaps are resin rich areas, so a higher value of gap fraction means impoverishing the material properties of that element.

Fayazbakhsh et al.[36] presented a graph in which the elastic properties E_1, E_2 and G_{12} were plotted versus the gap area in percentage. It can be shown that the polynomial functions depicted in the graph correspond to the 'modified' rule of mixtures. The conventional rule of mixture estimates the composite

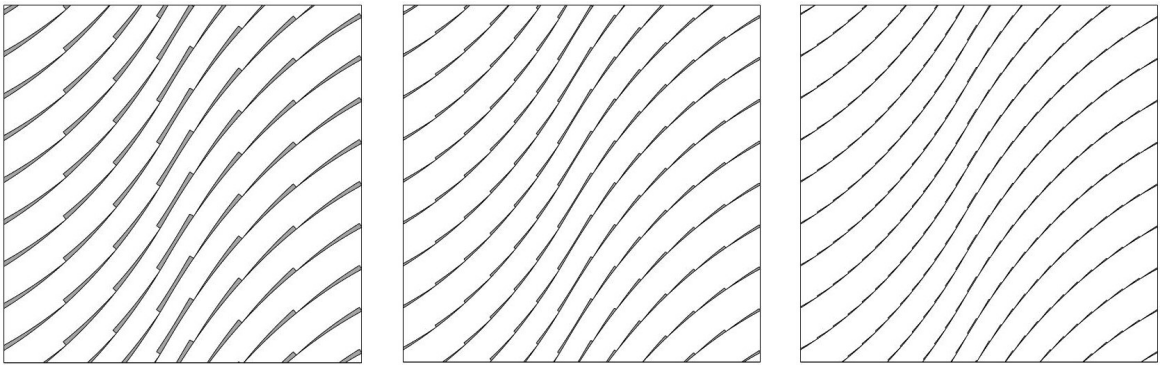

(a) 8 tows of 12.7×10^{-3} m wide (b) 16 tows of 6.35×10^{-3} m wide (c) 32 tows of 3.175×10^{-3} m wide

Figure 3.11: Gap formation in the $\langle 60, 30 \rangle$ ply based on the number of tows in a course and the tow width

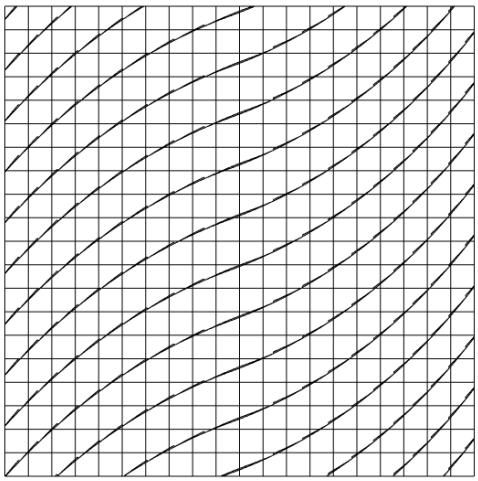

Figure 3.12: Intersection between the mesh plate and the gap distribution

material properties based on the weighted contribution of the fiber and matrix. Here, the constituents are the non-defective composite and matrix representing the gaps. The longitudinal elastic modulus, E_1, the transverse modulus, E_2, and the in-plane shear modulus, G_{12}, can be calculated using Equations 3.6, 3.7 and 3.8, respectively.

$$E_1 = A_c E_{1c} + A_m E_m \tag{3.6}$$

$$E_2 = \frac{E_{2c} E_m}{A_m E_{2c} + A_c E_m} \tag{3.7}$$

$$G_{12} = \frac{G_{12c} G_m}{A_m G_{12c} + A_c G_m} \tag{3.8}$$

where the subscript c represent the non-defective composite and the subscript m the matrix or gaps. The composite area fraction, A_c, and the gap area fraction, A_m, are equivalent to the volume fraction since the thickness is the same in the layer with or without gaps. Obviously, $A_c = 1 - A_m$.

Fayazbakhsh et al. [36] did not introduce the Poisson's ratio and the out-of-plane shear modulus. These properties as suggested by [54] can be obtained also by the 'modified' rule of mixture. To calculate

the Poisson's ratio , ν_{12}, and the out-of-plane shear modulus, G_{23}, Equations 3.9 and 3.10 can be used.

$$\nu_{12} = A_c \nu_{12c} + A_m \nu_m \tag{3.9}$$

$$G_{23} = A_c G_{23c} + A_m G_m \tag{3.10}$$

The material properties for each element are calculated according to Equations 3.6 - 3.10. Figure 3.13 illustrates the resulting scaled material properties for each element according to its gap area fraction.

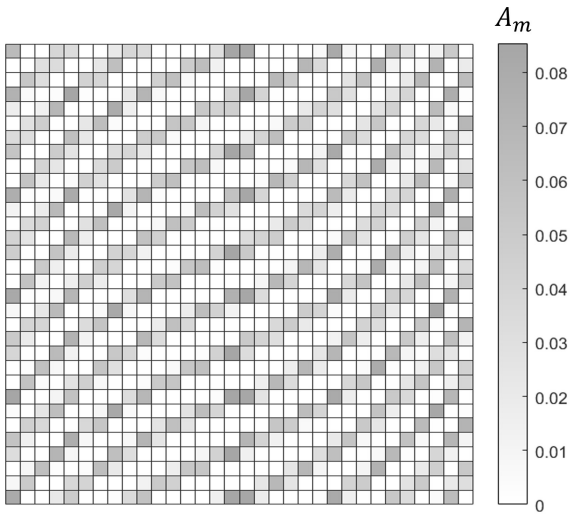

Figure 3.13: Scaled material properties according to gap area

Note that depending on the fiber angles T_0 and T_1, the gap formation varies. This implies that the gap areas and the corresponding material properties are calculated for each different ply of the laminate.

The scaled material properties for each element are used then to build the FE model, creating a material for each layer and for each element. Comparing Figures 3.12 and 3.13, one can observe that the scaled materials follow the gap distribution. This allows the effect of gaps in the VS laminate to be considered without explicitly describing their geometry in the FE model.

3.3.1 Verification study of Gap modeling

The case study presented by Fayazbakhsh et al. [36] was reproduced to validate the gap module developed. A rectangular panel with dimensions 0.254m × 0.4064m is considered. It was subject to axial compression in the negative y-direction. All edges were simply supported, i.e, no displacement out-of-plane was allowed. In addition, vertical in-plane displacement of the upper border was constrained. Figure 3.14 shows the load and boundary conditions applied.

0% coverage or full gap strategy was adopted to manufacture the variable stiffness panel. The material properties of the system carbon epoxy Cytec® G40-800/5276-1 are shown in Table 3.2. The laminate consisted of 16 plies, each 1.59×10^{-4} m thick. The number of tows in a course was 8 and the tow width 3.175×10^{-3} m.

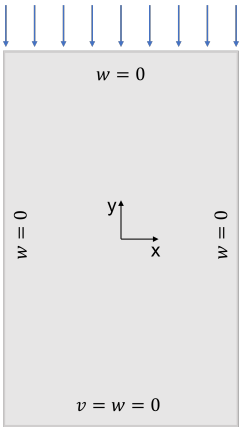

Figure 3.14: Load and boundary conditions applied to test case for gap modeling

Table 3.2: Material properties of carbon epoxy Cytec® G40-800/5276-1

	Composite	Resin
E_1 [GPa]	143.0	3.7
E_2 [GPa]	9.1	3.7
G [GPa]	4.8	1.4
ν_{12}	0.3	0.3

The authors chose two variable stiffness panels to study the influence of the gaps on the buckling load. They were named design A and design B. It must be noted that the authors defined the reference fiber path using a constant curvature path. It was a simplification of the formulation presented in Section 2.3 because only a circular arc defined the fiber path. In this thesis, a linear variation of the fiber angle is employed. Therefore, it is necessary to make an equivalence between the parameters that characterize the constant curvature path and the linear variation path.

The fiber angle at the center of the plate, T_0, and the curvature, k, are the parameters that defines the constant curvature path. The notation adopted for this fiber path is (T_0, k). The fiber angle, φ, varies along the path according to Equation 3.11.

$$sin\varphi = sinT_0 + k\,|x| \tag{3.11}$$

where x is the distance measured from the plate center. It is then trivial to obtain the fiber angle at the edge of the plate, T_1. Note that the authors took the y-direction as a reference for measuring the fiber angles, while in this thesis the reference is the x-direction. The angles are complementary.

Table 3.3 shows the laminate configuration for design A and design B defined with both constant curvature and linear variation parameters. Table 3.3 also indicates a constant stiffness quasi-isotropic laminate. It was used as a baseline to normalize the design A and design B buckling loads.

To ensure that the equivalent parameters for the fiber trajectory are correct, FE analyses are first performed for laminates A and B without gaps. The buckling loads resulting from the analyses of both

Table 3.3: Laminate configuration for baseline and designs A and B reported by Fayazbakhsh [36] and the equivalents utilized in this thesis

Design	Layup
Baseline	$[45/0/-45/90]_{2s}$
A-constant curvature	$[\pm(43, 0.48)/\pm(44, -1.57)/\pm(35, -1.57)/\pm(38, -1.57)]_s$
A-linear variation	$[\pm\langle 47, 42\rangle/\pm\langle 46, 60\rangle/\pm\langle 55, 68\rangle/\pm\langle 52, 65\rangle]_s$
B-constant curvature	$[\pm(43, 0.48)/\pm(48, -1.57)/\pm(30, -1.57)/\pm(26, -1.57)]_s$
B-linear variation	$[\pm\langle 47, 42\rangle/\pm\langle 42, 57\rangle/\pm\langle 60, 72\rangle/\pm\langle 64, 76\rangle]_s$

linear variation and constant curvature fiber paths are shown in Table 3.4. The table also provides the percent error between the present model and Fayazbakhsh model. The percent error is due to the fact that the fiber angle along the path for constant curvature is slightly higher than for the linear variation. In any case, the error is less than one percent, so it can be said that the equivalence between angles has been calculated accurately.

Table 3.4: Comparison between the normalized buckling loads for laminates without gaps reported by Fayazbakhsh[36] and those obtained by the present model

	Design A	Design B
Fayazbakhsh[36]	1.37	1.31
Present model	1.37	1.32
Percent error	$<1\%$	$<1\%$

The results of the FE analyses for the laminates with embedded gaps are shown in Table 3.5. Both models experience a reduction in the buckling load due to the incorporation of gaps. Therefore, the gaps have a substantial impact on the structural performance of the laminate. In this case, the percent error between the two models is higher. The discrepancy is because the choice of fiber path influences the gap area percentage.

Table 3.5: Comparison between the normalized buckling loads for laminates with embedded gaps reported by Fayazbakhsh[36] and those obtained by the present model

	Design A	Design B
Fayazbakhsh[36]	1.20	1.15
Present model	1.25	1.20
Percent error	4.5%	4.6%

The average gap area percentage for the laminate is then obtained. It is calculated as the sum of the gap area in each ply divided by the total laminate area. Table 3.6 shows the average gap area percentage for both models and both designs. It is clear that there is a difference in the value of gap area. Laminates generated with a constant curvature fibre path exhibit a larger gap area than those with linear variation. Figure 3.15 shows the gap distribution of $+(44, -1.57)$ ply of the design A reported by Fayazbakhsh[36] and its equivalent of linear variation fiber path. It can be seen that the geometry of the constant curvature path involves more number of tow-drops, increasing the gap area in the laminate. Hence, it is reasonable that the linear variation laminates have a slightly higher buckling load as the gap area is smaller. The error is still less than 5%, so it is considered that the model developed captures correctly the effects of the gaps.

Table 3.6: Comparison between the average gap area percentage reported by Fayazbakhsh[36] and that obtained by the present model

	Design A	Design B
Fayazbakhsh [36]	12.4%	12.3%
Present model	8.3%	8.4%

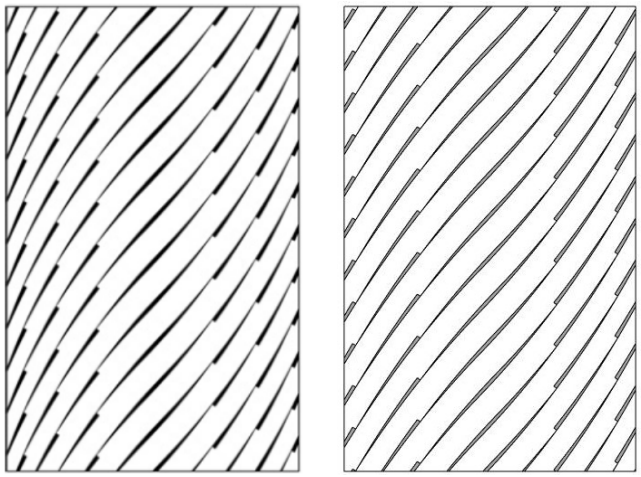

(a) $+(44, -1.57)$ ply (b) $+\langle 40, 60\rangle$ ply

Figure 3.15: Comparison between the gap distribution reported by Fayazbakhsh [36] and the equivalent of the present model

3.4 Modeling of Curvilinearly Grid-Stiffened Panels

3.4.1 Geometry parametrization of Curvilinear Stiffeners

As discussed in Section 2.5, the approach presented by [34, 42, 43] is modified to parameterize the stiffener geometry. Three points are used to determine the stiffener shape by means of a cubic spline. The start

and end points, A and B, are assumed to be located at the plate edges. They are parametrized by the plate perimeters, ε_A and ε_B. The perimeter parameter ε is defined on the plate boundary and varies from 0 to 1, where 1 is the whole plate perimeter. The placement of the stiffener on the plate is then controlled by the perimeter parameters. The control point, C, is assumed to be in the perpendicular direction to the midpoint D of the straight line A-B. It is parametrized by the curvature parameter α. The curvature parameter is the normalized distance measured on the perpendicular line from the midpoint to the control point. Therefore, the stiffener geometry would be parameterized by three design variables: ε_A, ε_B and α. A scheme of the geometry parametrization explained above is shown in Figure 3.16.

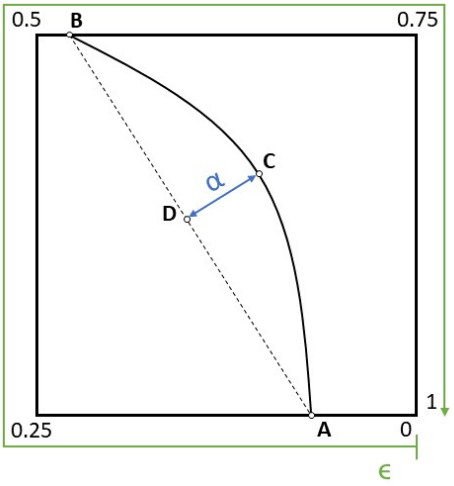

Figure 3.16: Geometry parametrization of a curvilinear stiffener

A total of four stiffeners are considered attached to the plate. This means that the number of design variables would be twelve. These design variables would be in addition to the design variables for the plate curvilinear fibres. Twelve design variables provide a wide range of possible stiffener layouts, however, they involve a high computational cost in the optimization process. Therefore, the following assumptions are necessary to reduce the number of design variables for the stiffener layout:

1. The start point, A, is located at the bottom edge of the plate.
2. The end point, B, is placed at the plate upper edge on the same vertical as the start point.
3. The four stiffeners are symmetrically placed on the plate.

The first and second assumptions mean that the stiffener placement is controlled by one perimeter parameter, ε, and not two as before. The third assumption implies that the geometric parameterization of one stiffener is sufficient for the entire layout. Consequently, the stiffener layout is governed by two design variables: ε and α. Figure 3.17 illustrates the stiffener layout that is considered in this thesis.

The stiffeners are modeled in Abaqus using the spline tool. This tool requires the coordinates of the three points. Therefore, it is necessary to convert the parametrization to x-y coordinates. Table 3.7 indicates the relationship between the value of the perimeter parameter, ε, and the x-y coordinates on the boundary of the square plate of a half-side. These equations are used to calculate the coordinates of the start and end point of the stiffeners.

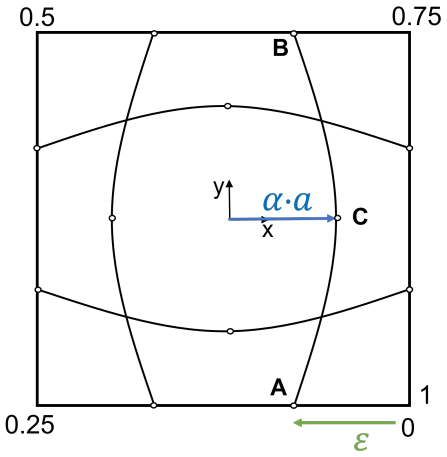

Figure 3.17: Stiffener layout employed in the present model

Table 3.7: Relationship between the perimeter parameter, ε, and the x-y coordinates on the boundary of the square plate of a half-side

ε	x	y
$[0, 0.25]$	$a - 8a\varepsilon$	$-a$
$[0.25, 0.5]$	$-a$	$-3a + 8a\varepsilon$
$[0.5, 0.75]$	$-5a + 8a\varepsilon$	a
$[0.75, 1]$	a	$7a - 8a\varepsilon$

The coordinates of the the control points are trivial to calculate. For a vertically oriented stiffener, the y-coordinate is zero and the x-coordinate is α multiplied by a if the stiffener is on the right side. If the stiffener is on the left side, multiply by $-\alpha$. For a horizontally oriented stiffener, the x-coordinate is zero and the y-coordinate is α multiplied by a if the stiffener is on the upper side. If the stiffener is on the lower side, multiply by $-\alpha$.

It should be noted that, instead of choosing this parameterization approach, the stiffeners could be modeled directly by the coordinates of the points. However, modeling a 3-point stiffener in the most general form involves 6 coordinates, while only 3 parameters $(\varepsilon_A, \varepsilon_B, \alpha)$ are required to characterize it. Therefore, the parameterization explained here needs a smaller number of design variables to define the stiffener layout. And although assumptions were made to reduce the stiffener layout two parameters, the script has been coded in a general way, so it can also model 3-parameter stiffeners if considered. In addition, the difference in the computational time between the two approaches is negligible.

With this approach, the number of design variables is decreased and the choice of appropriated bounds for the design variables is easier. It also facilitates to control that the stiffeners lie inside the panel.

3.4.2 Stiffener Cross-Section

Once the stiffener path is parameterized, its cross section is defined. The stiffeners would be manufactured with an AFP machine by successively placing one tow on top of another. This results in a rectangular stiffener cross-section. Therefore, two dimensions are required to describe the cross-section: the stiffener thickness, t_s, and the stiffener height, h_s. The stiffener depth ratio is defined as h_s/t_s. The influence of the stiffener depth ratio on the panel buckling load and mode shape was studied by W.Zhao and R.Kapania [42]. In their work, the stiffness thickness was fixed while the stiffenes height was varied.

Numerical results showed that the buckling load increased significantly as the stiffener depth ratio increased from 0 to 8. The stiffener height enhances the panel transverse stiffness and, therefore, a higher buckling load can be reached. Here, both the plate and stiffeners buckle out-of-plane resulting in a global buckling mode.

For stiffener depth ratios between 8 and 12, the buckling load did not increase with the stiffener height and remained nearly constant. In this case, when the stiffener height exceeds the optimal value, the transverse stiffness at the plate nodes along the stiffener line becomes very large and the stiffeners can be considered as a simply supported boundary condition. Thus, the stiffeners act as 'panel breakers' and the plate buckles locally between the stiffeners.

Beyond a stiffener depth ratio of 12, the buckling load decreased with the stiffener height. There is almost no panel buckling of the panel, instead the stiffener itself buckles.

In the present model, the stiffener thickness is set equal to thickness of the plate, t_p. The stiffener depth ratio is fixed to $h_s/t_s = 5$, thus global buckling or plate local buckling behaviours are expected. Stiffener blade buckling is not considered.

The stiffeners are attached eccentrically to the plate. The stiffener eccentricity is defined in Equation 3.12 as the the offset between the stiffener centroid and the panel middle plane [42].

$$e = \frac{1}{2}(h_s + t_p) \tag{3.12}$$

Figure 3.18 schematizes the cross-sectional view of the panel showing the thickness, height and eccentricity of the stiffeners, as well as the plate thickness and the thickness of each ply of the laminate. Note that in the present thesis the stiffener laminate is assumed to be perpendicular to the plate midplane as can also be seen in Figure 3.18.

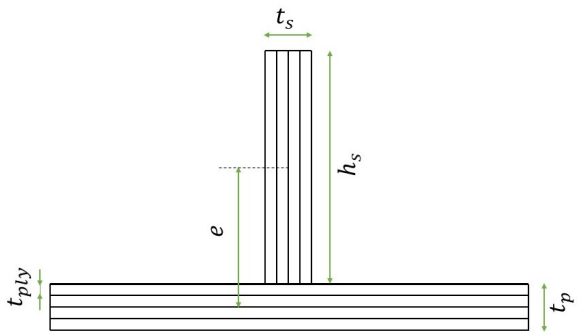

Figure 3.18: Scheme of the panel cross section

3.4.3 Modeling Stiffeners by Beam elements

The stiffeners are idealized by beam elements, specifically Abaqus B31 element. B31 element is a 2-node linear beam Timoshenko type. Timoshenko beams allow for transverse shear deformation [47].

The beam element in Abaqus does not support a composite laminate definition. However, a beam can be assigned a section with an orthotropic material and an orientation. The beam cross section is defined as a rectangular profile of t_s by h_s, the dimensions to define the stiffener blade. Since the beam element accepts orthotropic properties, the material used for the stiffener is the same as for the plate.

The key aspect here is to set the strong material direction coincident with the longitudinal direction of the stiffener. This simulates that the fibers are aligned with the local orientation of the beam, i.e, the fibers follow the stiffener path. Thus, the stiffeners can be modeled with a zero angle laminate. The zero angle fiber ply in the stiffener is shown to provide a larger bending stiffness to the plate, enhancing the structural stability of the design [42]. Figure 3.19 shows the local directions for the material properties of the stiffeners.

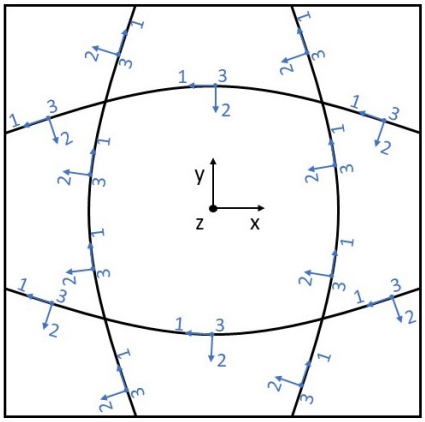

Figure 3.19: Local material orientation for the the stiffeners

3.4.4 Tie Constraint

Abaqus' built-in *tie constraint* has been used to attach the stiffeners to the plate. The *tie constraint* ties two separate surfaces together so that there is no relative motion between them [47]. Its major advantage is that it allows fusing together a pair of regions with dissimilar meshes, as it is the case here. Therefore, it is not necessary for the stiffener nodes to coincide with the plate nodes, which reduces the complexity of the setup.

In the tie constraint, one surface is designated as the master surface and the other surface as the slave surface. The plate has been chosen to be the master surface and the set of stiffeners is the slave surface. Abaqus forms constraints between the slave nodes and the master nodes by generating tie coefficients. The tie coefficients are used to interpolate quantities from the master nodes to the point where the slave node projects onto the master surface.

A position tolerance criterion is used to determine whether or not the slave nodes are constrained to the the master surface. This criterion is based on the distance between the slave nodes and the

master surface, i.e, slave nodes that are within the set distance will be tied to the master and slave nodes that do not meet this criterion will not be constrained. As mentioned above, the stiffeners are attached eccentrically to the plate. Recall also that the stiffeners are modeled by beam elements and the plate by shell elements. The centroid of the beam and the shell midsurface are then at a distance of e (stiffener eccentricity defined in Equation 3.12). Therefore, to constraint all slave nodes to the master, the position tolerance distance has been set to the value of e. Figure 3.20 shows the offset e between the slave nodes (corresponding to the centroid of the beam) and the master nodes (corresponding to the reference midsurface of the shell).

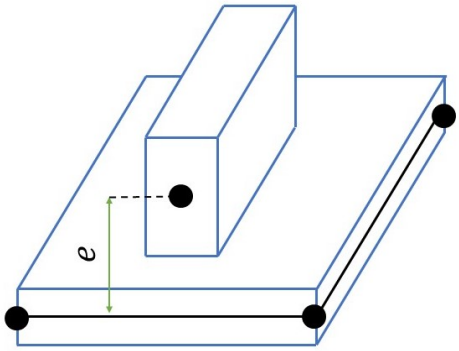

Figure 3.20: Offset between the beam nodes and shell nodes

3.4.5 Verification study of Curvilinearly Grid-Stiffened Panels

Zhao et al. [55] developed a finite element approach to study the vibration and buckling behaviour of a curvilinearly grid-stiffened panel. The buckling load results are employed here to validate the code for modeling curvilinear stiffeners, in this case using Abaqus. A simply supported square panel with dimensions 800 mm × 800 mm subjected to in-plane biaxial loads was considered. The panel thickness was set to $t_p = 8\,\text{mm}$ and the stiffener width was the same as the panel thickness, $t_s = t_p$. Different stiffener heights, h_s, were established to investigate the effect of the stiffener depth ratio , h_s/t_s, on the buckling response of the grid panel. Figure 3.21 shows the loading and boundary conditions applied to the panel and indicates the dimensions of the cross-section of the panel.

The panel and stiffeners were made of composite material, specifically T300/5208 graphite-epoxy composite. The material properties are as follows: $E_1 = 132.38\,\text{GPa}$, $E_2 = E_3 = 10.76\,\text{GPa}$, $G_{12} = G_{13} = 5.65\,\text{GPa}$, $G_{23} = 3.38\,\text{GPa}$, $\nu_{12} = \nu_{13} = 0.24$, $\nu_{23} = 0.49$ and $\rho = 1800\,\text{kg/m}^3$.

The layup for the panel consisted of eight layers in a symmetric cross-ply configuration: $[(0/90)_2]_s$. The composite panel has constant stiffness , i.e. the fibers are straight. To model straight fibers, $T_0 = T_1$ has been set in the code. Note that the variable stiffness composite panels have been validated with the case study presented in Section 3.2.1. Therefore, it has been proceeded to validate the curvilinear composite stiffeners.

The stiffener laminate was perpendicular to the panel midplane and also had eight layers. The strong material direction was considered to coincide with the longitudinal direction of the stiffeners, so an angle

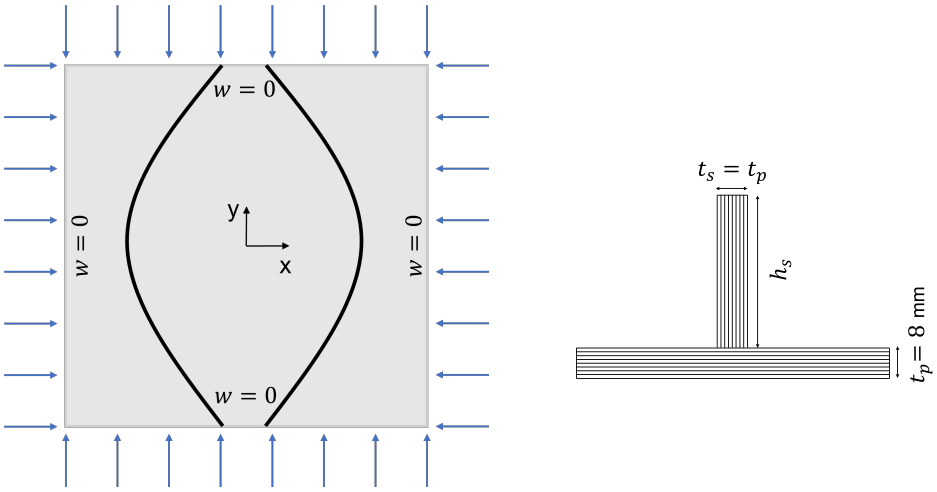

(a) Load and boundary conditions (b) Cross-section of the panel

Figure 3.21: Test case for curvilinear stiffeners modeling

of zero degrees was applied to all layers.

Two symmetrical stiffeners around the y-axis were eccentrically attached to the panel. The stiffener location was defined by the perimeter parameter ε and the stiffener shape by the curvature parameter α. The definition of these parameters is slightly different between the approach taken by Zhao et al. [55] (see Figure 2.14) and the one adopted in this thesis (see Figure 3.16). The values of parameters with the approach of this thesis are $\varepsilon = 0.1112$ and $\alpha = 0.25$.

The plate was modeled by shell elements and the stiffeners by beam elements. The number of elements utilized for meshing the plate was 144 and for each stiffener was 15. Linear buckling analysis were then performed, modifying the stiffener depth ratio. The buckling loads were normalized with respect to the buckling load of the unstiffened cross-ply laminate. The buckling load reported by Zhao et al. [55] for the baseline panel had a value of 56.1 N/mm, the same value as that obtained by Abaqus.

The normalized buckling loads for three different cases of stiffener depth ratio, h_s/t_s, are shown in Table 3.8. It also indicates the percent error between the normalized buckling loads reported by Zhao et al. [55] and those resulting from the present model. The percent error is less than 2%. Therefore, the present code for modeling curvilinear composite stiffeners is validated.

Table 3.8: Comparison between the normalized buckling loads reported by Zhao et al. [55] and those obtained by the present model

	$h_s/t_s = 0.1$	$h_s/t_s = 2.5$	$h_s/t_s = 5$
Zhao et al. [55]	1.01	3.90	7.30
Present model	1.02	3.84	7.22
Percent error	0.5%	1.5%	1.2%

3.5 Mesh Convergence

A mesh convergence study should be performed to determine the minimum number of elements that will guarantee adequate Finite Element Analysis (FEA) results and a reasonable computation time. The mesh is said to be converged when further mesh refinement produces a negligible change in the solution. Here, the element size is iteratively decreased until the buckling load provided by the FEA tends towards a unique value.

The convergence study is conducted for a simply supported composite panel subjected to biaxial compression. The dimensions of the panel are $1\text{m} \times 1\text{m}$. The laminate for both the plate and the stiffener consists of four layers, each with a thickness of $t_{ply} = 1.27 \times 10^{-4}\text{m}$. Thus, the thickness of the plate and the stiffeners are the same and equal to $t_p = t_s = 5.08 \times 10^{-4}\text{m}$. The height of the stiffeners is set to $h_s = 2.54 \times 10^{-3}\text{m}$. The material properties for both the plate and stiffeners are indicated in Table 5.2. The design variables that define the optimization problem $\left(T_0^1, T_1^1, T_0^2, T_1^2, \varepsilon, \alpha\right)$ have been arbitrarily chosen for the mesh convergence study. The sole condition was that the curvature constraint was satisfied. The stacking sequence for the plate laminate is set to $\left[\langle 30, 60\rangle \,/\, \langle -50, -25\rangle\right]_s$. The stiffener location and curvature are fixed to $\varepsilon = 0.1$ and $\alpha = 0.5$.

The plate and the stiffeners are meshed separately. Therefore, a mesh convergence is first conducted only for the plate to determine the size of the plate element. Next, the mesh of the plate is fixed and the convergence study for the stiffener element size is performed. In addition, since the optimization is carried out for panels with and without the effect of gaps, convergence studies are presented for both scenarios. Note that square shell elements are used to model the plate and beam elements for the stiffeners.

Successive FEA simulations are carried out by reducing the element size until mesh convergence is reached. To determine which element size will provide reliable results with a reasonable computational time, the percent error with respect to the buckling load of the minimum element size considered is calculated. The minimum element size is assumed to provide the actual buckling load.

The percent error is defined as the difference between the buckling load corresponding to an element size minus the actual buckling load divided by the actual buckling load and multiplied by 100 (see Equation 3.13).

$$\text{Percent error } \% = \frac{\text{Buckling load} - \text{Actual buckling load}}{\text{Actual buckling load}} \cdot 100 \tag{3.13}$$

Results for the plate mesh convergence without gaps are given in Table 3.9. The convergence is achieved from an element size of 0.04 m onwards since the percent error is less than 0.5%. The element size equal to 0.03125 m has been chosen to model the plate, which corresponds to a total of 1024 elements.

Table 3.9: Convergence study for the plate without gaps

Element Size [m]	0.2	0.125	0.1	0.0625	0.05	0.04	0.03125	0.025	0.02	0.015625	0.0125	0.01
Buckling load [N/m]	53.252	50.384	49.760	49.088	48.932	48.832	48.756	48.716	48.688	48.668	48.656	48.644
Percent error %	9.473	3.577	2.294	0.913	0.592	0.386	0.230	0.148	0.091	0.049	0.025	-

Having studied the mesh convergence for the plate without gaps, the element size for the stiffeners is then determined. Table 3.10 indicates the stiffener element size, the corresponding buckling load of the panel (plate + stiffeners), and the percent error. The size of the elements selected has been 0.045 m, which in most cases corresponds to 24 elements per stiffener, i.e., a total of 96 elements for the four stiffeners. The curvature of the stiffener changes in the optimization process, which means that, depending on the curvature value, the number of elements to model the stiffener may change slightly.

Table 3.10: Convergence study for stiffeners with fixed mesh plate without gaps

Element Size [m]	0.09	0.08	0.06	0.045	0.035	0.03
Buckling load [N/m]	127.628	127.484	127.224	127.204	127.184	127.164
Percent error %	0.365	0.252	0.047	0.032	0.016	-

The same procedure has been followed to study the mesh converge for the case that considers gaps. Results for the plate mesh and the stiffener mesh are provided in Tables 3.11 and 3.12. The plate element size and the stiffener element size chosen are the same as in the case without gaps, since the Defect Layer Method allows the gaps to be located independently of the number of elements [35]. Hence, the size of elements in the FE model is only dictated by the convergence of the buckling load.

Table 3.11: Convergence study for the plate with gaps

Element Size [m]	0.2	0.125	0.1	0.0625	0.05	0.04	0.03125	0.025	0.02	0.015625	0.0125	0.01
Buckling load [N/m]	52.068	49.256	48.652	47.976	47.828	47.748	47.676	47.644	47.620	47.608	47.604	47.600
Percent error %	9.387	3.479	2.210	0.790	0.479	0.311	0.160	0.092	0.042	0.017	0.008	-

Table 3.12: Convergence study for stiffeners with fixed mesh plate with gaps

Element Size [m]	0.09	0.08	0.06	0.045	0.035	0.03
Buckling load [N/m]	126.420	126.288	126.024	126.012	125.992	125.972
Percent error %	0.356	0.251	0.041	0.032	0.016	-

Note that the element sizes selected here are also used for panels with other laminates, boundary conditions, or load cases.

Chapter 4

Optimization Framework

In this chapter, the definition of the optimization problem is presented. Section 4.1 indicates the chosen objective function, the design variables and manufacturing constraints. These constraints in terms of curvature for the skin and stiffener fibers are detailed in Section 4.2. Section 4.3 provides the theoretical basis of Genetic Algorithms and specifies the genetic parameters and functions selected. Finally, Section 4.4 explains the methodology followed to integrate the finite element module into the optimization module

4.1 Problem Statement

GA is employed as the optimizer in this thesis. An optimization problem is defined by an objective function, f, which is maximized (or minimized) with respect to the design variables, $\mathbf{x}$, and is often subject to constraints, g.

In this work, the objective of the optimization is to maximize the buckling load of composite panels with curvilinear fibers and grid stiffeners. To this end, the objective function to be minimized is the inverse of the normalized buckling factor, $\overline{BF}$. It has been chosen to minimize the objective function since the GA available in MATLAB does not support maximization. The Buckling Factor (BF) is defined as the ratio of the buckling load and the applied load. The buckling factor is normalized to the buckling factor obtained in the first evaluation of the objective function, BF_1 (see Equation 4.1). The BF has been normalized so that the value of the objective function is of a similar order of magnitude to that of the design variables.

$$\overline{BF} = \frac{BF}{BF_1} \tag{4.1}$$

The design variables of the problem can be divided into two sets: those of the skin fibers and those of the stiffener layout. The skin fibers follow a curvilinear path in which the orientation varies according to the x-direction. To define the path of the skin fibers according to Equation 3.1, two fiber angles and a characteristic length are needed. The present work considers the plate dimensions fixed and the fiber angles as the design variables. Therefore, there will be two design variables for each i different ply of the laminate: T_0^i and T_1^i. Two different plies are considered, resulting in four design variables for the skin laminate: T_0^1, T_1^1, T_0^2, T_1^2. The stiffener layout is determined by the ε location parameter and the

α shape parameter, which constitute the other two design variables. Note the thickness and height of the stiffeners are fixed in the optimization. Hence, a total of six design variables define the problem. A more detailed description on how the plate fibers and the stiffener layout are modeled can be found in the previous sections 3.2 and 3.4.1, respectively.

Manufacturing constraints in terms of maximum curvature allowable by the AFP machine are imposed for both skin and stiffener fibers. The number of curvature constrains will be equal to the number of i different plies of the skin laminate plus the curvature constraint for the stiffener layout. Section 4.2 explains how the curvature of the skin and stiffener fibers is computed.

The optimization formulation for the design problem can be expressed as:

$$\begin{aligned} \text{Minimize} \quad & f = \frac{1}{\overline{BF}} \\ \text{w.r.t.} \quad & \mathbf{x} = \left[T_0^i, T_1^i, \varepsilon, \alpha\right] , \\ \text{subject to} \quad & g_i = \frac{\left|\kappa^i_{max,f}\right|}{\kappa_{AFP}} - 1 \leq 0 \quad \text{for} \quad i = 1, 2, ..., m, \\ & g_{i+1} = \frac{|\kappa_{max,s}|}{\kappa_{AFP}} - 1 \leq 0 \end{aligned} \tag{4.2}$$

The range of the design variables has been chosen so that their order of magnitude is similar. The range is indicated in Table 4.1. Note that the fiber angles, T_0^i and T_1^i, will be multiplied by 90 and ε and α will be converted to x,y coordinates when the FE model is built.

Table 4.1: Range of the design variables

	T_0^i	T_0^i	ε	α
Lower bound	-1	-1	0	-1
Upper bound	1	1	0.25	1

It is recalled that ε controls the stiffener placement on the plate. The assumptions made in 3.4.1 for the geometry parametrization of the stiffener layout mean that the reference stiffener is constrained to be placed at the plate bottom edge, so the range of ε can vary from 0 to 0.25. The design variable α governs the curvature by means of the stiffener control point coordinates. The range of α is from -1 to 1, which in the FEM model results in the x-coordinates to vary between $-a$ and a, thus covering the whole plate width. It also ensures that the stiffener does not surpass the limits of the plate.

4.2 Manufacturing Constraints

The manufacturing constraint imposed in the design of variable-stiffness panels is the maximum curvature allowable by AFP machines. This constraint is also called the minimum turning radius of the machine. Both terms, maximum curvature or minimum turning radius, are equivalent as they are the inverse of each other (see Equation 4.3).

$$\kappa_{max} = \frac{1}{R_{min}} \tag{4.3}$$

The maximum curvature depends, among other factors, on the tow width. A wider tow means increasing the compression of the fibers along the inside of the curve. Therefore, a larger tow width implies a higher value of the minimum turning radius (or a lower maximum curvature). According to [4], the common minimum turning radius for an AFP machine that uses a 32 tow course with 3.175×10^{-3} m wide tows (as it is the case) is 0.635 m. Hence, the maximum curvature of the AFP machine is fixed to κ_{AFP} =1.57 m^{-1}.

The curvature constraint is imposed on both the skin and the stiffeners as they are made of curvilinear fibers. Since the trajectory of the fibers is 2D, the definition of the curvature for a planar function is employed. The curvature at a point of a function, $y(x)$, is given in terms of the first and second derivatives of $y(x)$ by Equation 4.4.

$$\kappa = \frac{f''(x)}{(1 + (f'(x))^2)^{3/2}} \tag{4.4}$$

Equation 4.4 requires an analytical function to describe the trajectory of the fibers. In the case of plate fibers is trivial as $f(x)$ represents the fiber path defined by the linear variation of the fiber angle. However, the stiffeners are modeled directly in Abaqus, which makes it more difficult to find such function. Here below, it is explained how to implement the curvature constraint in the optimization framework, first for the skin fibers and then for the stiffener fibers.

4.2.1 Skin Fibers Curvature

The layers of the skin would be manufactured by the shifted method. In the shifted method, the fiber paths have identical orientation as the reference path. This means that the curvature constraint for the whole ply is reduced to calculate the curvature for the reference path. In addition, the reference path is antisymmetric with respect to the y-axis, so the curvature can be calculated only for positive values of x. As mentioned above, $f(x)$ stands for the fiber path $y(x)$ defined in Equation 3.2. Equation 4.4 requires the expression of the first and second derivatives. They can be calculated as indicated in Equations 4.5 and 4.6.

$$\frac{dy}{dx} = tan\theta \tag{4.5}$$

$$\frac{d^2y}{dx^2} = \frac{d}{dx}(tan\theta) = \frac{1}{cos^2\theta}\frac{d\theta}{dx} = \frac{1}{cos^2\theta}\frac{(T_1 - T_0)}{a} \tag{4.6}$$

The curvature can then be obtained in terms of T_1, T_0, $\theta(x)$ and a, as shown in Equation 4.7.

$$\kappa_f = \frac{(T_1 - T_0)/a}{cos^2\theta(1 + tan^2\theta)^{3/2}} \tag{4.7}$$

If the trigonometric relationship 4.8 is considered,

$$1 + tan^2\theta = \frac{1}{cos^2\theta} \tag{4.8}$$

the expression for the curvature of the fiber path is simplified as:

$$\kappa_f = \frac{T_1 - T_0}{a} cos\theta \tag{4.9}$$

Equation 4.9 is employed to evaluate the curvature of the reference path at each positive x-position. The x-positions are the coordinates of the center of each element of the mesh plate.

Once the curvature of each point has been calculated, the maximum in absolute value is obtained. The absolute value is used since the curvature is a signed quantity. The maximum curvature of the fiber path, $\kappa^i_{max,f}$, is then compared to the maximum curvature of the AFP machine, κ_{AFP}. The constraint implemented is shown in Equation 4.10. Note that there will be as many curvature constraints as different i layers of the laminate.

$$\frac{\left|\kappa^i_{max,f}\right|}{\kappa_{AFP}} - 1 \leq 0 \tag{4.10}$$

The contour plot of the Figure 4.1 shows how the maximum fiber curvature changes, $\kappa_{max,f}$, as a function of the fiber angles T_0 and T_1. Thus, depending on the maximum curvature imposed in the constraint, the feasible design space of T_0 and T_1 will vary. A restrictive value of the curvature allowed by the AFP machine will result in a reduction of the fibre angle combination possibilities.

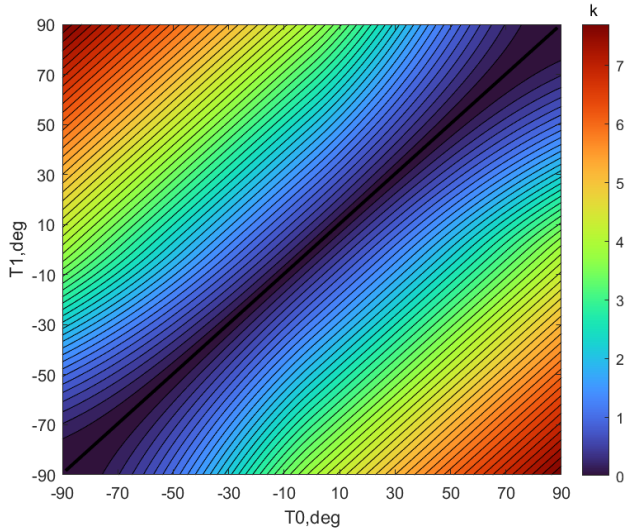

Figure 4.1: Feasible design space of T_0 and T_1 depending on curvature value

4.2.2 Stiffener Fibers Curvature

To evaluate the curvature of the stiffeners, an analytical function is first found. This function must be at least second differentiable as it is required by Equation 4.4. The stiffeners are modeled using the spline tool in Abaqus. Knowing how Abaqus/CAE draws the spline is the key to determine that function.

From Abaqus Documentation [47], one can read that the spline curve is calculated by Abaqus/CAE using a cubic spline fit between all the points along the spline. Therefore, the curve shape is influenced by the location of the points. The use of a cubic spline fit implies that the first and second derivatives of the spline are continuous . In addition, it can be observed that the cubic spline becomes a straight line at the start and end points. This condition is termed as a natural spline. Hence, the objective is to obtain the cubic spline function given a number of data points. Once this function is determined, it is possible to interpolate the value of an arbitrary point on the stiffener and compute its curvature. The mathematical formulation to find the spline function is described hereunder.

A cubic spline is a piece-wise third-order polynomial. There is then a different cubic polynomial for each interval between data points or knots, as expressed in Equation 4.11.

$$f_{i,i+1}(x) = a_{i,i+1}x^3 + b_{i,i+1}x^2 + c_{i,i+1}x + d_{i,i+1} \tag{4.11}$$

where $f_{i,i+1}(x)$ is the cubic polynomial that connect the knots i and $i+1$. Then for n data points, there are $n-1$ cubic polynomial and, consequently, $4(n-1)$ unknown coefficients. The $4(n-1)$ conditions to solve the unknowns are:

1. The function values must be equal at the interior knots ($2(n-1)-2$ conditions).
2. The first and last functions must pass the start and end knots (2 conditions).
3. The first derivatives at the interior knots must be equal ($n-2$ conditions)
4. The second derivatives at the interior knots must be equal ($n-2$ conditions)
5. The second derivatives at the start and end knots must be zero (2 conditions)

Figure 4.2 shows a cubic spline of n data points and $n-1$ functions.

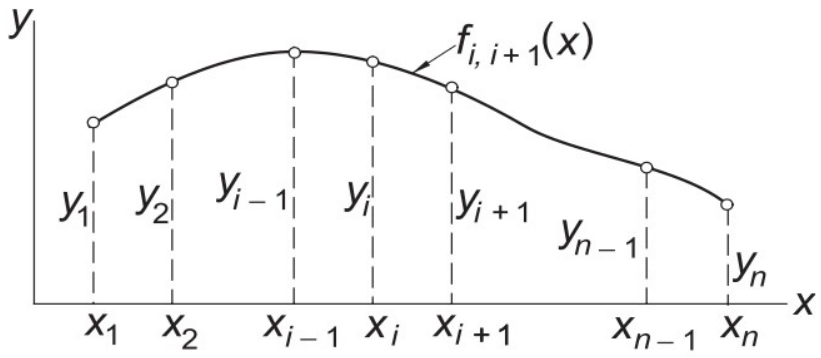

Figure 4.2: Cubic spline interpolation reproduced from [56]

Although the cubic spline could be obtained as indicated above, an alternative method has been followed to gain computational efficiency. This method only requires to solve $n-2$ equations. The approach taken is based on references [56] and [57].

The first step of the method is to realize that if each pair of points is joined by a third-order polynomial, the second derivative within each interval is a straight line. Equation 4.11 is differentiated twice and expressed in Equation 4.12 by a linear Lagrange interpolating polynomial.

$$f''_{i,i+1}(x) = k_i \frac{x - x_{i+1}}{x_i - x_{i+1}} + k_{i+1} \frac{x - x_i}{x_{i+1} - x_i} \tag{4.12}$$

where $f''_{i,i+1}(x)$ is the second derivative at any point in the segment $i, i+1$, k_i and k_{i+1} are the second derivative at knots i and $i+1$, respectively. Equation 4.12 proves to be a straight line connecting the second derivative at the first knot with the second derivative at the second knot.

The next step is to integrate Equation 4.12 in which two unknown constants will appear. The first derivative, $f'_{i,i+1}(x)$, and the function, $f_{i,i+1}(x)$, are expressed in Equations 4.13 and 4.14, respectively.

$$f'_{i,i+1}(x) = \frac{k_i (x - x_{i+1})^2 - k_{i+1} (x - x_i)^2}{2 (x_i - x_{i+1})} + A - B \tag{4.13}$$

$$f_{i,i+1}(x) = \frac{k_i (x - x_{i+1})^3 - k_{i+1} (x - x_i)^3}{6 (x_i - x_{i+1})} + A (x - x_{i+1}) - B (x - x_i) \tag{4.14}$$

where A and B are constants of integration. Although these two terms could be written as the usual form $Cx + D$, setting $C = A - B$ and $D = -Ax_{i+1} + Bx_i$ yields to a more convenient computation.

These constants of integration, A and B, can be obtained by applying the first condition listed before, i.e., $f_{i,i+1}(x)$ must be equal to $f_{i,i+1}(x_i)$ at x_i and $f_{i,i+1}(x)$ must be equal to $f_{i,i+1}(x_{i+1})$ at x_{i+1}. For the shake of brevity, the terms $f_{i,i+1}(x)$ and $f_{i,i+1}(x_i)$ are renamed as y_i and y_{i+1} respectively. The expressions for A and B can be found in Equations 4.15 and 4.16.

$$A = \frac{y_i}{x_i - x_{i+1}} - \frac{k_i}{6} (x_i - x_{i+1}) \tag{4.15}$$

$$B = \frac{y_{i+1}}{x_i - x_{i+1}} - \frac{k_{i+1}}{6} (x_i - x_{i+1}) \tag{4.16}$$

Substituting A and B, the function of the cubic spline results in Equation 4.17.

$$\begin{aligned} f_{i,i+1}(x) = {} & \frac{k_i}{6} \left[\frac{(x - x_{i+1})^3}{(x_i - x_{i+1})} - (x - x_{i+1}) (x_i - x_{i+1}) \right] \\ & - \frac{k_{i+1}}{6} \left[\frac{(x - x_i)^3}{(x_i - x_{i+1})} - (x - x_i) (x_i - x_{i+1}) \right] \\ & + \frac{y_i (x - x_{i+1}) - y_{i+1} (x - x_i)}{(x_i - x_{i+1})} \end{aligned} \tag{4.17}$$

Although it could seem that Equation 4.17 is much more complicated than the usual form of the cubic polynomial (Equation 4.11), this new expression just involves two unknowns: the second derivatives at the start knot, k_i, and end knot, k_{i+1}, of the segment.

The second derivatives at the interior knots can be calculated by the continuity of first derivatives: $f'_{i-1,i}(x_i) = f'_{i,i+1}(x_i)$. This condition is applied in Equation 4.13 to all interior knots. It generates a system of $n - 2$ equations with n unknowns second derivatives, as expressed by Equation 4.18.

$$k_{i-1} (x_{i-1} - x_i) + 2k_i (x_{i-1} - x_{i+1}) + k_{i+1} (x_i - x_{i+1}) = 6 \left(\frac{y_{i-1} - y_i}{x_{i-1} - x_i} - \frac{y_i - y_{i+1}}{x_i - x_{i+1}} \right) \tag{4.18}$$

The condition that the spline is natural implies that the second derivatives at the start and end knots of the spline are set to zero: $k_1 = k_n = 0$. This reduces the unknowns to $n - 2$. Moreover, the system of equations 4.18 is tridiagonal which is easy to solve by Lower–Upper (LU) decomposition. In LU decomposition, a tridiagonal matrix is factored into a lower triangular matrix L and an upper triangular matrix U, so that the product of the LU matrices gives the original matrix. LU decomposition is an effective method for solving systems of linear equations [57].

The mathematical method explained is implemented to obtain the spline function that describes the stiffener path. It is worth mentioning that this formulation is only valid when the points are to form a function in the x-y plane and are ordered from smallest to largest. This implies that depending on how the stiffener is modeled, the points must be converted to the x-y plane. The angle between the line joining

the start and end point of the stiffener and the x-axis is calculated. If the angle is zero, the stiffener is aligned with respect to the x-axis and no further operation is performed. If the angle is nonzero, the data points are converted to points in the xy-plane by a rotation matrix.

In this work, three points are used to model the stiffener, so there are two segments and one interior knot as shown in Figure 4.3. Following the formulation, the interpolated functions of the two segments

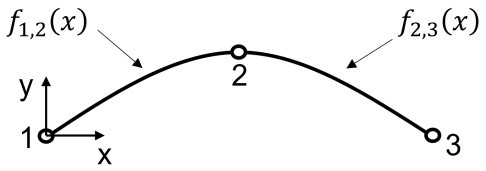

Figure 4.3: Spline functions of the stiffener

are determined. The curvature is calculated for 100 points of the stiffener. To know to which segment each point belongs, the bisection method is applied. Finally, the maximum curvature of the stiffener, $\kappa_{max,s}$, is obtained and compared to the maximum curvature allowable by the AFP machine, κ_{AFP}. Note that the four stiffeners are equal, so the values of the curvature are only calculated for one of them. The constraint is shown in Equation 4.19.

$$\frac{|\kappa_{max,s}|}{\kappa_{AFP}} - 1 \leq 0 \tag{4.19}$$

4.3 Genetic Algorithm

Genetic algorithm is the optimizer adopted in the present thesis. The Abaqus module used to calculate the buckling load (the objective function) acts like a black box towards MATLAB (the optimizer module). Thus, the sensitive information of the problem is not accessible. In addition, the optimization of VS laminates with curvilinear stiffeners usually exhibits local minima. Consequently, the global optimization methods like GA are better options compared to gradient-based optimization methods. Several optimization runs should be performed to ensure that the global optimum is found. Although the genetic algorithm is time-consuming, the problem is defined with a reduced number of design variables, which makes the optimization computation time affordable.

In this section, the basics of the genetic algorithm are first explained. Next, the penalty algorithm used to evaluate the fitness score of the individual is described. The genetic operators are then specified. Finally, the values of the genetic parameters chosen to perform the optimization problem are indicated. In this thesis, the optimization framework is implemented in MATLAB, thus the parameters and functions described here are those available in its library.

4.3.1 GA Fundamentals

Genetic algorithms are stochastic search methods that were first devised by John Holland [58] and his collaborators in the mid-sixties. GA mimics the natural selection process of biologic evolution, following the Darwinian principle of "the survival of the fittest". Simply put, individuals in a population compete

for resources and the successful ones have more offspring than the others. The genes of the fittest parents are propagated through the next generation, creating offspring that are likely to be superior to either parent. As a result, the subsequent generation is better adapted to the environment. Each individual represents a candidate solution: a possible panel design for the optimization problem. The individuals are traditionally coded as a finite-length binary string (chromosome). The components of the string would be the gene analogs.

The genetic algorithm starts by creating a random initial population. Each individual of the population is evaluated to compute its fitness value. GA then generates a new population by means of three main operators - selection, crossover, and mutation- giving more possibilities to reproduce the individuals with better fitness scores. The population size is maintained constant throughout the process and, therefore, the old population is replaced by the new one. Each new generation is expected to have better partial solutions (fitter individuals) than the preceding generations. Several generations later, the population evolves towards an optimal solution. GA ends the iterative process when the stopping criteria are met. In this thesis, the stopping criteria are implemented as the maximum number of generations performed by the algorithm and the average change in fitness value being less than or equal to a specified tolerance.

4.3.2 Penalty Method

The present optimization problem involves constraints related to the maximum curvature allowed by the AFP machine. The constrained optimization problem is converted into an unconstrained problem by a penalty function. The penalty algorithm is available in MATLAB GA library and based on K.Deb's work [59]. The method proposed by K.Deb uses a tournament selection operator with two solutions compared at a time to ensure the following criteria:

i When two feasible solutions are compared, the one with better objective function value is chosen

ii When one feasible and one infeasible solutions are compared, the feasible solution is chosen

iii When two infeasible solutions are compared, the one with smaller constraint violation is chosen

Here, penalty parameters are not necessary because none of the three scenarios compare solutions that require both objective function and constraint violation information at the same time. In addition, the comparison of infeasible solutions in terms of constraint violation has a practical sense, since computing the objective function of an infeasible design is a time-consuming task. The penalty function employed in this method is expressed in Equation 4.20.

$$F(\mathbf{x}) = \begin{cases} f(\mathbf{x}), & \text{if} \quad g_i(\mathbf{x}) \leq 0, \quad i = 1, 2, ..., m \\ f_{max} + \sum_{i=1}^{m} \langle g_i(\mathbf{x}) \rangle, & \text{otherwise} \end{cases} \tag{4.20}$$

Therefore, the fitness score of a feasible individual is simply the value of its fitness function (usually the objective function). Whereas if the individual is infeasible, the penalty function is the worst fitness function value of the feasible individuals in the population, f_{max}, plus the sum of the constraint violations of the infeasible individual. If there are no feasible individuals in the population, f_{max} is equal to zero. Note that all m constraints are normalized to avoid any bias of a particular constraint.

This constraint handling scheme without the need of a penalty parameter is possible because genetic algorithms use a population of solutions in every iteration and a pair-wise comparison of solutions is possible using the tournament selection operator [59]. This is a major advantage, as it avoids the difficulty of setting the appropriate penalty parameters, which require extensive experimentation.

4.3.3 Genetic Operators

The GA utilizes individuals from the present population to create the offspring that will form the next generation. First, the algorithm selects a set of individuals (parents) that will contribute their genes to their offspring. The fittest individuals tend to be selected more frequently.

Several selection methods are available. Here, the tournament selection with size 2 has been chosen. Tournament selection consists of running tournaments among a few individuals, in this case two, chosen randomly from the population. The winner of each tournament (the fittest) is set to be a parent.

Once the parents have been selected, the genetic algorithm creates three categories of offspring for the subsequent generation: elite children , crossover children, and mutation children.

Elite children are the fittest individuals of the current generation. The number of these individuals that automatically passed on to the next generation can be specified. Therefore, the best designs will remain unchanged. A high value of elite children means that they will govern the population and the search can be less effective.

Crossover children are generated by exchanging information from two individuals in the current generation. It allows the algorithm to extract the best genes from different individuals and combine them to hopefully create a superior offspring. There are various crossover functions that can be selected. The crossover scattered is the one chosen for the present optimization. It creates a random binary vector and selects the genes where the vector is a 1 from the first parent, and the genes where the vector is a 0 from the second parent, and combines the genes to form the child [60]. Figure 4.4 shows an example of how the scattered crossover operator works.

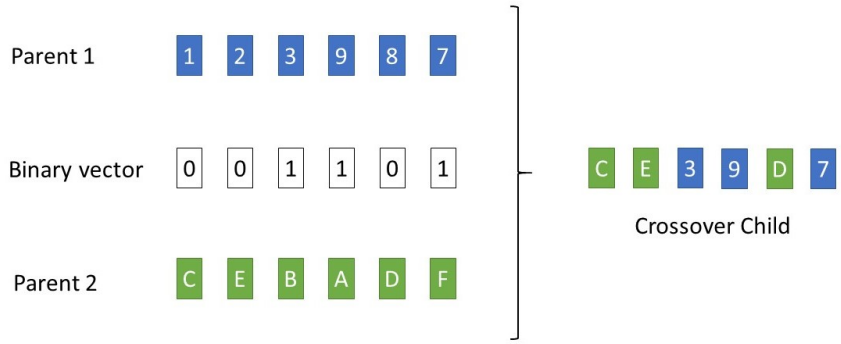

Figure 4.4: Crossover scattered

A mutation child is created by inserting random changes (mutations) to a single individual in the current generation. Mutation provides diversity in the population, which increases the probability that fitter individuals will be generated. It broadens the search space for the optimal solution, increasing

both computational time and the reliability of the solution. It also prevents the GA from prematurely converging to a local optimum.

In the present thesis, the following values of GA parameters have been chosen based on the author's experience as a compromise between the sufficient reliability of the optimal solution and a reasonable calculation price. Regarding the population size, a large value does not achieve a sufficient mix of individuals at a reasonable computational price, while in a small population there is not enough genetic material to ensure a high diversity of individuals. It is clear that the population size should increase with the problem size. In this regard, a population size at least ten times the number of design variables is recommended [59]. Since the present optimization problem involves six design variables, a population size of sixty individuals has been chosen. The stopping criterion in terms of maximum number of generations has been set to 60 generations. Other parameters including the number of elite children and the crossover fraction have been set to 3 and 0.6 , respectively.

4.4 Integration of Modules

The methodology followed to integrate the finite element module into the optimization module is explained in this section. The present optimization framework has two modules: the MATLAB module and the Abaqus module.

The MATLAB module performs the optimization. The maximum curvature of the skin and stiffener fibers is computed in this module. The geometry of gaps, if considered, is also obtained here. The Abaqus module executes the Python script in which the information to build the FE model, such as the plate geometry, materials, boundary conditions, loads or mesh options is written. This Python script is coded to model variable stiffness laminates with curvilinear stiffeners. Abaqus then conducts the linear buckling analysis and provides the first eigenvalue, which is the buckling factor used in the objective function. The interaction between the two modules is presented in the optimization flowchart of Figure 4.5. A brief overview of the optimization framework is explained hereafter.

A random initial design of the panel is first set by MATLAB. MATLAB then checks whether or not the design violates the curvature constraint. If the constraint is violated, a new design is generated. If it is satisfied, MATLAB moves to the objective function. The function calls Abaqus directly if the gap effect in the laminate is not considered. If so, the gap module is executed. Abaqus then receives the MATLAB inputs that are the value of the design variables and the material properties. This information is used to build the FEM of the panel. Abaqus performs the buckling linear analysis. The output is a text file in which the first buckling eigenvalue is written. In the MATLAB module, the objective function reads the text file and calculates the normalized buckling factor. The process is repeated until the convergence is reached. The optimized panel design is then obtained.

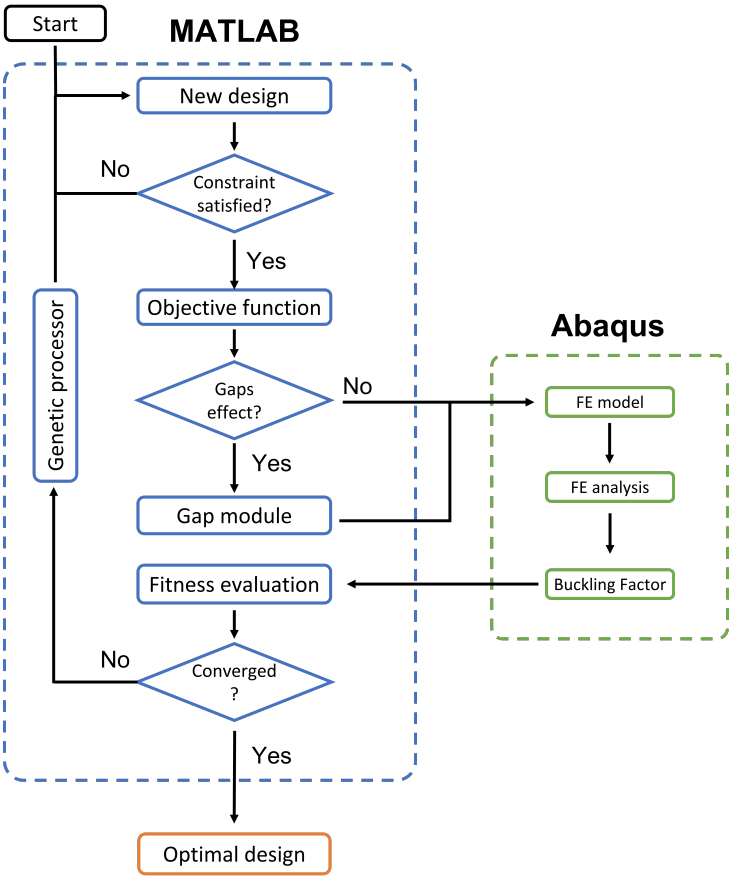

Figure 4.5: Flowchart of the optimization framework

Chapter 5

Results

This chapter first introduces the case studies to be optimized. The geometry, laminate properties, boundary conditions and load cases considered are described in Section 5.1. The results obtained from the optimization are then presented and discussed. Section 5.2 focuses on the optimized design for the first load case and Section 5.3 deals with the optimized panels considering the second load case.

5.1 Case Studies

In this work, a square composite panel of dimensions $2a \times 2a$ is optimized. The value of a is set to 0.5 m. Two stacking sequences are considered for the plate laminate: $\left[\left\langle T_0^1, T_1^1 \right\rangle / \left\langle T_0^2, T_1^2 \right\rangle\right]_s$ (laminate A composed of 4 plies in total), and $[\pm \left\langle T_0^1, T_1^1 \right\rangle / \pm \left\langle T_0^2, T_1^2 \right\rangle]_{2s}$ (laminate B composed of 16 plies in total). The superscript refers to the 2 different plies of the laminate. Each ply has a thickness, t_{ply}, of 1.27×10^{-4} m, a typical value for a prepeg thermoset.

The thickness of the stiffener, t_s, is equal to that of the plate, t_p, i.e., both laminates have the same number of plies. The stiffener height, h_s, is five times the stiffener thickness. The strong material direction is assumed to coincide with the longitudinal direction of the stiffener, which means an angle of zero degrees for the plies of the stiffener laminate. The stiffener laminate is perpendicular to the plate midplane. The stiffeners are eccentrically attached to the plate. Table 5.1 reports the values of the ply, plate and stiffener thicknesses and stiffener heights for both laminates. Figure 5.1 schematizes the panel and indicates its dimensions.

Table 5.1: Dimensions of the panel cross-section

Laminate	t_{ply} [m]	t_p [m]	t_s [m]	h_s [m]
$\left[\left\langle T_0^1, T_1^1 \right\rangle / \left\langle T_0^2, T_1^2 \right\rangle\right]_s$	1.27×10^{-4}	5.08×10^{-4}	5.08×10^{-4}	2.54×10^{-3}
$[\pm \left\langle T_0^1, T_1^1 \right\rangle / \pm \left\langle T_0^2, T_1^2 \right\rangle]_{2s}$	1.27×10^{-4}	2.032×10^{-3}	2.032×10^{-3}	1.016×10^{-2}

The parameters to define the tow course, which are the the tow width and the number of tows in a course, are set to $t_w = 3.175 \times 10^{-3}$ m and $n_t = 32$, respectively. These parameters affect the gap

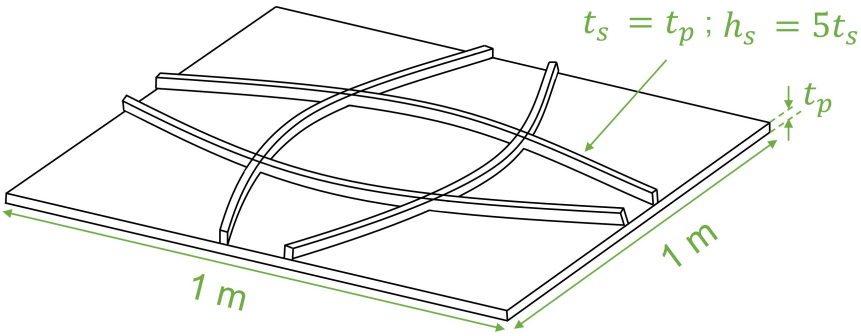

Figure 5.1: Scheme of the panel to be optimized

formation within each ply and limit the allowable curvature of the AFP machine to $\kappa_{AFP} = 1.57\,\mathrm{m}^{-1}$.

The material properties of both the skin and the stiffeners correspond to an standard modulus graphite plus epoxy resin material, commonly used in aeronautics. Representative values, taken from [55], are given in Table 5.2. The material properties of a generic epoxy resin, employed to fill the gaps, are also indicated in Table 5.2.

Table 5.2: Material properties

Graphite-Epoxi		Epoxi	
E_1	132.38 GPa		
E_2	10.76 GPa	E_m	3.7 GPa
E_3	10.76 GPa		
ν_{12}	0.24		
ν_{13}	0.24	ν_m	0.3
ν_{23}	0.49		
G_{12}	5.65 GPa		
G_{13}	5.65 GPa	G_m	1.4 GPa
G_{23}	3.38 GPa		

When panels with gaps are optimized, Poisson's ratios are assumed equal ($\nu_{12} = \nu_{13} = \nu_{23}$) because a rule of mixture for ν_{23} has not been stated.

Boundary conditions and load cases influence substantially the buckling load and modal shape, thus several case studies are optimized in this thesis. Certain boundary conditions and load cases have been selected to represent what a wing panel of an aircraft may experience. Panel edges at $x = -a, x = a$ would simulate the ribs and panel edges at $y = -a, y = a$ would simulate the spars. The different scenarios are presented next.

The three different boundary conditions addressed in this thesis are:

- All plate edges are simply supported. This case is denoted by SSSS.

- Two plate edges are simply supported at $y = -a, y = a$ and the other two are clamped at $x = -a, x = a$. This case is denoted by SSCC.
- All plate edges are clamped. This case is denoted by CCCC.

Here, for the simply supported boundary condition there is no out-of-plane displacement, i.e., $w = 0$. The clamped boundary condition restricts, in addition to the out-of-plane displacement, the rotations along the x-axis and y-axis, i.e., $w = \theta_x = \theta_y = 0$. In all cases, to avoid body solid rigid motion, the bottom left corner and bottom right corner are constrained to $v = 0$ and $u = v = 0$, respectively.

The two load cases modeled in this thesis are as follows:

- Biaxial compressive load case.
- Biaxial compressive load plus in-plane shear load.

Therefore, a total of six combinations of boundary conditions and load cases are considered for the optimization problem. These combinations are schematized in Figure 5.2. Note that the loads and boundary conditions are applied at the edges of the midplane of the plate.

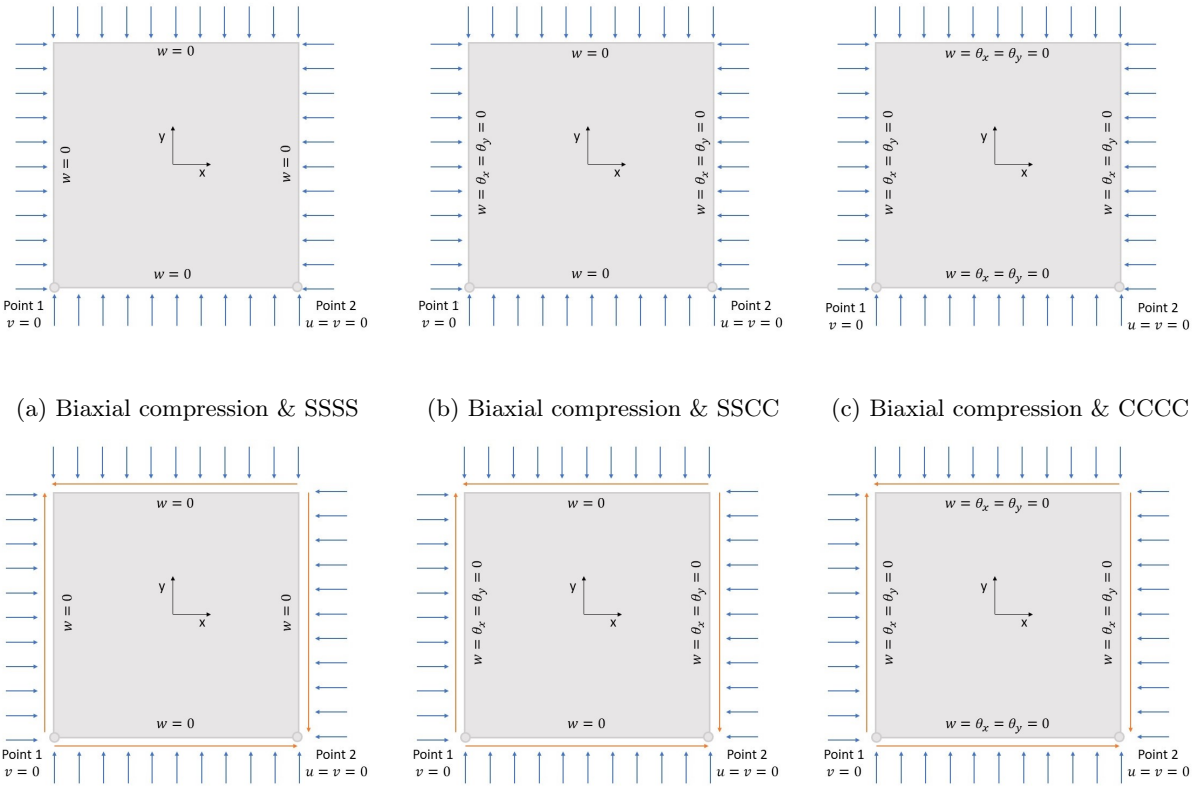

(a) Biaxial compression & SSSS (b) Biaxial compression & SSCC (c) Biaxial compression & CCCC

(d) Biaxial compression+Shear & SSSS (e) Biaxial compression+Shear & SSCC (f) Biaxial compression+Shear & CCCC

Figure 5.2: Combinations of load cases and boundary conditions

The optimization results are compared to a constant stiffness composite panel with straight stiffeners.

The stacking sequence for the case of a 4 plies laminate is [±45/0/90] and for the 16 plies laminate is $[\pm 45/0/90]_{2s}$. The straight stiffeners are placed equidistant from each other. It should be noted that for a fairer comparison between the curvilinear fiber design and straight fiber design, the latter should also be optimized. However, due to time constraints, the straight fiber designs described above are used.

Hereafter, the results of the optimization are presented and discussed, first for the biaxial compression load case and then for the biaxial compression plus in-plane shear load case.

5.2 Biaxial compression load case

In this section, the results of the optimized ideal panels, i.e., without gaps, are first analyzed. Next, the optimized panels considering the gap effect are presented. Four case studies have been optimized for panels subjected to biaxial compressive load: the first one with laminate A (4 plies) and SSSS boundary conditions, the other three with laminate B (16 plies) and boundary conditions of SSSS; SSCC; CCCC. Table 5.3 reports the buckling load obtained with the straight fiber design for this four scenarios. These buckling loads will be used to calculate the percent improvement over curvilinear fiber panels.

Table 5.3: Buckling load for the straight fiber design panel subjected to biaxial compression load

Laminate	Boundary Conditions	Buckling Load $[N/m]$
[±45/0/90]	SSSS	96
$[\pm 45/0/90]_{2s}$	SSSS	17260
	SSCC	36080
	CCCC	40160

5.2.1 Results of ideal panel optimization

Table 5.4 indicates the results of the optimization for the four cases: the value of the design variables, the maximum curvature of the fibers of ply 1 (κ_1), ply 2 (κ_2), and stiffeners (κ_s), the critical buckling load and the improvement with respect to straight fiber design. The configuration for ply 1, ply 2, the stiffener layout, and the first buckling mode for each of the four case studies are shown in Figure 5.3.

The optimized panel with laminate A (4 plies) subjected to biaxial compression and SSSS boundary conditions is first analyzed. The fiber angles of ply 1 and ply 2 are almost the same in absolute value. The fiber angles of ply 1 have a positive sign while the fiber angles of ply 2 have a negative sign, thus forming a quasi-balanced laminate for the plate. The maximum curvature of the fiber paths for both plies and for the stiffeners is the maximum curvature imposed as a constraint. This reveals that the curvature of the AFP machine acts as an active constraint preventing the design of more curved fiber panels that could give a higher buckling load. The resulting buckling load has a value of 150 N/m. The panel buckles in a global manner. The improvement compared to the straight analogue is 57%, showing that in this case

Table 5.4: Optimization results of ideal panels subjected to a biaxial compression load

Total plies	Boundary Conditions	$T_0^1\,(^\circ)$	$T_1^1\,(^\circ)$	$T_0^2\,(^\circ)$	$T_1^2\,(^\circ)$	ε	α	Max Curvature $[m^{-1}]$	Buckling Load $[N/m]$	Improvement (%)
4	SSSS	14.2	60.9	-11.6	-57.8	0.110	0.387	$\kappa_1 = 1.57$ $\kappa_2 = 1.57$ $\kappa_s = 1.57$	150	57
16	SSSS	13.9	59.5	18.5	66.2	0.0987	0.475	$\kappa_1 = 1.54$ $\kappa_2 = 1.57$ $\kappa_s = 1.57$	24210	40
16	SSCC	27.5	56	29.3	20.4	0.159	-0.337	$\kappa_1 = 0.876$ $\kappa_2 = 0.289$ $\kappa_s = 0.377$	41360	15
16	CCCC	50.2	38.9	-62.1	-21.6	0.177	-0.193	$\kappa_1 = 0.305$ $\kappa_2 = 1.30$ $\kappa_s = 1.32$	49770	24

the possibility of tailoring the stiffness by means of curvilinear fibers substantially enhances the buckling performance.

The optimization results of the panel with laminate B (16 plies) under biaxial compression and SSSS have some similarity with the results obtained from the previous case. The values of the fiber angles of ply 1 and ply 2 are nearly equal in absolute value to those of the laminate A. The placement and shape of the stiffeners are also analogous to the previous case. The maximum curvature of ply 1 fibers does not reach the maximum allowed, but is very close to it. The maximum curvature for fiber paths of ply 2 and stiffeners is the maximum imposed curvature. Therefore, the optimized panel implies exploiting the tow steering capability to the fullest allowable, as was also the case with the previous panel. These similarities were to be expected since the boundary conditions and the load case were the same. The buckling load obtained is 24 210 N/m. A value much higher than in the case of the laminate A, since the total number of plies not only involves the thickness of the laminate but also the dimensions of the stiffeners, enhancing the load-bearing capacity of the panel. The buckling mode is also global. The improvement with respect to the straight fiber panel is 40%.

The next case optimized has been the panel with laminate B subjected to biaxial compression under SSCC. A different behavior is encountered. The fibers of ply 1 exhibit a significant curvature, but far from the maximum allowed. The maximum curvature of the ply 2 fibers and of the stiffeners has a modest value. The two clamped edges (SSCC) imply a significant increase in buckling load and a change in the buckling mode shape with respect to the SSSS case. Now the panel buckles locally with the buckle peaks at the top and bottom edges and not in the center. The buckling load has a value of 41 360 N/m. The improvement over the straight fiber configuration is 15%. In this case, the tow steering capability has not revealed a major advantage for the panel buckling performance.

The last case optimized for the biaxial compression load is the panel with laminate B under CCCC.

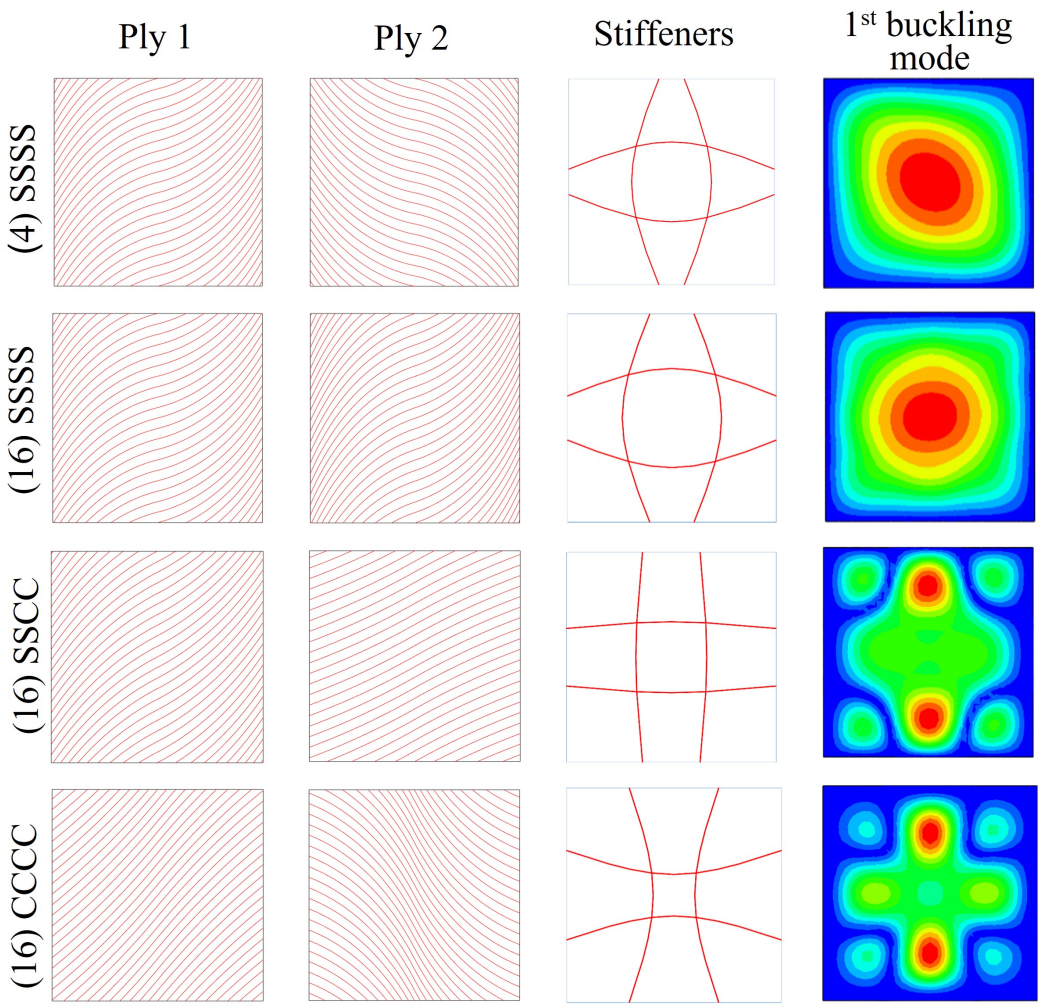

Figure 5.3: Optimized ideal panels subjected to biaxial compression

Although the fibers of ply 1 do not present a high curvature, the fibers of ply 2 are considerably curved. The stiffeners curve significantly towards the center of the panel. The maximum permitted curvature is not reached in any of the cases. The four clamped edges lead to a high buckling load. The resulted buckling load for the optimum panel is 49 770 N/m and the plate buckles in a local manner. The improvement with respect to the straight fiber design is 24%.

5.2.2 Results of the panel optimization considering gap effect

Table 5.5 reports the results of the panel optimization considering the gap effect. It also indicates the average gap area encountered for a ply of the laminate. It is calculated as the sum of the gap area in each ply divided by the total laminate area. Figure 5.4 illustrates the plies configuration, stiffener layout and the first buckling mode.

The results of the optimization for panels considering the gap effect have a certain similarity with respect to those obtained with ideal panels. The laminate A (4 plies) subjected to the SSSS boundary condition presents high values of curvature near or at the limit of the maximum curvature for both skin and stiffener fibers. The gaps formed in the VS laminate deteriorate the buckling performance, however,

Table 5.5: Optimization results of panels considering gap effect, subjected to biaxial compression load

Total plies	Boundary Conditions	T_0^1 (°)	T_1^1 (°)	T_0^2 (°)	T_1^2 (°)	ε	α	Max Curvature $[m^{-1}]$	Gap Area (%)	Buckling Load $[N/m]$	Improvement (%)
4	SSSS	15.4	60.7	-9	-54.6	0.138	-0.364	$\kappa_1 = 1.51$ $\kappa_2 = 1.55$ $\kappa_s = 1.57$	2.03	145	51
16	SSSS	15.6	57.4	-15.6	-62.2	0.104	0.433	$\kappa_1 = 1.40$ $\kappa_2 = 1.55$ $\kappa_s = 1.57$	2.07	24190	40
16	SSCC	34	23.6	-20	-50.4	0.160	-0.280	$\kappa_1 = 0.333$ $\kappa_2 = 0.990$ $\kappa_s = 0.018$	1.76	41010	14
16	CCCC	55.2	21	-38.8	-56.6	0.183	-0.197	$\kappa_1 = 1.11$ $\kappa_2 = 0.481$ $\kappa_s = 1.57$	1.86	49360	23

the average gap area for the optimized panels is not much higher than 2%, so the critical load does not decrease significantly. The buckling load has a value of 145 N/m. The first buckling mode shape is of global nature. The improvement over the straight fiber panel is 51%.

Regarding to the laminate B (16 plies) under SSSS boundary condition, similar results are obtained. The skin fibers are of high curvature, close to the maximum allowed. The stiffeners reach the maximum curvature. The average gap area is 2.07%. The buckling load is 24 190 N/m and the panel buckles globally. The improvement achieved is 40%.

A different pattern is found for the SSCC boundary condition. In this case, the skin fibers show considerable curvature, but do not approach the maximum. The average gap area is 1.76%, which is lower than in cases where the skin fibers reach the maximum curvature. The stiffeners are of very low curvature. The buckling load is 41 010 N/m and the plate buckles locally. The improvement obtained is 14%, mainly caused by the skin fibers, since the stiffener layout is almost equal to the straight fiber configuration.

In the last boundary condition (CCCC), the skin fibers are significantly curved but not to the maximum allowed. The average gap area is 1.86%. The stiffeners are the ones that reach the maximum curvature. The buckling load is 49 360 N/m. The panel buckles in a local manner with peaks on the top and bottom edges. The improvement obtained is 23%.

5.3 Biaxial compression plus Shear load case

For this load case, only laminate B (16 plies) has been optimized. The same boundary conditions have been addressed: SSSS, SSCC and CCCC. First, the results of the optimization of ideal panels are introduced. Then, the optimized panels considering the gap effect are presented. The buckling load of the straight fiber design subjected to biaxial compression plus in-plane shear for each boundary conditions is

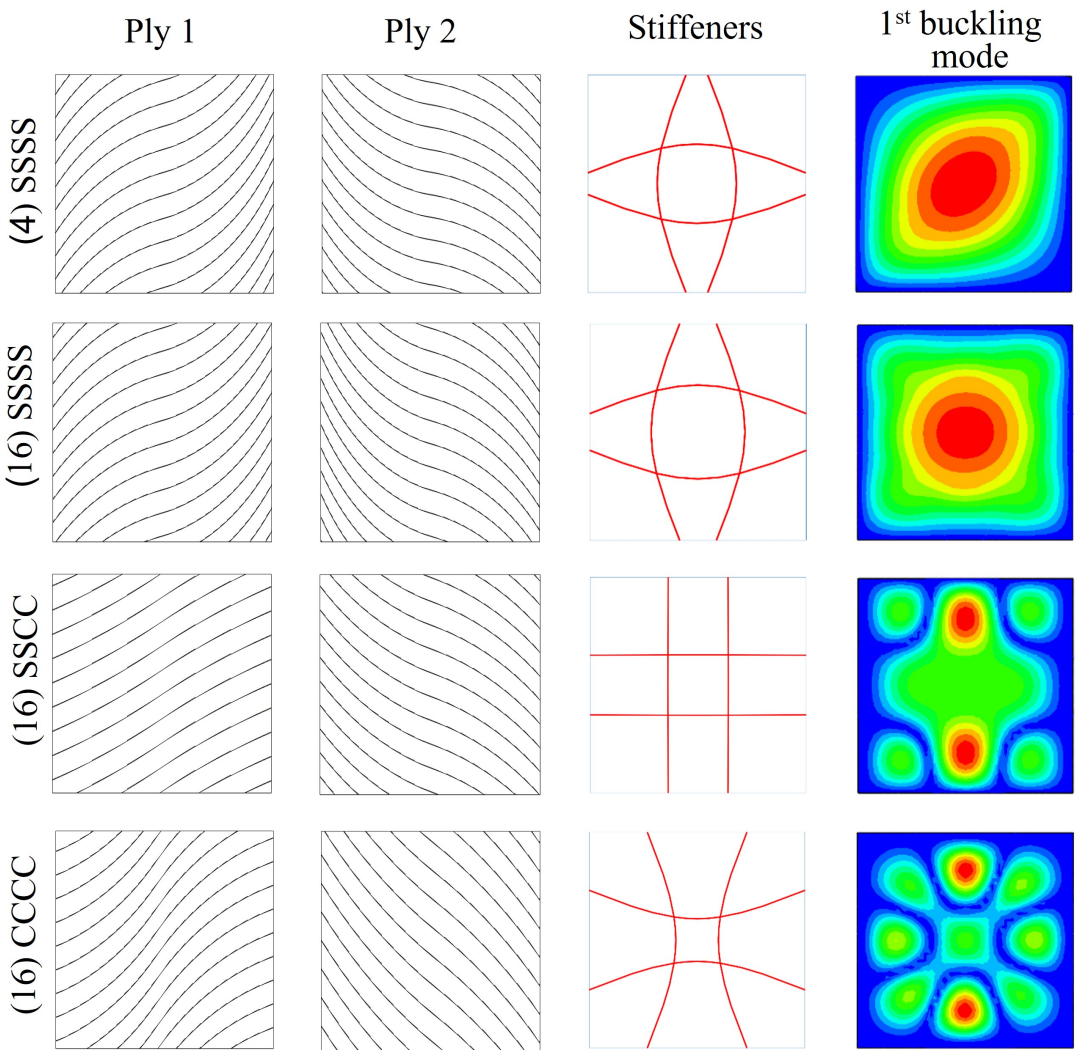

Figure 5.4: Optimized panels considering gap effect, subjected to biaxial compression

indicated in Table 5.6.

5.3.1 Results of ideal panel optimization

The results of the optimization of ideal panels subjected to biaxial compression plus in-plane shear are given in Table 5.7. The configuration of ply 1 and ply 2, the stiffener layout, and the first buckling mode are illustrated in Figure 5.5.

The ideal panel with laminate B (16 plies) subjected to biaxial compression plus shear load under SSSS boundary conditions is the first discussed. The fiber paths of ply 1 present a considerable curvature. The fiber paths of ply 2 and of the stiffener reach the maximum curvature allowable. When the boundary condition is SSSS, it appears that the preferred design panels are those that take full advantage the capability to curve the composite fibers. The resulting buckling load has a value of 41 000 N/m. The buckling shape is of global nature. The improvement with respect to the straight fiber counterpart is 27%.

In the case of SSCC boundary condition, the fibers of the plate laminate exhibit significant curvature;

Table 5.6: Buckling load for the straight fiber design panel subjected to biaxial compression plus shear load

Laminate	Boundary Conditions	Buckling Load $[N/m]$
$[\pm 45/0/90]_{2s}$	SSSS	32300
	SSCC	61610
	CCCC	70360

Table 5.7: Optimization results of ideal panels subjected to biaxial compression plus shear load

Total plies	Boundary Conditions	T_0^1 (°)	T_1^1 (°)	T_0^2 (°)	T_1^2 (°)	ε	α	Max Curvature $[m^{-1}]$	Buckling Load $[N/m]$	Improvement (%)
16	SSSS	20.2	55.0	17.3	63.1	0.100	0.464	$\kappa_1 = 1.13$ $\kappa_2 = 1.51$ $\kappa_s = 1.57$	41000	27
16	SSCC	37.9	11.2	16.1	63.0	0.169	-0.311	$\kappa_1 = 0.913$ $\kappa_2 = 1.56$ $\kappa_s = 0.249$	69050	12
16	CCCC	36.2	23.9	20.3	68.7	0.0976	0.353	$\kappa_1 = 0.390$ $\kappa_2 = 1.57$ $\kappa_s = 0.790$	85620	22

the fibers of ply 2 actually reach the curvature limit. By contrast, the value of the maximum curvature of the stiffeners is low and the layout is close to the straight fiber design. The buckling load is 69 050 N/m and the panel buckles globally. An improvement of 12% is obtained mainly due to the skin fibers.

In the last optimized case, all edges clamped boundary condition (CCCC), the fiber paths of ply 1 show a modest curvature, while the fiber paths of ply 2 adopt the maximum imposed curvature. The stiffener layout has a moderate curvature and does not reach the maximum allowable. The resulting buckling load is 85 620 N/m and there is local buckling of the plate. The improvement achieved over the straight fiber configuration is 22%.

5.3.2 Results of panel optimization considering gap effect

Table 5.8 reports the optimization results of panels with embedded gaps subjected to biaxial compression plus in-plane shear. Figure 5.6 shows corresponding plies configurations, stiffener layout and bucking mode shape.

The case of SSSS boundary condition involves again high values of curvature close or at the maximum allowed for the skin fibers and the stiffeners. The average gap area is 2.08%. The buckling load obtained is 40 870 N/m and the panel buckles globally. The improvement with respect to the straight fiber counterpart is 26%.

Optimization results for the boundary condition (SSCC) indicate that the skin fibers are greatly

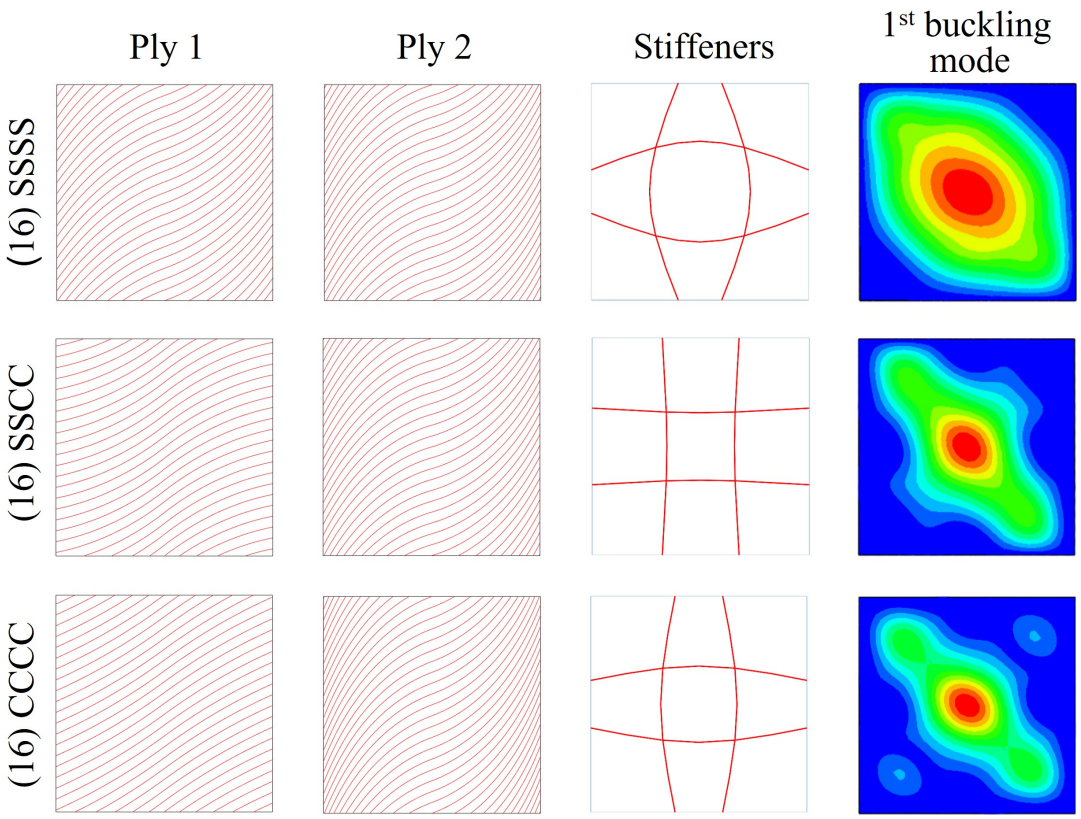

Figure 5.5: Optimized ideal panels subjected to biaxial compression plus shear

curved but a quasi-straight configuration for the stiffeners. The average gap area has a value of 1.97%. The buckling load achieved is 69 010 N/m. The improvement over the straight fiber design is 12%. This modest value is mainly due to the configuration of the skin fibers, since the optimized design of the stiffener layout has resulted to be very similar to that of the straight fiber panel.

For the CCCC boundary condition case, the fibers of the skin are considerably curved. The average gap area is 2.26%, the highest value of all optimized cases. It is because the high value of $T_0^1 = 72.7°$ in ply 1 leads to increased gap formation. Regarding to the stiffener layout, it shows a moderate curvature. The buckling load has a value of 81 450 N/m and the plate buckles locally. The improvement achieved over the straight fiber design is 16%.

5.4 Discussion of Results

The results yielded by the optimization of ideal panels and the optimization of panels with gaps have some similarity. In both scenarios, the values of the fiber angles, T_0 and T_1, are in the range from 10 to 70 (in absolute value). The difference between the fiber angles is about 40 degrees, which implies a considerable curvature of the skin fibers. That configuration of T_0 and T_1 and the chosen manufacturing parameters for the course (32 tows of 3.175×10^{-3} m wide) results in the average gap area not exceeding 2.3% for any optimized ply. Therefore, although the inclusion of gaps certainly worsens the bearing capacity of the panel, these optimized laminates with a low gap area do not suffer a significant decrease

Table 5.8: Optimization results of panels considering gap effect, subjected to biaxial compression plus shear load

Total plies	Boundary Conditions	T_0^1 (°)	T_1^1 (°)	T_0^2 (°)	T_1^2 (°)	ε	α	Max Curvature $[m^{-1}]$	Gap Area (%)	Buckling Load $[N/m]$	Improvement (%)
16	SSSS	15.9	61	-13.6	-60.2	0.0949	0.488	$\kappa_1 = 1.50$ $\kappa_2 = 1.57$ $\kappa_s = 1.47$	2.08	40870	26
16	SSCC	42.4	10.4	16.8	62.4	0.161	-0.295	$\kappa_1 = 1.09$ $\kappa_2 = 1.51$ $\kappa_s = 0.052$	1.97	69010	12
16	CCCC	72.7	36.2	26.3	64.2	0.099	0.322	$\kappa_1 = 1.01$ $\kappa_2 = 1.17$ $\kappa_s = 0.665$	2.26	81450	16

in the buckling critical load. Curvilinear fibers that induce gaps are preferred to straight fibers that do not cause those gaps. Note that designs with straight fibers are allowed in the optimization. For all cases, an improvement is achieved with respect to the straight fiber design.

As for the grid layout, the stiffeners are generally located in intermediate positions neither near the center nor near the edges of the panel. The stiffener curvature depends on which boundary condition is optimized. Since stiffeners are not considered to induce gaps, the resulting layouts are similar for both scenarios: ideal laminates and laminates with embedded gaps. This repeatability indicates that the Genetic Algorithm finds the optimum design for the stiffeners.

It has been demonstrated that the boundary conditions substantially influence on the panel buckling performance. Panels under SSSS boundary condition exhibit high curvature for both the skin and stiffener fibers, reaching in most cases the maximum allowed. Here, the curved fibers provide more efficient load paths than the straight fiber counterparts. Thus, the capability to tailor the stiffness variation is fully exploited, enhancing the buckling response of the panel. For the SSSS boundary condition, the greatest improvement over the straight fiber design has been achieved. The optimized panels considering the gap effect show a 51% improvement for biaxial compression and 26% improvement for biaxial compression plus in-plane shear.

For panels under SSCC boundary condition, the results of the optimization show that the skin fibers are significantly curved but the stiffeners are of very low curvature. The resulting optimized stiffener layout is similar to the straight stiffener design. In this case, curvilinear stiffeners have not demonstrated a major advantage in panel buckling behavior, as the design of quasi-straight stiffeners is preferred. Therefore, the improvement achieved over the straight fiber configuration is mainly due to the curvilinear fibers of the skin. The improvement for panels with embedded gaps is 14% for biaxial compression and 12% for biaxial compression plus in-plane shear. These improvement values are the lowest achieved among the boundary condition cases studied.

The optimized panels under CCCC boundary condition present moderate values of curvature for both skin and stiffener fibers, in some cases reaching the maximum allowable value. The improvement of panels with gaps compared to the straight fiber design for the biaxial compression loading case is 23% and for

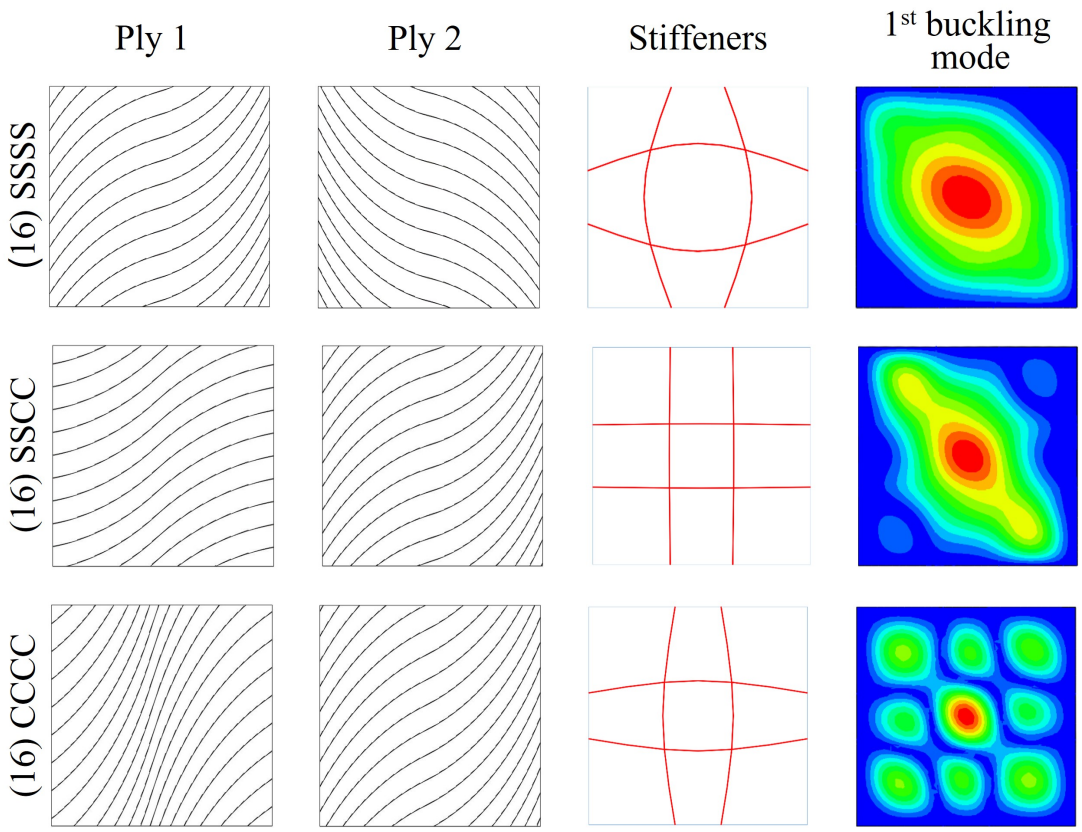

Figure 5.6: Optimized panels considering gap effect, subjected to biaxial compression plus shear

biaxial compression plus in-plane shear is 16%. It is an intermediate case between the SSSS and SSCC boundary conditions.

Chapter 6

Conclusions

The achievements and the conclusions drawn in this thesis are discussed in Section 6.1. Section 6.2 presents several aspects that may be of interest for future research.

6.1 Conclusions

In this thesis, a framework has been developed to optimize the buckling performance of variable stiffness panels with curvilinear stiffeners.

First, variable-stiffness laminates were modeled. To that end, the curvilinear fiber paths were described by the linear variation of the fiber angle. The fiber orientation was set to vary in the horizontal direction. This approach requires only two parameters to characterize the fiber path: the fiber angle at the center and at the side of the panel. A complete ply was constructed by shifting consecutive courses, identical to the reference course, in the vertical direction. That is, the shifted method was employed. The manufacturing aspects of the AFP machine were considered in the modeling phase of VS laminates. The maximum curvature allowed by the AFP machine was imposed on the skin fiber paths to avoid wrinkling. The effect of the manufacturing-induced gaps was incorporated by first locating the gaps present in the VS laminates. Then the material properties were scaled according to the gap area.

A curvilinear grid-stiffened layout was also designed. The curvilinear stiffeners were modeled by a cubic spline. Four symmetrical stiffeners eccentrically attached to the plate were considered. The stiffener layout was defined by two parameters. One parameter controlled the stiffener location on the plate and the other the stiffener curvature. The composite fibers followed the curvilinear path of the stiffener, forming a zero-angle laminate. The maximum curvature allowed by the AFP machine also constrained the in-plane curvature of the stiffener paths.

The optimization was performed by Genetic Algorithm. GA was chosen as the optimizer to avoid the calculation of the derivatives of the objective function and constraints and to not converge to a local minimum. The panels were defined by a reduced number of design variables which made the computational time affordable. Optimal designs for VS laminates with curvilinear stiffeners were obtained for different loading cases and boundary conditions. Two load cases were addressed: a biaxial compression

and biaxial compression plus in-plane shear. Three boundary conditions were considered: all edges of the plate simply supported (SSSS), two edges simply supported and two edges clamped (SSCC), and all edged clamped (CCCC). A constant stiffness quasi-isotropic laminate with equidistant straight stiffeners was used as a basis for comparison.

Regarding the skin laminate, there was a chance that the skin laminates were composed of straight fibers, however, all optimized laminates presented fibers with curvature. Curvilinear fibers produced more efficient load paths than the straight fibers, enhancing the bearing capability of the skin. The curvature of the skin fibers was dependant on the boundary condition studied. Panels under SSSS boundary condition showed highly curved skin fibers, reaching or being close to the maximum allowable value. Panels under SSCC and CCCC boundary conditions presented lower, but still significant, curvature values for the skin fibers.

It was observed that the manufacturing-induced gaps in VS laminates worsened the buckling performance of the panel. Since the optimized panels presented a low gap area, the buckling load did not excessively decrease compared to the ideal panels. Curvilinear skin fibers that induce gaps were preferred to straight fibers that do not cause those gaps.

As for the grid layout, the stiffeners were placed in intermediate positions, neither towards the center of the panel nor towards the edges. The stiffener curvature also changed according to which boundary condition was optimized. The curvature of the stiffeners reached the maximum allowed when the panels were optimized under SSSS boundary condition. For the SSCC boundary condition, quasi-straight stiffeners were preferred. In this case, curved stiffeners did not demonstrate a major advantage in panel buckling behavior. The optimized stiffeners under CCCC boundary conditions showed a considerable curvature.

It was shown that tailoring the stiffness variation by using curvilinear fibers can improve the buckling performance of the panel. The improvement in the buckling load compared to the straight fiber design depended on the load case and boundary conditions. Panels under SSSS boundary conditions showed the highest improvement: a 51% for biaxial compression and 26% for biaxial compression plus in-plane shear. In the case of the SSCC boundary condition, the improvement achieved was the lowest: a 14% for biaxial compression and 12% for biaxial compression plus in-plane shear. The SSCC boundary condition presented intermediate values of improvement: a 23% for biaxial compression and 16% for biaxial compression plus in-plane shear

The optimization framework developed has proven to be an efficient tool to design composite panels with curvilinear fibers and curvilinear stiffeners It can help the designer to evaluate in which scenarios these panels provide the greatest benefit.

6.2 Future Work

The optimized case studies present an overview of the possible benefits of VS panels reinforced with curvilinear stiffeners. However, there are several aspects that remain to be addressed in the future.

To qualitatively assess in which situations these panels will perform better than straight fiber designs,

various load cases and boundary conditions, as well as other dimensions of the skin and stiffeners, should be studied.

The design space could be expanded by optimizing the thickness and height of the stiffeners or defining different stiffener layouts. Various reference paths for the skin fibers could be implemented to fully explore the tailoring capability of curvilinear fibers. Other laminate stacking sequences can be optimized, for example, with more different plies or removing the symmetry and balance conditions.

For the sake of model simplicity, the panels optimized in the present thesis are assumed to be flat. However, the panels could be modeled with a slight curvature to more closely resemble the wing and fuselage skins of the aircraft. In this regard, panels with a hole could be investigated to simulate the fuselage skin window.

The optimization performed seeks to maximize the buckling load but is easily adaptable to other objective functions. Other design objectives and constraints may be panel mass, fundamental frequency, deformations, ply failure, interlaminar stress, etc. In addition, parallel processing could be used to conduct various finite element analyses, accelerating the optimization runtime.

The number of tows in a course, the tow width and the coverage percentage affect the gap and/or overlap distribution in VS layers. Studies varying these manufacturing parameters could be carried out to investigate their effect on the panel buckling performance.

Post-buckling behavior and experimental validation of composite panels with curvilinear fibers and curvilinear stiffeners could be other fields of future research.

Bibliography

[1] F.C. Campbell. *Manufacturing technology for Aerospace structural materials.* Number 2006927672. Elsevier, 1 edition, 2006. ISBN-13: 978-1-85-617495-4.

[2] United States Government General Accountability Office. Aviation safety - status of FAA's actions to oversee the safety of composite airplanes. *Report to Congressional Requesters*, GAO-11-849, September 2011.

[3] Justin Hale. Boeing 787 from the ground up. *A quarterly publication BOEING.COM/COMMERCIAL/AEROMAGAZINE*, QTR-04-06.

[4] A.W.Blom. *Structural performance of fiber-placed, variable-stiffness composite conical and cylindrical shells.* PhD thesis, Delft University of Technology, 2010.

[5] M.Bahar and M.Sinapius. Adaptive feeding roller with an integrated cutting system for automated fiber placement (afp). *Journal of Composites Science*, 4(3):92, 2020. doi:10.3390/jcs4030092.

[6] C.Waldhart. Analysis of tow-placed, variable-stiffness laminates. Master's thesis, Faculty of the Virginia Polytechnic Institute and State University, 1996.

[7] S.Ijsselmuiden. *Optimal design of variable stiffness composite structures using lamination parameters.* PhD thesis, Delft University of Technology, 2011.

[8] B.Kim, K.Potter, and P.Weaver. Continuous tow shearing for manufacturing variable angle tow composites. *Composites Part A: Applied Science and Manufacturing*, 43:1347–1356, 2012. doi:10.1016/j.compositesa.2012.02.024.

[9] B.Kim, K.Potter, and P.Weaver. Computer aided modelling of variable angle tow composites manufactured by continuous tow shearing. *Composite Structures*, 129:256–267, 2015. doi:10.1016/j.compstruct.2015.04.012.

[10] B.Kim, K.Potter, and P.Weaver. Manufacturing characteristics of the continuous tow shearing method for manufacturing of variable angle tow composites. *Composites Part A: Applied Science and Manufacturing*, 61:141–151, 2014. doi:10.1016/j.compositesa.2014.02.019.

[11] S.Nagendra, S.Kodiyalam, and J.Davis. Optimum design of composite structures with curved fiber courses. *Collection of Technical Papers-AIAA/ASME/ASCE/AHS/ASC Structures, Structural Dynamics and Materials Conference*, 2:1031 – 1041, 1995.

[12] S.Honda and Y.Narita. Natural frequencies and vibration modes of laminated composite plates reinforced with arbitrary curvilinear fiber shape paths. *Journal of Sound and Vibration*, 331(1): 180–191, 2012. doi:10.1016/j.jsv.2011.08.019.

[13] L.Parnas, S.Oral, and Ü.Ceyhan. Optimum design of composite structures with curved fiber courses. *Composites Science and Technology*, 63(7):1071–1082, 2003. doi:10.1016/S0266-3538(02)00312-3.

[14] R.Olmedo and Z.Gurdal. Buckling response of laminates with spatially varying fiber orientations. *Collection of Technical Papers - AIAA/ASME Structures, Structural Dynamics and Materials Conference*, pages 2261–2269, 1993. doi:10.2514/6.1993-1567.

[15] Z.Gürdal and R.Olmedo. In-plane response of laminates with spatially varying fiber orientations: Variable stiffness concept. *AIAA Journal*, 31(4):751–758, 1993. doi:10.2514/3.11613.

[16] B.Tatting and Z.Gürdal. Design and manufacture tow placed plates of elastically tailored. *NASA/CR*, 2002.

[17] Z.Gürdal, B.F.Tatting, and C.K.Wu. Variable stiffness composite panels: Effects of stiffness variation on the in-plane and buckling response. *Composites Part A: Applied Science and Manufacturing*, 39 (5):911–922, 2008. doi:10.1016/j.compositesa.2007.11.015.

[18] Z.Gürdal, B.Tatting, and K.Chauncey Wu. Tow-placement technology and fabrication issues for laminated composite structures. *Collection of Technical Papers - AIAA/ASME/ASCE/AHS/ASC Structures, Structural Dynamics and Materials Conference*, 4:2716–2733, April 2005.

[19] S.Honda, Y.Oonishi, Y.Narita, and K.Sasaki. Vibration analysis of composite rectangular plates reinforced along curved lines. *Journal of System Design and Dynamics*, 2(1):76–86, 2008. doi:10.1299/jsdd.2.76.

[20] S.Honda and Y.Narita. Vibration design of laminated fibrous composite plates with local anisotropy induced by short fibers and curvilinear fibers. *Composite Structures*, 93(2):902–910, 2011. doi:10.1016/j.compstruct.2010.07.003.

[21] S.Setoodeh, A.Blom, M.Abdalla, and Z.Gurdal. Generating curvilinear fiber paths. *AIAA/ASME/ASCE/AHS/ASC Structures. Structural Dynamics, and Materials Conference*, pages 1–13, May 2006.

[22] A.Alhaj Ahmad, M.Abdallah, and Z.Gürdal. Design tailoring for pressure pillowing using tow-placed steered fibers. *Journal of Aircraft*, 45(2):630–640, 2008. doi:10.2514/1.32676.

[23] Z.Wu, P.Weaver, G.Raju, and B.Kim. Buckling analysis and optimisation of variable angle tow composite plates. *Thin-Walled Structures*, 60:163–172, 2012. doi:10.1016/j.tws.2012.07.008.

[24] A.Blom, M.Abdalla, and Z.Gurdal. Optimization of course locations in fiber-placed panels for general fiber angle distributions. *Composites Science and Technology*, 70(4):564–570, 2010. doi:10.1016/j.compscitech.2009.12.003.

[25] X.Niu, T.Yang, Y.Du, and Z.Q.Xue. Tensile properties of variable stiffness composite laminates with circular holes based on potential flow functions. *Archive of Applied Mechanics*, 86(9):1551–1563, 2016. doi:10.1007/s00419-016-1126-8.

[26] S.Setoodeh, A.Blom, M.Abdalla, and Z.Gurdal. Design of variable-stiffness composite laminates for maximum in-plane stiffness using lamination parameters. *Collection of Technical Papers - AIAA/ASME/ASCE/AHS/ASC Structures, Structural Dynamics and Materials Conference*, 5: 3473–3481, April 2005. doi:10.2514/6.2005-2083.

[27] M.Abdalla, S.Setoodeh, and Z.Gurdal. Design of variable stiffness composite panels for maximum fundamental frequency using lamination parameters. *Composite Structures*, 81(2):283–291, 2007. doi:10.1016/j.compstruct.2006.08.018.

[28] S.Honda and Y.Narita. Design of composite plates with optimally distributed short fibers. *Proceeding of 16th International Conference on Composite Materials*, July 2007.

[29] S.W.Tsai and N.J.Pagano. Invariant properties of composite materials. *Archive of Applied Mechanics*, page 233–252, 1968. Technomic, Westport, PA.

[30] S.W.Tsai and H.T.Hahn. Introduction of composite materials. page 233–252, 1980. Technomic, Lancaster, PA.

[31] A.Alhajahmad and C. Mittelstedt. Buckling performance of curvilinearly grid-stiffened tow-placed composite panels considering manufacturing constraints. *Composite Structures*, 260:113271, September 2021. doi:10.1016/j.compstruct.2020.113271.

[32] B.Coburn, Z. Wu, and P. Weaver. Buckling analysis of stiffened variable angle tow panels. *Composite Structures*, 111:259–270, 2014. doi:10.1016/j.compstruct.2013.12.029.

[33] D.Wang, M.Abdalla, and W.Zhang. Buckling optimization design of curved stiffeners for grid-stiffened composite structures. *Composite Structures*, 159:656–666, 2017. doi:10.1016/j.compstruct.2016.10.013.

[34] K.Singh and R.Kapania. Buckling load maximization of curvilinearly stiffened tow-steered laminates. *Journal of Aircraft*, 56:2272–2284, 2019. doi:10.2514/1.C035358.

[35] M. Arian Nik. *Optimization of variable stiffness composites with embedded defects induced by Automated Fiber Placement*. PhD thesis, McGill University, 2014.

[36] K.Fayazbakhsh, M.Arian Nik, D.Pasini, and L.Lessard. Defect layer method to capture effect of gaps and overlaps in variable stiffness laminates made by automated fiber placement. *Composite Structures*, 97:245–251, 2013. doi:10.1016/j.compstruct.2012.10.031.

[37] A.Blom, C.Lopes, P.Kromwijk, Z.Gurdal, and P.P.Camanho. A theoretical model to study the influence of tow-drop areas on the stiffness and strength of variable-stiffness laminates. *Journal of Composite Materials*, 43(5):403–425, 2009. doi:10.1177/0021998308097675.

[38] V.Mishra, D.Peeters, and M.Abdalla. Stiffness and buckling analysis of variable stiffness laminates including the effect of automated fibre placement defects. *Composite Structures*, 226:111233, 2019. doi:10.1016/j.compstruct.2019.111233.

[39] T.Brooks and J.Martins. On manufacturing constraints for tow-steered composite design optimization. *Composite Structures*, 204:548–559, 2018. doi:10.1016/j.compstruct.2018.07.100.

[40] D.Liu, P.Hao, K.Zhang, K.Tian, B.Wang, G.Li, and W.Xu. On the integrated design of curvilinearly grid-stiffened panel with non-uniform distribution and variable stiffener profile. *Materials and Design*, 190:108556, 2020. doi:10.1016/j.matdes.2020.108556.

[41] L.Praticò, J.Galos, E.Cestino, G.Frulla, and P.Marzocca. Experimental and numerical vibration analysis of plates with curvilinear sub-stiffeners. *Engineering Structures*, 209:109956, 2020. doi:10.1016/j.engstruct.2019.109956.

[42] W.Zhao and R.Kapania. Buckling analysis of unitized curvilinearly stiffened composite panels. *Composite Structures*, 135:365–382, 2016. doi:10.1016/j.compstruct.2015.09.041.

[43] R.Kapania, J.Li, and H.Kapoor. Optimal design of unitized panels with curvilinear stiffeners. *Collection of Technical Papers - AIAA 5th ATIO and the AIAA 16th Lighter-than-Air Systems Technology Conference and Balloon Systems*, 3:1708–1737, 2005. doi:10.2514/6.2005-7482.

[44] R.Vescovini, V.Oliveri, D.Pizzi, L.Dozio, and P.Weaver. Pre-buckling and buckling analysis of variable-stiffness, curvilinearly stiffened panels. *Aerotecnica Missili & Spazio*, 99:43–52, 2020. doi:10.1007/s42496-019-00031-4.

[45] T.Dang, K.Kapania, W.Slemp, M.Bhatia, and S.Gurav. Optimization and postbuckling analysis of curvilinear-stiffened panels under multiple-load cases. *Journal of Aircraft*, 47:1656–1671, 2010. doi:10.2514/1.C000249.

[46] J.Xu, Q.Zhao, and P.Qiao. A critical review on buckling and post- buckling analysis of composite structures. *Frontiers in Aerospace Engineering*, 2(3):157–168, 2013.

[47] *Abaqus 6.14 Documentation*. Dassault Systemes, 2014. http://130.149.89.49:2080/v6.14/.

[48] S.Nagendra, R.T. Haftka, and z.Gürdal. Design of a blade stiffened composite panel by a genetic algorithm. *Collection of Technical Papers - AIAA/ASME Structures, Structural Dynamics and Materials Conference*, pages 2418–2436, 1993.

[49] P.Hao, C. Liu, X.Yuan, B.Wang, G.Li, T.Zhu, and F.Niu. Buckling optimization of variable-stiffness composite panels based on flow field function. *Composite Structures*, 181:240–255, 2017. doi:10.1016/j.compstruct.2017.08.081.

[50] L.Ingber. Simulated annealing: Practice versus theory. *Mathematical and Computer Modelling*, 18 (11):29–57, December 1993. doi:10.1016/0895-7177(93)90204-C.

[51] A.Alhaj Ahmad. *Design tailoring of panels for pressure pollowing using tow-placed steered fibers.* PhD thesis, Delft University of Technology, 2008.

[52] Z.Wu, , G.Raju, and P.Weaver. Framework for the buckling optimization of variable-angle tow composite plates. *AIAA Journal*, 53(12):3788–3804, 2015. doi:10.2514/1.J054029.

[53] V.Mishra. A methodology to predict the stiffness properties and buckling load of manufacturable variable stiffness panels. Master's thesis, Delft University of Technology, 2017.

[54] J.Kollenburg. The effects of local fibre steering. Master's thesis, Delft University of Technology, 2021.

[55] W.Zhao and R.Kapania. Vibration analysis of curvilinearly stiffened composite panel subjected to in-plane loads. *AIAA Journal*, 55(3):981–997, 2017. doi:10.2514/1.J055047.

[56] J.Kiusalass. *Numerical Methods in Engineering with MATLAB*, chapter 3. Cambridge University Press, second edition, 2010.

[57] R. Canale and S.Chapra. *Numerical Methods for Engineers*, chapter 18. McGraw-Hill, sixth edition, 2010.

[58] J. H. Holland. *Adaptation in Natural and Artificial Systems.* Ann Arbor: University of Michigan Press, 1975.

[59] K.Deb. An efficient constraint handling method for genetic algorithms. *Computer Methods in Applied Mechanics and Engineering*, 186(2-4):311–338, 2000. doi:10.1016/S0045-7825(99)00389-8.

[60] *Genetic Algorithm and Direct Search Toolbox ™ 2 User's Guide.* The MathWorks, Inc., 2004-2008. www.mathworks.com.